CHEMICAL REVIEWS

Review

pubs.acs.org/CR

Silicon–Germanium Nanowires: Chemistry and Physics in Play, from Basic Principles to Advanced Applications

Michele Amato,*[,†] Maurizia Palummo,*[,‡] Riccardo Rurali,*[,§] and Stefano Ossicini*[,∥,⊥]

[†]Institut d'Electronique Fondamentale, UMR8622, CNRS, Université Paris-Sud, 91405 Orsay, France

[‡]European Theoretical Spectroscopy Facility (ETSF), Dipartimento di Fisica, Università di Roma, "Tor Vergata", Via della Ricerca Scientifica 1, 00133 Roma, Italy

[§]Institut de Ciència de Materials de Barcelona (ICMAB–CSIC), Campus de Bellaterra, 08193 Bellaterra, Barcelona, Spain

[∥]"Centro S[3]", CNR-Istituto di Nanoscienze, Via Campi 213/A, 41125 Modena, Italy

[⊥]Dipartimento di Scienze e Metodi dell'Ingegneria, Centro Interdipartimentale En&Tech, Università di Modena e Reggio Emilia, Via Amendola 2 Pad. Morselli, I-42100 Reggio Emilia, Italy

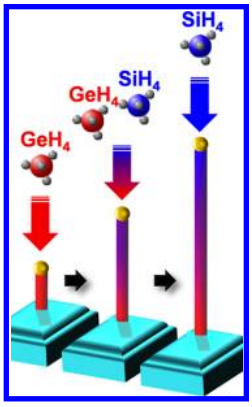

CONTENTS

1. INTRODUCTION

The trend predicted by Moore's law sets forth strict requirements on the electronic properties of materials that cannot always be satisfied by conventional semiconductors. Thus, the last twenty years and, in particular, the first decade of this century have witnessed a progressive interest in materials and devices with reduced size and dimensionality. Nanostructures and nanomaterials have been considered the key development for next generation technology, due their ease of processing, new properties and compatibility with the existent silicon (Si) microelectronics. Great progresses have been made, in particular regarding the use of Si nanostructures in microelectronics, photonics, and photovoltaics.[1−5]

However, the scaling down of semiconductor structures to nanometer sizes alone does not satisfy the need of new unique properties in a variety of applications. On the other hand, the manipulation through alloying together with the variation of the size provides a natural platform for the development and creation of materials that present the desired properties but, at the same time, can be easily integrated into the existent Si

Received: May 11, 2013
Published: November 22, 2013

   dx.doi.org/10.1021/cr400261y | Chem. Rev. 2014, 114, 1371−1412

technology. A meaningful example of this possibility is given by the use of silicon−germanium (SiGe) nanostructures.

The idea of combining the chemical and physical properties of Si and Ge represents a well-established strategy to engineer innovative materials and devices. In particular SiGe systems have garnered much attention as promising technology building blocks able to improve some of the properties of Si, producing enhanced versions of Si microlectronic devices, still maintaining its cheap fabrication processes. Indeed the smaller band gap of Ge compared to that of Si and the possibility to strain Si, due to the lattice mismatch of the two materials, offered the possibility to engineer the electronic band gap thereby increasing the devices inherent switching speeds due to the higher Ge mobility. The real strength of SiGe systems for electronics applications lies in the possibility to integrate analog, radio frequency, and digital on a single chip using existing complementary metal oxide semiconductor (CMOS) fabrications technologies, which is not possible with any other technologies (like, e.g., devices based on GaAs). Furthermore, SiGe materials are actively investigated in the field of silicon photonics and optoelectronics with the hope for the future to maintain the versatility and cheap costs of silicon technology to create complete optoelectronic systems. Thus, SiGe systems have been experiencing tremendous development, starting from more than four decades ago, as high quality SiGe thin layers and superlattices became the subjects of an intense research and development. Historically[6] the point of departure was the theoretical suggestion by Gnutzmann and Clausecker[7] that, due to zone folding effects in superlattices, it would be possible to obtain quasi-direct band gap semiconductors starting from the indirect band gap ones. The first experimental attempt to do this can be ascribed to Kasper et al.,[8] who using an ultrahigh vacuum (UHV) evaporation technique at a substrate temperature of 750 °C obtained heterostructures of medium quality, due to the large lattice mismatch. Improvements were made, in the 80s, by Bean et al.[9] using molecular beam epitaxy (MBE) and through lowering of the substrate growth temperature and by the Abstreiter's group, which, using the concept of strain symmetrization and growing an intermediate SiGe alloy buffer layer, was able to grown thick pseudomorphic multilayer structures.[10] In the 90s the first observations of band edge photoluminescence on fully strained SiGe alloys and Si/SiGe multiple quantum wells (MQWs) were thus reported[11,12] greatly exciting the entire field. Since then, major progresses in chemical synthesis, materials processing, device engineering, characterization and modeling have enabled the fabrication of devices with improved performance and reproducibility. As a result of these efforts, SiGe layered heterostructures boosted important technological breakthrough in solid-state electronics,[13] for example as heterojunction bipolar transistors (HJBT),[14] heterojunction internal photoemission photodetector,[15] metal-on-insulator field effect transistor (MOSFET) with high performance,[16] and modulation-doped field effect transistor (MODFET).[17,18] Many other devices, such as optical modulators, waveguides and detectors, resonant tunneling diodes, lasers, and quantum devices have been envisaged and proposed. Reviews of these exciting results for SiGe heterostructures were given in the last two decades by Schäffler[19] and Whall and Parker[13,20] and recently by Paul[21] and Lee et al.[22]

In the new millennium nano definitely enters into play. Nanostructures are low-dimensional confined systems, where quantum confinement can act in three spatial directions; therefore, one has two-dimensional (quantum wells), one-dimensional (quantum wires or nanowires), and zero-dimensional (quantum dots or nanocrystals) confined structures. Thus, concerning SiGe nanostructures a huge amount of literature has been devoted to Si/SiGe quantum well structures[23,24] and to the spontaneous formation, self-organization, and properties of SiGe quantum dots.[24,25]

In this review the interest is centered on SiGe nanowires (NWs), a particular class of semiconductor nanowires for which several methods of growth have been developed both in the bottom-up and in the top-down approach. The research activity in this field is one of the most rapidly developing areas in materials science. The confinement in one direction leads to unique transport properties of electrons, phonons, and photons, and additionally, SiGe NWs offer, unlike the corresponding pure Si and pure Ge NWs, the possibility to modulate the electronic, optical, and transport properties, not only by changing the size of the system, but even by varying the geometry of the Si/Ge interface and the relative composition of Si and Ge atoms. In fact one of the great advantages of these nanowires heterostructures is that two types of systems can be realized, axial heterostructures, in which sections of different materials with the same diameter are grown along the wire axis, and radial heterostructures, made by two coaxial cylinders: the internal one, the core, is made up of one type of material, and the external one, the shell, is made up of the other type. Thus, it is possible to say that the electronic properties of SiGe nanowires depend on two main factors: the first one is the extrinsic size effect, which is related to the variation of the size of the system and which can be analyzed by fixing the composition of the wire and varying its diameter; the second is the intrinsic bulk alloying effect, which is related to the geometry and the composition of the system and which can be analyzed by fixing the diameter of the wire and varying its composition.

Throughout all this review we will focus on bottom-up nanowires, where the constituent atoms assemble to form a larger structure, rather than on top-down nanowires, where the bulk material is nanostructured by techniques such as lithography or electrophoresis.[26] Top-down nanowires[27] are in principle more amenable to mass serial production, but atomically precise and truly nano structures, smooth facets, and some of the most important configurations that we will describe, such as core−shell structures, inherently belong with bottom-up synthetic nanowires. Nevertheless, some very interesting works based on top-down SiGe nanowires have been reported, covering many topics in fundamental physics, such as quantized conductance of nanoconstrictions,[28] single-electron devices,[29] Coulomb blockade,[30,31] and the magneto-resistance of quasi-ballistic wires.[32,33] The interested reader is referred to the original publications.

SiGe NWs are expected to be the target of intriguing technological applications in the field of high performance nanoelectronics (such as FETs and interconnections), thermoelectrics, photovoltaics, chemical energy storage, biomedicine, superconductivity, and spintronics. From another point of view, since in these materials the thickness matches the length scale of some quantum mechanical phenomena (a few hundreds of nanometers and less), their investigation offers a fruitful playground for basic research in material science.

Despite of the amount of literature devoted to this issue (for reviews partly dedicated to SiGe NWs see refs 34−38), a unified description of the theoretical concepts and experimental

results on the main properties of SiGe NWs is still lacking. The paper has a 3-fold goal, which consists in (i) presenting the current developments in SiGe NW understanding and technology by giving a comprehensive overview of the main experimental results related to their chemical and physical properties; (ii) providing an exhaustive review of the theoretical state-of-art, trying to bridge gaps between theoretical modeling and its consolidation into experiments, and (iii) collecting all of the advanced technological applications of these materials, highlighting their connections with basic solid-state phenomena.

The review is organized as follows. First, in section 2 the growth methods will be reviewed, also from an historical point of view, accounting for the main achievements and challenges specific to the synthesis of these systems, in particular regarding axial and radial heterostructures. In section 3 we will discuss the chemical and physical properties of SiGe NWs, namely the structural and electronic properties and their dependence on the composition and interface band-offsets and strain. This section will end with an overview of the importance and the role of SiGe nanowires in thermal transport. Section 4 is entirely devoted to a review of the role played by theory, modeling, and simulations in the descriptions of the unique properties of SiGe NWs with particular emphasis on the effects related to quantum confinement, size, shape, composition, local strain, interfaces states, and doping. In section 5 the paper will end with a description of the most recent advances in electronic devices based on SiGe nanowires. Final remarks and outlook will be presented in section 6.

2. GROWTH TECHNIQUES, MORPHOLOGY, AND STRUCTURAL PROPERTIES

Semiconductor nanowires are commonly grown through the vapor−liquid−solid (VLS) mechanism, which was first proposed in the 1960s by Wagner and Ellis[39] for the growth of Si whiskers. In a nutshell, the method consists in using a catalytic nanoparticle, typically Au, to promote the decomposition of an appropriate gaseous precursor. Let us see in more detail the case of the standard growth of a Si NW. First a Au nanoparticle is deposited onto a Si substrate. Au and Si react and form a Au−Si alloy droplet. Next, SiH_4 in vapor phase, the Si precursor, is inserted in the growth chamber and starts to be adsorbed in the Au−Si droplet. When supersaturation is reached, Si atoms precipitate and the nanowire starts its nucleation.

Many different flavors of this general recipe have been reported and some of the ingredients can change (precursor gas and catalytic nanoparticle), but the process always relies on the catalyzed decomposition of a precursor on a liquid metal droplet, which yields a growth rate which is orders of magnitude higher in one direction than in the others. The main distinctive element among different approaches to VLS is how the precursor is supplied and reach the catalytic droplet. (i) In chemical vapor deposition (CVD) a volatile gaseous precursor—SiH_4, Si_2H_6, or $SiCl_4$, to stick to the case of Si NWs—reaches the Au particle and decompose. (ii) In molecular beam epitaxy (MBE), a solid ultrapure Si source is heated until it starts to sublimate; then, a gaseous beam of Si atoms is directed to the substrate, where it reacts with the Au particle. (iii) In laser ablation, used to produce the first truly nanoscopic Si[40] and, as we shall see briefly, SiGe alloy NWs,[41] a high-power pulsed laser is used to ablate material from a mixed Si−Au target; the Si ablated from the target collides with inert-gas molecules present in the furnace and the atoms condense to liquid nanodroplets that contain both Si and the catalyst material. Other popular choices include oxide assisted growth, based in the evaporation of SiO,[42] solution-based techniques, where growth takes place in liquid media,[43] and metal-assisted etching.[44]

The goal of this section is reviewing the main achievements and challenges in nanowire growth which are specific of SiGe systems. For a comprehensive description of growth techniques, the interested reader is encouraged to see the reviews by Schmidt et al.[45] and Wang et al.[46] In section 2.1 we will show how a precise control of the composition in alloyed NWs leads to a new class of nanowires with tunable properties. In sections 2.2 and 2.3 we will discuss the formation of axial and radial Si/Ge interfaces for advanced devices. Notice that top-down nanofabrication is not considered here (see Wolfsteller et al.[47] for a comparison between bottom-up and top-down approach for the fabrication of SiGe heterostructures).

2.1. Alloyed Nanowires

The observation that the eutectic temperature of Au−Si and Au−Ge are practically identical suggested immediately the possibility of growing NWs that contained both species. Roughly speaking, if Si and Ge precursors are incorporated in the catalytic particle and therein decompose until supersaturation at the same temperature, it is in principle enough to add simultaneously both precursors in the growth chamber. This was first accomplished by Duan and Lieber[41] in 2000 by laser-assisted catalytic growth.[48]

Despite the initial advantage of similar eutectic temperatures, however, the synthesis of SiGe alloy NWs using gaseous precursors is complicated by the different thermal stabilities of SiH_4 and GeH_4. As a result of different decomposition reaction rates of the precursors, Ge NWs grow efficiently at 260−500 °C, while the growth of Si NWs is optimum in the 400−500 °C range. This behavior was observed in their experiment by Duan and Lieber,[41] where, due to the nonuniform temperature distribution inside the furnace, Si-rich NWs were obtained in the hotter central region, while Ge-rich NWs were obtained at the colder end. These results demonstrated that alloy NWs with different compositions could be grown in a single experiment. However, the main goal of alloying is the creation of an artificial material whose properties can be tuned by precise control of the composition. Hence, laser ablation does not seem to be the most suitable choice. Ideally, one would like to achieve full control on the composition of the alloy by tuning the fundamental growth parameters: the inlet gas composition (or ratio), i.e., $R = [GeH_4/(GeH_4 + SiH_4)]$, the growth temperature, and the total pressure.

Significant progress in this direction was reported by Lew et al.[49] where SiGe alloy NWs were grown by CVD from SiH_4 and GeH_4. Initially, at 275 °C no growth was observed, while subeutectic growth of Ge NWs has been previously reported. SiGe NWs growth was observed upon raising the temperature to 350 °C. Wires with uniform diameter along all their length were obtained for growth temperature of up to 400 °C. In this narrow window T is high enough to promote VLS growth but also low enough to prevent a noncatalyzed deposition of Ge on the wire sidewalls. Indeed, above 400 °C tapering was observed and it increased approximately linearly with temperature.

In the optimum 350−400 °C temperature range the composition can be varied through the inlet gas ratio R, at least in the 0.01−0.038 range where the dependence is linear

dx.doi.org/10.1021/cr400261y | Chem. Rev. 2014, 114, 1371−1412

and Ge concentrations between 0.12 and 0.26 were obtained (the growth parameters of this and other works reviewed in this section are summarized in Table 1). Larger values of the gas inlet ratio lead to Ge coating and tapering. The maximum Ge concentration that can be obtained in these growth conditions is $x \approx 0.66$. To increase x further the temperature has to be slightly reduced and with T = 325 °C and R = 0.2−0.4, concentrations up to 0.85 and 0.95 were achieved (Table 1).[50]

Table 1. Ge Concentration in $Si_{1-x}Ge_x$ Alloy NWs as a Function of Temperature T, Pressure P and Gas Inlet Ratio $R = GeH_4/(GeH_4 + SiH_4)$[a]

T (°C)	P (Torr)	Si precursor	Ge precursor	R	x
350−400	13	SiH_4	GeH_4	0.01	0.12[49]
350−400	13	SiH_4	GeH_4	0.038	0.25[49]
325	13	SiH_4	GeH_4	0.2	0.85[50]
325	13	SiH_4	GeH_4	0.4	0.95[50]
370−390	200	SiH_4	GeH_4	1.0	0.35[51]
370−390	200	SiH_4	GeH_4	1.0	0.55[51]
370−390	200	SiH_4	GeH_4	1.0	0.65[51]
370−390	200	SiH_4	GeH_4	1.0	0.70[51]
370−390	200	SiH_4	GeH_4	1.0	0.80[51]
370−390	200	SiH_4	GeH_4	1.0	0.85[51]
350	50	SiH_4	GeH_4	0.02	0.74[52]
350	100	SiH_4	GeH_4	0.02	0.66[52]
350	200	SiH_4	GeH_4	0.02	0.59[52]
350	300	SiH_4	GeH_4	0.02	0.45[52]
350	500	SiH_4	GeH_4	0.02	0.39[52]
350	750	SiH_4	GeH_4	0.02	0.35[52]
350	1000	SiH_4	GeH_4	0.02	0.27[52]
400	5	Si_2H_6	GeH_4	0.89	0.13[53]
400	20	Si_2H_6	GeH_4	0.89	0.32[53]
400	60	Si_2H_6	GeH_4	0.89	0.52[53]
500	20	Si_2H_6	GeH_4	0.50	0.13[53]
500	80	Si_2H_6	GeH_4	0.50	0.17[53]
500	160	Si_2H_6	GeH_4	0.50	0.26[53]
400	60	Si_2H_6	GeH_4	0.89	0.53[53]
450	60	Si_2H_6	GeH_4	0.89	0.48[53]
500	60	Si_2H_6	GeH_4	0.89	0.41[53]
440	4−5	Si_2H_6	GeH_4	0.33*	0.08*[54]
440	4−5	Si_2H_6	GeH_4	0.40*	0.10*[54]
440	4−5	Si_2H_6	GeH_4	0.50*	0.17*[54]
440	4−5	Si_2H_6	GeH_4	0.67*	0.20*[54]
440	4−5	Si_2H_6	GeH_4	0.80*	0.25*[54]
375	4.6	SiH_4	GeH_4	0.048	0.2*[55]
375	4.6	SiH_4	GeH_4	0.065	0.26*[55]
375	4.6	SiH_4	GeH_4	0.09	0.34*[55]
375	4.6	SiH_4	GeH_4	0.15	0.46*[55]

[a]Alloy compositions are normally determined by energy-dispersive x-ray spectroscopy (EDX) or, less frequently, by Raman spectroscopy.[55−60] Values marked with * are estimated from the figures of the original references.

Although the gas inlet ratio, in the appropriate T range, provides intuitively the best control over the composition, Givan and Patolsky[52] showed that similar results can be achieved by tuning the total growth pressure. The main advantage of this approach is that the growth temperature and the gas inlet ratio can be chosen to be low enough to minimize tapering (T = 350 °C, R = 0.02) and the composition can be controlled by a single growth parameter. Pressure was varied from 50 to 1000 Torr, and two regimes could be roughly distinguished: (i) P < 500 Torr, the Ge content increases sharply with P; (ii) P > 500 Torr, a milder linear dependence was observed. Tapering is absent or negligible throughout the pressure range explored. The pressure dependence of the composition has been tracked down to the decomposition rates of SiH_4 and GeH_4: while both increase with P concentration, yielding higher overall growth rates, germane decomposition rate can be up to 2 orders of magnitude higher. Data of unimolecular decomposition refer to higher temperatures than those relevant for the growth of SiGe NWs, but extrapolation to lower temperatures leads to even higher germane-to-silane pressure dependent decomposition rates. The same group later showed that pressure is also the key parameter to reduce random kinking in Ge-core/Si-shell NWs.[61]

An additional degree of freedom in the growth process that has been exploited to control the morphology of SiGe NWs is the use of additional gases, other than the precursors. Although the control of the composition remains the most critical issue in the growth of alloyed NWs, in principle one wants also smooth surfaces and uniform diameter throughout the length of the NW. Lee et al.[59] obtained longer and straighter NWs, without tapering, when the H_2 flux was increased from 100 to 200 sccm. Similar observations were reported by Potié et al.[58] upon addition of an optimum flow of HCl in the gas phase. In both cases the surface coverage with H and Cl seems to inhibit Au migration along the wire sidewalls, which helps preventing tapering of the NW. Additionally, Cl passivation has proven to be efficient in hindering silane adsorption, thus noncatalyzed radial growth. Interestingly, the HCl gas flow has a noticeable correlation with the Ge content, improving its incorporation in the alloy NW. Potié et al.[58] showed that, while Ge fraction saturates at ∼0.5 at 400 °C, it can increase up to ∼0.75 with a flow of 40 sccm of HCl. The role of O_2 flow in the synthesis of coaxial $Si_{1-x}Ge_x$ NWs have also been studied recently,[62] demonstrating the selective fabrication of $Ge/Si_{1-x}Ge_x$ or $SiO_2/Si_{1-x}Ge_x$ heterostructured wires.

$Si_{1-x}Ge_x$ NWs have been reported to grow along the ⟨110⟩, ⟨111⟩, and ⟨112⟩ axis (see for instance ref 49). Dailey et al.[53] reported a nice correlation between the growth orientation and the alloy composition: wires with a low Ge concentration, tend to mimic Si NW morphology, ⟨111⟩ oriented with Au decorated sidewalls at low precursor pressure, ⟨112⟩ oriented with clean sidewalls at high precursor pressure, while wires with a high Ge fraction present the typical features of Ge NWs of similar diameter (>20 nm), and ⟨111⟩ oriented with no Au on the sidewalls. Correlation of the wire diameter with the Ge content has also been reported.[63]

Recently, the importance of obtaining a uniform distribution of atoms into alloyed wires has been clearly pointed out by Ma et al.[64] By combining mechanical properties measurements and atomistic simulations, they demonstrated that, in alloyed SiGe NWs grown with the VLS method, the presence of interstitial Ge atoms can strongly affect the mechanical response of the wire, modifying its fracture strength and fracture strain. In particular, they used a nanomanipulator in a focused ion beam (FIB) system combined to a scanning electron microscope (SEM) to perform tensile experiments. In a first step, they measured the fracture strength and strain in SiGe NWs finding a nonlinear dependence of these quantities on the Ge content. Then, they employed a rapid thermal annealing (RTA) process to remove incorporated interstitial atoms and performed the same type of mechanical investigation. Surprisingly, after the RTA process, the fracture strength and strain were found to

dx.doi.org/10.1021/cr400261y | Chem. Rev. 2014, 114, 1371−1412

have a linear increasing relationship that is proportional to the Ge concentration. This pointed out the central role of interstitial defects on the structural stability of the wires.

The effect of dopant incorporation, necessary for device design, on the morphology, growth rate, and alloy composition has been studied by Givan et al.[65] Diborane (B_2H_6) and phosphine (PH_3) were used to achieve *p*- and *n*-type doping, respectively. *p* doping perturbs minimally the morphology and growth kinetic of the $Si_{1-x}Ge_x$ NW: no tapering is observed, the growth rate is minimally affected and the Ge concentration exhibits only a slight decrease. On the other hand, B doping appears to be more critical, making more difficult to obtain smooth nanowires with a controllable composition. The presence of diborane favors the decomposition of silane and silicon is more easily incorporated in the nanowire. While this fact can lead to an increase of the growth rate of up to the 35%, the Ge/Si ratio is halved for all the doping level considered. Additionally, B doping results in a noticeable tapering (0.5−1 nm/μm), which increases with the doping level.

2.2. Axial Heterostructures

Two-dimensional heterojunctions between semiconductors have been the privileged playground for the study of many fundamental properties in mesoscopic physics as well as the basic building block for several electronic and optoelectronic devices.

In two-dimensional interfaces, however, requirements on the lattice match of the two materials are quite stringent to obtain dislocation-free junctions. One-dimensional systems allow envisaging a broader class of possible heterostructures, because the lattice misfit can be more easily accommodated due to the new boundary conditions; that is, the stress can be released by radial expansion.

Si and Ge have a lattice mismatch of ∼4.2%. This rather large value, besides making the growth of defect-free 2D-interfaces challenging,[66,67] is responsible for sophisticated growth mechanism as the well-known Stranski-Krastanov growth, used to grow Ge quantum dots on Si substrates.

The first successful attempt at growing an axially modulated SiGe one-dimensional nanostructure was reported by Wu et al.[68,69] They used an ingenious combination of laser ablation and CVD growth to synthesized Si/SiGe superlattice NWs (Figure 1). The process consists in carrying out a conventional VLS-CVD growth of a Si NW, while a pulsed laser is periodically turned on and off. When the laser is on, pulsed ablation of a Ge target provides the Ge vapor for the SiGe alloyed segment. In this way the superlattice periodicity is simply controlled through the on/off frequency of the laser (5 s on, 25 s off in the experiment of Wu et al.[68]).

The successful engineering of devices based on hetero-junctions requires the interfaces between different materials to be as sharp as possible. However, in all of the early reports of $Si/Si_{1-x}Ge_x$ axial junctions in nanowires,[68,70] the interfaces were very diffuse, posing serious questions concerning the efficiency of the envisioned devices. Similar observations have been reported when standard CVD[71] and MBE growth are used.[72,73]

The difficulties encountered in obtaining abrupt interfaces motivated Clark et al.[74] to study whether or not they were due to fundamental impediments or could be bypassed. Their main finding was that the abruptness of the interface is of the order of the diameter of the NW, with the ledges being well fitted by an error function or an exponential decay, when the composition changes from Si to $Si_{1-x}Ge_x$ or vice versa (Figure 2). The fundamental bottleneck is the delay required to achieve a steady-state composition in the liquid droplet. In simple terms, when the chamber gas is enriched with GeH_4 the liquid droplet is still supersaturated mostly with Si alone and it will take a certain time until the Si:Ge ratio of the liquid phase will be the same than in the gas phase. During the transient, a nanowire segment with a composition gradient will grow.

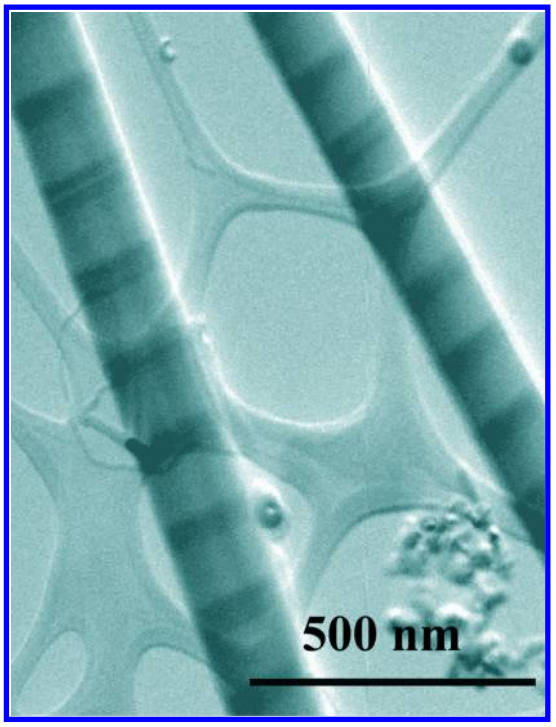

Figure 1. STEM image of two heterostructured Si/SiGe nanowires in bright field mode. The scale bar is 500 nm. Reprinted with permission from ref 68. Copyright 2002 American Chemical Society.

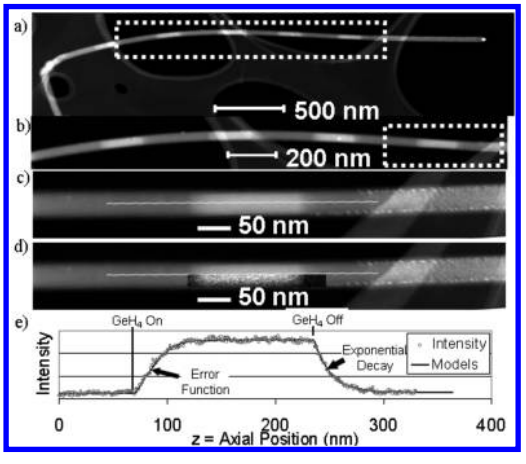

Figure 2. (a) Annular dark-field STEM image of a $Si/Si_{1-x}Ge_x$ heterostructured nanowire comprised of 6 $Si_{1-x}Ge_x$ blocks separated by Si segments. (b) Higher magnification ADF-STEM image revealing Si segments are longer than $Si_{1-x}Ge_x$. (c) Higher magnification ADF-STEM image that allows appreciating the nonabrupt interface of one of the $Si_{1-x}Ge_x$ segments. (d) ADF-STEM image with overlay of Ge energy dispersive spectrometer (EDS) map revealing that HAADF image is dominated by atomic number contrast. (e) Intensity profile of the last $Si_{1-x}Ge_x$ segment; the asymmetric interfaces are well-described by an error function and an exponential decay. Reprinted with permission from ref 74. Copyright 2008 American Chemical Society.

dx.doi.org/10.1021/cr400261y | *Chem. Rev.* 2014, 114, 1371−1412

The fundamental nature of this reservoir effect has been described by a theoretical model by Li et al.[75] According to this model, sharp Si−Ge heterojunctions cannot be obtained within standard VLS as a direct result of the high precursor solubilities. Hence, while the large solubility of Si and Ge at the eutectic point is a great advantage for the growth of uniform NWs, it becomes the main limiting factor when it comes to obtaining sharp interfaces in Si−Ge heterostructures. This also explains why sharper interfaces can be obtained in III−V NWs such as InAs-InP,[76] thanks to the low solubility in the catalyst of the elements of group V. It is noteworthy that, although the model of Li et al.[75] was developed for standard CVD growth, its predictions turned out to be quantitatively accurate also for hybrid techniques involving laser ablation[74] or pulsed laser deposition.[77]

The problem of abrupt interfaces is apparently irresolvable within VLS growth. When the gas precursor is switched from silane to germane with the goal of achieving a Si/Ge interface, the droplet must be depleted of Si before a pure Ge NW can be grown. Wen et al.[78] circumvented this problem by combining VLS growth with vapor−solid−solid (VSS) growth. Solid catalysts have already been used to grow Si and Ge NWs.[79,80] While they present some specific advantage, solid Al catalysts yield *p*-type doped Si NW with no need for other precursors, they suffer from very low growth rate, because the growth temperature must be considerably lower than in VLS. The idea of Wen et al.[78] is simple (i) they start growing a Si NW within VLS, (ii) they decrease the temperature and switch to VSS growth, and (iii) once the droplet is emptied of its Si content, they switch from SiH_4 to GeH_4 and start growing the Ge segment. During the first step the high Si solubility of VLS results in a high growth rate and it is harmless to the interface sharpness, as a pure Si segment is being grown. When GeH_4 is added into the reaction chamber the nanowire is already growing within VSS and the intrinsically low solubility of Si and Ge in the solid phase allows abrupt interfaces. With this method Wen et al.[78] obtained Si−Ge heterojunctions as sharp as 1 nm for a NWs with diameter of 18 nm (Figure 3). A versatile catalyst suitable to both VLS and VSS growth of Si and Ge NWs was prepared by adding Al to Au (previously used for VSS growth of Si[79] and Ge NWs,[80] respectively). More recently the same method has been demonstrated also with Ag/Au solid catalyst.[81]

The model of Li et al.,[75] the early report of Clark et al.,[74] and the successful growth of sharp Si−Ge interfaces of Wen et al.[78] showed the key role played by the precursor solubility. Despite the remarkable abruptness obtained, however, the combination of VLS and VSS seems to be practical only when a short Ge segment has to be grown. Otherwise, the slow growth rate of VSS would not be compatible with the wire length and throughput required by nanowire-based devices. A solution, of course, would be switching back to VLS growth after the interface has been formed, but this has not yet been demonstrated.

For these reasons, as pointed out in the Introduction, efforts have been made to stick with VLS growth and other approaches to tune the solubility of the semiconductor precursors in the catalytic droplet have been investigated. Perea et al.[82] accomplished this goal by in situ alloying of the Au catalysts. The central idea is that the eutectic solubility of Ge in a $Au_{1-x}Ga_x$ liquid nanoparticle depends on the Ga concentration x of the alloyed catalysts. Hence, a Ge NW is initially grown from a Au droplet ($x = 0$) as in conventional VLS; when an interface needs to be formed, a controlled flow of trimethylgallium (TMGa) is added in the reactor, inducing alloying of the $Au_{1-x}Ga_x$ droplet, where Ge is less soluble. Next, TMGa and GeH_4 are removed from the CVD chamber, while SiH_4 is added and temperature is increased from 380 to 495 °C (remember that Si NWs efficiently grow at higher temperatures than Ge NWs). Following this recipe, interfaces as sharp as 6 and 11 nm for 30 and 60 nm thick wires, respectively, were

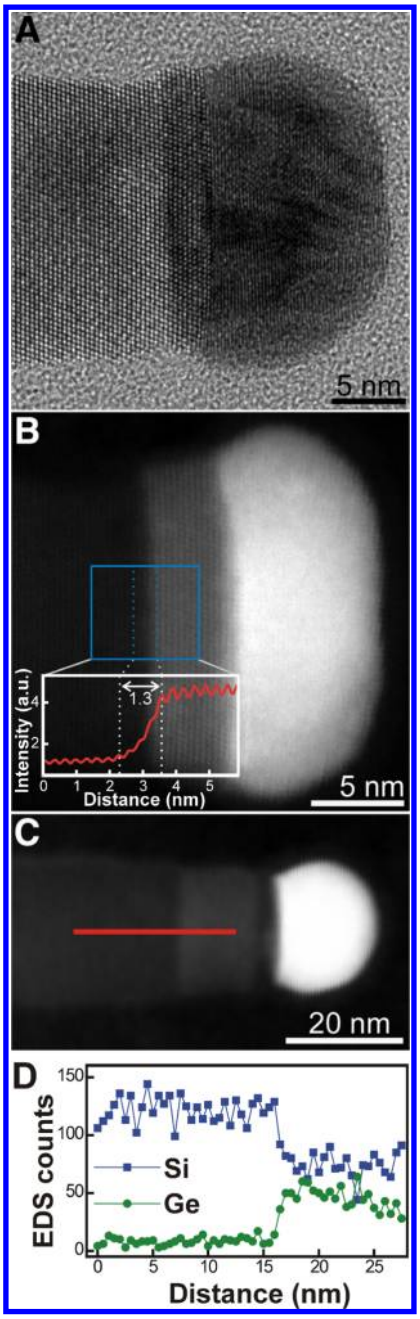

Figure 3. (A) High-resolution TEM image of a Si−Ge heterostructured nanowire. The Si NW was grown rapidly with the VLS method, then cooled, and grown for several minutes in the VSS mode, followed by growth of a Ge segment. (B) HAADF-STEM image of a similar wire grown under the same conditions. The inset shows the intensity profile across the interface. The width of the interface is 1.3 nm. (C) HAADF-STEM image of a $Si/Si_{1-x}Ge_x$ NW. (D) EDS line profile of Si and Ge across the $Si/Si_{1-x}Ge_x$ junction, as indicated in panel C, revealing a sharp transition of less than 2 nm from Si to SiGe. Reprinted with permission from ref 78. Copyright 2009 AAAS.

dx.doi.org/10.1021/cr400261y | *Chem. Rev.* 2014, 114, 1371−1412

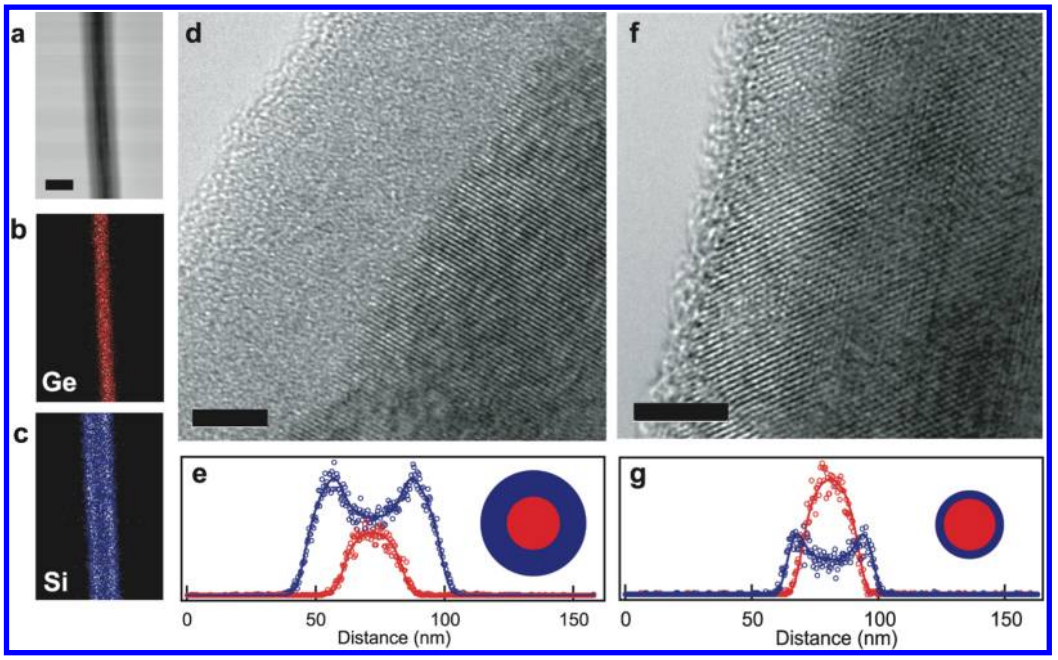

Figure 4. (a) Bright-field image of an unannealed Ge-core/Si-shell NW with an amorphous p-Si shell. Scale bar is 50 nm. (b,c) Scanning TEM elemental maps of Ge and Si concentrations of the nanowire shown in panel a. (d) High-resolution TEM image of a nanowire grown under the same conditions as the wire in panel a–c. Scale bar is 5 nm. (e) Elemental mapping cross-section showing the Ge (red circles) and Si (blue circles) concentrations. (f) High-resolution TEM image of annealed Ge-core/Si-shell NW with a crystalline *p*-Si shell. Scale bar is 5 nm. (g) Elemental mapping cross-section that gives a 5-nm shell thickness with a sharp interface consistent with the TEM image in panel f. Reprinted with permission from ref 87. Copyright 2002 Nature Publishing Group.

obtained. Ga–Au alloys have also been used to catalyze the growth of $Si_{1-x}Ge_x$ NWs.[83]

These efforts in achieving sharp axial heterojunctions in SiGe NWs have recently culminated in the report of an atomically abrupt interface.[84] Elegant in its simplicity, the method used by Geaney et al. consisted in using a Sn catalyst within a solvent vapor growth system.[85,86]

2.3. Radial Heterostructures

An important class of advanced devices that we will discuss in section 5 are based on core–shell nanowires. Radial heterostructures are in principle more challenging than axial ones because they require the ability of controlling axial versus radial growth at the same time that the inlet gas precursors are switched.

SiGe and GeSi core–shell NWs were first reported by Lauhon et al.,[87] where axial VLS growth of a Ge or a Si NW was followed by uncatalyzed, homogeneous vapor-phase deposition on the nanowire sidewalls of the complementary chemical species (Figure 4). With this approach they demonstrated Ge core–*p*-Si shell, as well as Si core–Ge shell NWs. All of the structures were monocrystalline, though Si shells, initially amorphous, needed a 600 °C thermal annealing to crystallize. Interface abruptness is not a major issue here, as the two growth steps involved are based on different synthesis mechanisms, i.e., VLS axial catalyzed growth vs uncatalyzed radial growth, and Si and Ge precursors do not mix.[88] As a matter of fact, interfaces as sharp as 1 nm were obtained.[87]

It should be stressed here that the recrystallization of the amorphous Si shell by thermal annealing likely leads to a strain relaxed heterostructure, similarly to the low pressure epitaxy carried out by Dayeh et al.[89] and described below. Although as a general rule in nanowire strains are more easily released laterally, this is not always the case and residual strains can have measurable effects on the electronic properties. Strain engineering, as a matter of fact, has traditionally been a way of tuning and improving the electronic characteristics of planar $Si_{1-x}Ge_x$ nanostructures and relies on a precise control of the strain level of the heteroepitaxy.[23,24]

Ge-core/Si-shell NWs have several advantages over the other possible coaxial SiGe structure, Si-core/Ge-shell NWs: (i) a better confinement of carriers in the core: band-offsets are such that holes are better confined than electrons or holes in a Si-core/Ge-shell, (ii) carrier mobilities in Ge are higher than in Si, and (iii) Si shells are more amenable to chemical passivation by thermal oxidation, as SiO_2 provide a more stable and higher quality surface passivation than any Ge oxide. These three factors together have been shown to lead to field-effect transistors (FETs) with significantly better performances than FETs based on single-element Ge or Si nanowires.[90] Therefore, since the seminal work of Lauhon et al.,[87] research efforts have mostly concentrated on coaxial NWs with a Ge-core and a Si-shell. Recently, it has been even shown that, via selective etching of the Ge core, these coaxial structures can serve as template for Si nanowire–nanotube heterostructures.[61]

The different optimal growth temperatures of Si and Ge are again at the core of a problem which is specific to the Ge-core/Si-shell architecture. After the axial growth of the Ge NW is stopped, the growth temperature must be increased for the conformal deposition of the Si-shell (Si optimally grows at higher temperatures than Ge, as discussed in section 2.1). At these conditions, however, the VLS-catalyzed synthesis of a Si NW from the tip of the Ge NW cannot be avoided, with growth rates of the undesired axial segment of the same order of the radial shell deposition. If the shell growth temperature and the SiH_4 partial pressure are decreased, the axial growth of a Si NW is inhibited, though this happens at expenses of a rough and nonconformal Si-shell. If the shell required is

dx.doi.org/10.1021/cr400261y | *Chem. Rev.* 2014, 114, 1371–1412

sufficiently thin, the growth could be in principle performed at the optimal temperature, as it would result in only a short axial segment of Si NW. Nevertheless, in this temperature range Au diffusion on the sidewalls of the nanowire is activated. Au impurities yield deep gap states that act as efficient recombination centers; thus, their presence is detrimental to the performance of many devices. On top of that, sidewall Au impurities can promote radial catalyzed growth that leads to tapered morphology.

A simple solution to this puzzle was proposed by Goldthorpe et al.:[91] before depositing the Si-shell, they etched the Au nanoparticle from the Ge NW tip. In this way Au cannot diffuse or promote VLS axial growth of a Si NW. Alternatively, to avoid the use of contaminants, it has been shown that the low temperature growth of a short segment of Si on top of the Ge NW can suppress diffusion, due to the lower mobility that Au has on Si rather than on Ge surfaces.[92,93]

While the sharpness of the Si/Ge junction is no longer a major issue in core−shell radial heterostructures, the contact area is much larger and it becomes more critical guaranteeing smooth and defect-free interfaces. In particular, theoretical models predict that only under restrictive conditions Si/Ge coaxial heterostructures are able to accommodate the full 4% lattice misfit without the creation of dislocations to relieve the stress.[94−98] These predictions agree with the experimental observation of periodic modulation of the Si-shell thickness, where both the periodicity and the amplitude of the surface roughness were found to increase linearly with the Ge-core diameter.[91] (i) At first, when the shell deposition begins, the amplitude of the surface roughening starts increasing; (ii) when enough elastic energy is built up at the valleys of the periodic modulation, dislocations nucleate and the amplitude of the roughening remain constant. Further synchrotron X-ray diffraction experiments indicate that the formation of these dislocations, mostly extrinsic stacking faults, leads to a substantial relieve of the axial strain but little relaxation of the radial strain. More recently, the same group carried out a systematic study of the strain relaxation as a function of the shell thickness in Ge-core/Si-shell NWs, estimating the critical shell thickness and determining dislocation mechanism that limits the coherency of the interface.[89] For instance they showed that a 16 nm radius Ge NW with a 3 nm Si shell is shown to accommodate 3% strain at equilibrium, three times larger than the 1 nm equilibrium critical thickness for planar Si/Ge heteroepitaxial growth.

Pushed by the observation that Si-shell are bedeviled by severe roughening, the same group carried out additional growth and characterization experiments in an effort to find the right recipe to obtain smooth Si-shells. They came up with two complementary strategies that allowed them obtaining a large class of dislocation-free Ge-core/Si-shell NWs.[99] The first idea originates from the observation of the periodic modulation previously observed, stemming from the low stability of {112} facets and the energetic convenience of replacing them with lower energy planes (the hills-and-valleys morphology observed). Therefore altering the surface energies involved, could avoid the facet break-up. Hence, instead of ⟨111⟩ wires bounded by {112} facets, they grew Ge NWs with diameters smaller than 20 nm that favor the ⟨110⟩ orientation, and are thus bounded by {111} and {110} facets.[99] Incidentally, this is likely the reason why Lu et al.,[100] who grew ⟨112⟩ NWs, were able to obtain dislocation-free Si-shells. The theoretical calculations of Cao et al.[101] suggests that the roughening of the Si-shell begins when the growth process changes from the Frank-van der Merwe to the Stranski-Krastanow mode.

The other approach proposed consists in carrying out the Si-shell deposition in presence of Cl, which competes for surface sites and hinders adatom diffusion that drives the surface roughening. Noteworthy, this effect could be accountable for the smooth surfaces obtained by Lauhon et al.,[87] who grew B-doped Si-shells. The B atoms, whose tendency to surface segregation is known, could behave like Cl atoms and difficult adatom diffusion.

The observation that the presence of other chemical species can have an effect on the shell morphology is very important, because many applications require doped Si-shells, where the appropriate dopant precursor must be mixed to SiH_4 . This led Zhao et al.[102] to study the effect of P and B, as common *n*- and *p*-type dopants, of the growth kinetics of the Si-shell. Growth times are found to change dramatically depending on the doping species: while diborane (B_2H_6) acts as a catalyst and enhances Si deposition rate by reducing SiH_4 decomposition energy, phosphine (PH_3) blocks surface sites of the Ge core and inhibits SiH_4 decomposition, yielding a lower growth rate of the Si-shell.

Although Ge-core/Si-shell NWs are more appealing for device applications, as discussed above, we note that Si-core/Ge-shell NWs present some specific additional challenges for what concerns the control of their morphology. The strain in thin film deposition of Ge on top Si promotes the nucleation of Ge islands due the well-known Stranski-Krastanow growth. This mechanism yields the formation of epitaxial 3D faceted Ge islands also on Si NWs.[103] Experimental evidence suggests that smooth and uniform coaxial Si-core/Ge-shell NWs can be obtained only for core diameters below a certain threshold,[87,103] as also predicted by theoretical modeling.[97]

All of the examples of growth techniques presented above clearly show that SiGe NWs can be produced in a controlled way following well established methods. They represent a real and concrete potential to replace traditional semiconductors used in microelectronics and to design innovative devices.[104] Their great advantage with respect to other nanomaterials is that they, in principle, offer the opportunity to be implemented on an existing semiconductor infrastructure and can hence benefit from continuous improvement in CMOS technology.[105] However, despite this great promise, this vision is still far to be realized because of some technological limitations that have to be overcome. As clearly pointed out by Thelander et al.[105] the main challenges that, not only SiGe one-dimensional systems, but nanowires in general have to face can be summarized as follows: (1) Contamination issues. The contamination of the wire with the metal catalyst deriving from the CVD growth should be reduced or completely suppressed. The presence of metal atoms in the wire can be responsible for an unavoidable modification of its electronic structure and, thus, of its technological performance. Several cleaning solutions should be developed and introduced in the fabrication process. (2) Device fabrication and variability. To develop a nanowire-based fabrication technology for transistors, several issues have to be still explored such as: (i) control of wire's dimensions and of the surface properties, (ii) control of the gate length and threshold voltage of the transistor in order to make up of dopants inefficiency at nanoscale, (iii) reduction of Schottky barrier at the interface between nanowires and metal contacts in order to improve transistor performances, and (iv) exploitation of new geometries, such as devices with a three-dimensional

nanowire-based channel[104,106] (in which the gate electrode is wrapped around the channel) to obtain larger electron mobility.

3. CHEMICAL AND PHYSICAL PROPERTIES

Recent years have witnessed an enormous progress in the methods of synthesis of SiGe nanowires, making them very attractive for their high mobility and band gap engineering, in the field of photovoltaics, nanoelectronics, optoelectronics and nanomedicine. Nevertheless, their use in real device applications is still limited due to the extreme difficulty in the control of the different growth parameters, as we discussed in section 2, and in the understanding of their relation with the desired structural, electronic, transport, and optical properties. For this reason a large part of the works that we are reviewing in this section aims at clarifying which is the relation between growth parameters, shape, homogeneity, crystallinity of SiGe nanowires, and their chemical and physical properties.

The chemical and physical properties of pure Si and Ge nanowires have been extensively reviewed elsewhere, covering growth techniques, experimental measurements, and theoretical calculations.[3,34−38] In this section we focus on the distinctive properties of SiGe nanowires that derive directly from the mixture of these two elements, both in the form of random alloys and axial or radial interfaces.

3.1. Electronic Properties

Silicon has been the material of choice for semiconductor devices in the latest decades and, although periodically other materials are proposed, it remains the undisputed king of the electronic realm. Sometimes, however, we would like silicon to have just slightly different properties. A simple route to this fine-tuning is adding some amount of germanium to the recipe, creating alloy or more complex interfaces. While this can also be pursued with bulk materials, nanowires offer much more flexibility to achieve such modulation of the electronic properties. Defect-free Si/Ge interfaces and alloys with a fully tunable composition are feasible from the morphological viewpoint and can be synthesized, while this is not always the case with their bulk counterparts.

Indeed, we will review many experimental reports showing that, unlike the corresponding pure Si and pure Ge nanowires, SiGe nanowires do offer the possibility to modulate the electronic properties, not only changing the size but also varying the relative composition of silicon and germanium atoms or the geometry of the Si/Ge interfaces. These additional degrees of freedom can be exploited at growth time in order to tune the nanowire properties to a desired target and to give rise to a wide variety of rich physical and chemical behaviors. As we will see in the following, scanning electron microscopy (SEM), transmission electron microscopy (TEM), and Raman and energy-dispersive X-ray (EDX) spectroscopy are the privileged tools to characterize the crystalline structure and the local atomic composition of these wires.

3.1.1. Modulation of the Electronic Properties by Composition Control. Motivated by the long years of experience on SiGe bulk and thin-film alloys, the electronic, transport, and optical properties of one-dimensional $Si_{1-x}Ge_x$ alloy NWs have been first investigated with the idea to use them as possible active elements in electronic and optoelectronic devices. Indeed, several groups have demonstrated the kinetic control of the catalytic decomposition of the chemical precursors during chemical vapor synthesis, to grow single-crystalline random $Si_{1-x}Ge_x$ alloy nanowires, against the general tendency toward phase segregation of the corresponding bulk crystal (see section 2.1).

For several applications the band gap width plays a decisive role and the possibility of tuning it is extremely appealing. In single-species nanowires this goal can be pursued by driving the system into the quantum confinement regime, where the band gap scales inversely with the wire diameter. In SiGe NWs, however, the same objective can also be accomplished by controlling the composition, a task that is in principle easier and that does not require sub-20 nm wires. Remarkably, Yang et al.[51] demonstrated the possibility to tune the gap by intrinsic alloy and extrinsic size effects. They clearly reported an optical band gap modulation in single crystalline CVD grown $Si_{1-x}Ge_x$ NWs with a variation of the absorption edge from the visible to infrared range (1.1−0.65 eV), varying the Ge composition x from 0 to 1. This work is of particular interest for Si-based opto-electronics and photonics. Their TEM analysis reveals the nanowires crystallinity and that they grew mainly along the ⟨110⟩ direction but shows a variation of the growth direction for wires of different diameter. The Si:Ge composition has been obtained by EDX spectra; no evidence of strong phase inhomogeneity is observed, confirming the possibility of forming random substitutional alloy $Si_{1-x}Ge_x$ nanowires, differently from thin-film where the tendency to segregate is observed. The optical gap modulation is illustrated in Figure 5,

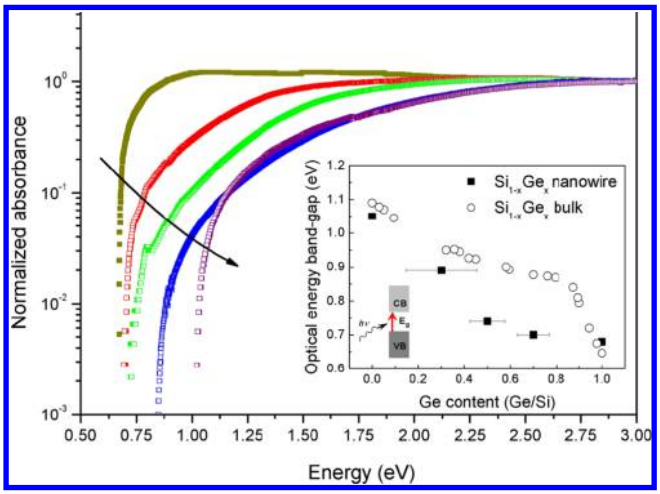

Figure 5. Optical absorption spectra measured in ref 51 near the energy-gap at 300 K for five $Si_{1-x}Ge_x$ nanowires (with mean diameters greater than 40 nm) with x = 1, 0.7, 0.5, 0.3, and 0. For qualitative comparison the absorbance is normalized with the values at 3 eV in each sample. The inset shows the variation with Ge concentration of the optical band-edges in NWs and in the corresponding bulk crystals. Reprinted with permission from ref 51. Copyright 2006 American Chemical Society.

where the absorption spectra of $Si_{1-x}Ge_x$ nanowires with x = 0, 0.3, 0.5, 0.7, and 1 and average diameters larger than 40 nm are reported. The inset of this figure clearly shows that, similarly to bulk SiGe alloy, the optical gap decreases increasing the Ge concentration but that the NWs gaps are smaller. Notably, in the same work the authors report a visible blue shift of the optical onset in pure Si and Ge nanowires decreasing the diameter near the respective exciton Bohr radii. This envisages the possibility to use this size effect to further modulate the optical properties of SiGe NWs.

Lu et al.[57] carried out a detailed study of the Raman scattering from larger diameter crystalline $Si_{1-x}Ge_x$ nanowires

dx.doi.org/10.1021/cr400261y | Chem. Rev. 2014, 114, 1371−1412

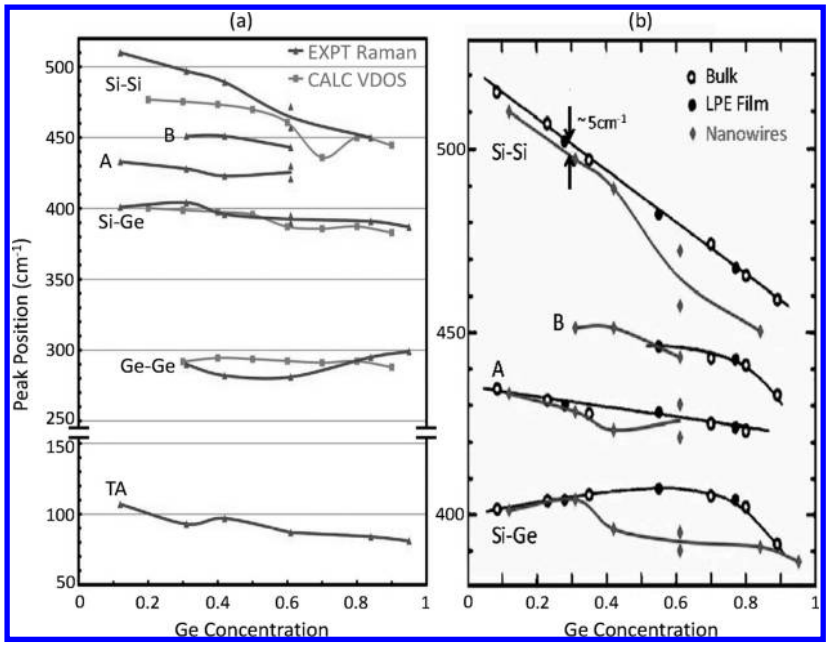

Figure 6. (a) Comparison of experimental Raman peaks of $Si_{1-x}Ge_x$ NWs as measured in ref 57 and the vibrational density of states (VDOS) band maxima calculated in ref 107 for nanoparticles. (b) Comparison of experimental Raman peaks of $Si_{1-x}Ge_x$ NWs with bulk and liquid-phase epitaxy film. Reprinted with permission from ref 57. Copyright 2008 American Chemical Society.

(80−100 nm) grown along the ⟨111⟩ direction. Varying x from 0 to 1 these authors showed that the intensity and the position of the three bands strongly depend on the composition and that the Si−Si band position is the most sensitive to the Ge concentration and rapidly down shifts with increasing x (this can then be used to estimate the Ge concentration in the nanowire). Additionally, another broad band around 75−110 cm^{-1} has been observed in this work and identified as due to transverse acoustic modes. The dependence of these four peaks positions and of other two shoulders (A,B in the figure) with Ge concentration is shown in Figure 6a. Remarkably, all of the measured data reasonably agree with the calculated vibrational density of states of $Si_{1-x}Ge_x$ nanoclusters,[107] suggesting that the Raman matrix elements are slightly dependent from the frequency. Only for the Ge−Ge mode an opposite behavior is observed, but a clear explanation is still lacking. A comparison with bulk and liquid-phase epitaxy (LPE) films Raman spectra is also provided (see panel b of the same figure). It indicates that the biggest discrepancy with respect to bulk and LPE counterparts, occurs for the Si−Si mode which has a much larger softening with increasing the Ge concentration, with a linear behavior up to 0.5.

Similar Raman and electron microscopy studies have also been used to address the effective uniformity in the Ge distribution along the radial direction. Kawashima et al.[108] found that in $Si_{1-x}Ge_x$ alloy nanowires, grown by Au-catalyzed CVD, the oxidation process induces a segregation of Ge atoms toward the external SiO_2 shell, resulting in a large inhomogeneity of the Ge radial composition. They showed that in order to minimize this inhomogeneity, SiGe nanowires should be oxidized at a lower rate and keeping the Ge diffusion rate high. By a detailed analysis of the Raman spectra, Nishimura et al.[109] went further and showed that $Si_{1-x}Ge_x$ nanowires, beside a not uniform Ge axial distribution, can even have a core−shell structure with a low-Ge composition core grown by the VLS process covered with a high-Ge composition shell grown by conformal deposition. Indeed they observed that the Si−Si mode is split in two peaks whose intensity and position vary along the NW axis. As seen in Figure 7b, both frequencies of the Si−Si low (due to high Ge-concentration region) and high-energy (due to low Ge-concentration region) mode decrease as a function of the distance from the catalyst, while their intensity ratio increases (Figure 7a). These results

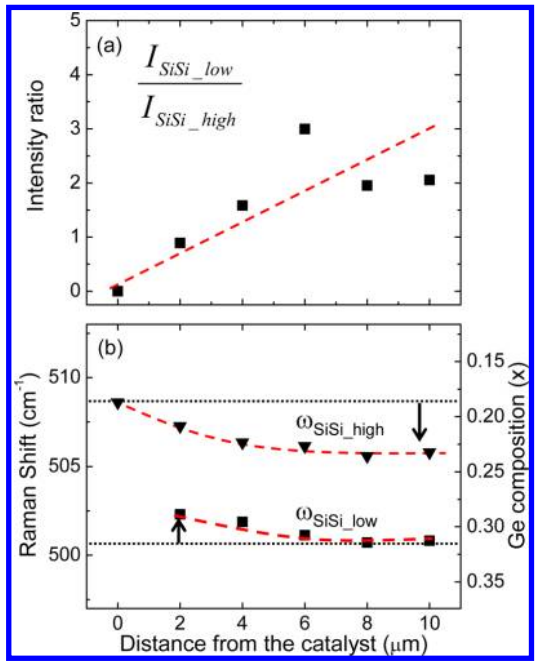

Figure 7. Low- and high-wavenumber Si−Si modes as a function of distance from the catalyst: (a) intensity ratio and (b) Raman shift. The dashed curves are guides to the eyes. The horizontal dotted lines in panel b indicate the wavenumber of the low-wavenumber mode at the catalyst side and that of the high-wavenumber mode at 10 μm. Reprinted with permission from ref 109. Copyright 2002 American Institute of Physics.

dx.doi.org/10.1021/cr400261y | *Chem. Rev.* 2014, 114, 1371−1412

combined with the slightly conical shape of $Si_{1-x}Ge_x$ NWs indicate a low-Ge concentration in the core region.

The experimental demonstration of the manipulability of the energy gap by controlling the alloy composition opened the way to even more sophisticated approaches to band gap engineering. Not only the composition of Si and Ge can be tuned, but it can also be varied in a controlled way during the growth and thus along the wire axis. $Si_{1-x}Ge_x$ NWs where x varies continuously from 0 to 1, turning gradually an all-Si into an all-Ge NW, have been reported. This in principle gives a wire whose band gap varies from E_{gap}^{si} = 1.1 eV at one end to E_{gap}^{Ge} = 0.75 eV to the other (or the corresponding quantum confined larger values).

A representative example of the current capabilities of controlling and characterizing the axially graded heteropitaxy of crystalline $Si_{1-x}Ge_x$ NWs can be found in the work of Yang et al.,[110] where wires of 20−30 nm diameter are synthesized by Au catalyst-assisted CVD approach. Their TEM images show that nanowires grew mostly along the ⟨110⟩ direction and that a continuously graded heteroepitaxy of Si and Ge occurs, not easily achievable in the corresponding thin film heteroepitaxy, although with some degree of residual strain. The reported Raman spectra do not manifest quantum confinement effects and show a strong similarity to those measured in bulk $Si_{1-x}Ge_x$ alloys suggesting a small amount of strain in these one-dimensional nanostructures. Three main phonon vibration modes associated with Si−Si (500 cm^{-1}), Ge−Ge (270 cm^{-1}), and Si−Ge (400 cm^{-1}) bonds are measured in two different regions of the wire, called A and B (see Figure 8a), as shown in Figure 8e, in good agreement with the results of Lu et al.[57] discussed earlier. Consistent with previous observations in bulk $Si_{1-x}Ge_x$ alloys and nanospheres, the frequency of the ν_{Si-Si} mode red-shifts with increasing the local Ge concentration. Different from bulk alloys, a remarkable optical anisotropy has been observed: the Raman intensity is almost double for light excitation polarized along the wire axis and also Raman scattered radiation results mainly polarized along this direction, as shown in Figure 8h. The large compositional changes along the nanowire axis were used by Dayeh et al.[111] to tailor charge transport and to engineer a device able to outperform the single-species counterparts (see section 5.1.1 below).

The ultimate demonstration of the properties modulation of an alloy nanowire along its axis was reported by Kim et al.[112] They investigated the carrier dynamics in axially graded $Si_{1-x}Ge_x$ NWs by scanning photocurrent imaging, showing that the dark conductivity, the photoconductivity and also the photoconductive gain can be modulated by varying the Ge content, opening new perspectives for the heteroepitaxial integration of broadband Si nanophotonic components. The measured photocurrent intensity progressively diminished from one end of the nanowire to the other, as the Ge content is gradually diluted. From the measurement of the dark current/voltage characteristics, the mobility of several $Si_{1-x}Ge_x$ NW segments is extracted resulting particularly enhanced in the Ge-rich regions. Furthermore, the effective internal gain, defined as the ratio between the number of collected carriers and the absorbed photons per unit time $G_{eff} = (I_{ph}/e)/(\eta P_{eff}/h\nu)$, results higher at lower absorbed power density P_{eff} in the Ge-rich nanowires, as shown in Figure 9a. In this way increasing values of saturation power densities can be extracted and this suggests that the surface-state density is progressively higher with increasing Ge content (see Figure 9b).

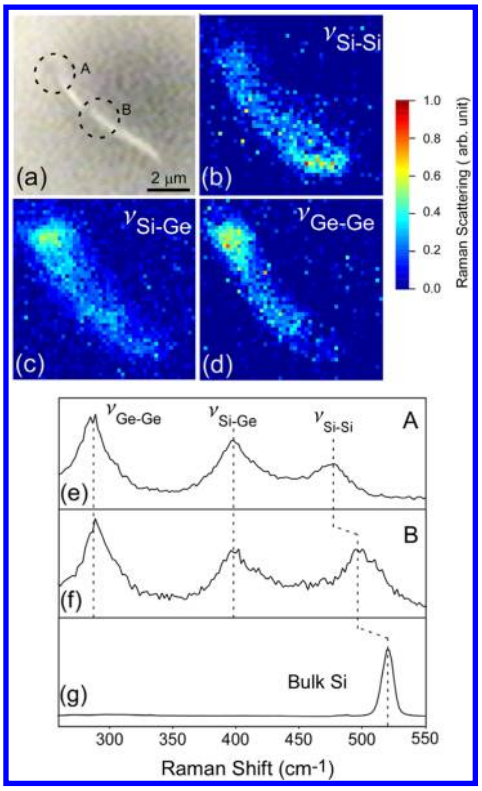

Figure 8. Typical Raman peaks and band assignment as obtained in ref 110 at two different points [called A and B, panel a] of a $Si_{1-x}Ge_x$ nanowire [panels e and f], and for bulk silicon [panel g]; Panel h shows the Raman intensities plot of the three main peaks as a function of detection polarization for parallel and perpendicular polarization excitation. Panels b−d are the confocal Raman images obtained by integrating the Si−Si, Si−Ge, and Ge−Ge Raman modes, respectively. Adapted and reprinted with permission from ref 110. Copyright 2008 American Institute of Physics.

Beyond pure $Si_{1-x}Ge_x$ alloy nanowires, $Si_{1-x}Ge_x$ oxide nanowires have been also synthesized and in particular their optical properties have been investigated.[113] Indeed nanostructured oxides are of particular interest to build functional devices for opto-electronic applications. Due to the presence of anion vacancies and cations with mixed valence states the electronic, optical and magnetic properties can be tuned. The authors of ref 113 show that $Si_{1-x}Ge_x$ oxide NWs of a certain diameter have a blue-shifted room temperature photoluminescence (415 nm, 2.97 eV) with respect to Si oxide NWs (470 nm, 2.63 eV) of a similar diameter and could be used for higher-frequency optical devices. Similarly to Si-oxide nanowires, this strong light emission has been attributed to the presence of oxygen vacancies, which are revealed by X-ray photoelectron spectroscopy (XPS) measurements.

3.1.2. Interfaces at Work: Strain, Band-Offset, and Carrier Gases. As we have seen in section 2, beyond SiGe alloy nanowires, it is possible to grow SiGe NW heterojunctions with axial or radial core−shell heterointerfaces. Rather than from composition, as in alloy NWs, the rich physics of these systems stems from the nature of the interface, namely the strain of the mismatched lattice and the band-offset of the two materials.

Any attempt of heteroepitaxy involving bulk Si and Ge irremediably ends up with the formation of dislocations that develops as a direct consequence of the strain induced by the 4% lattice mismatch. Actually, this strain can have an important

dx.doi.org/10.1021/cr400261y | Chem. Rev. 2014, 114, 1371−1412

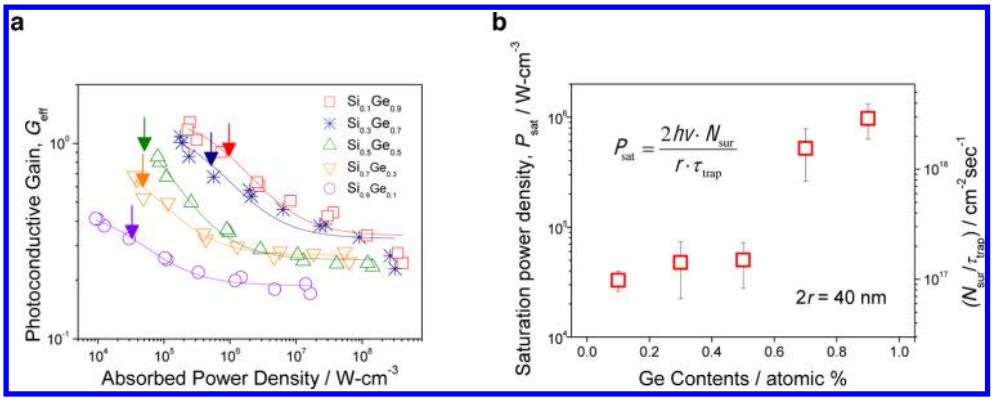

Figure 9. (a) Internal photoconductive gain as a function of absorbed power density. Arrows indicate the saturation power density of each $Si_{1-x}Ge_x$ NW segment and solid lines are phenomenological fits. (b) Powerdensity (P_{sat}) and the extracted density of surface states per capture lifetime as function of Ge concentration. Reprinted with permission from ref 112. Copyright 2011 Wiley-VCH Verlag GmbH & Co. KGaA, Weinheim.

role and is the driving force of the well-known but nontrivial Stranski-Krastanow method that leads to the nucleation of Ge quantum dots on Si. Nevertheless, in axial Si/Ge NWs, the strain induced by the lattice mismatch is partially relieved at the interface by lateral displacement of atoms, and the resulting defect-free interfaces can be exploited in the engineering of efficient nanodevices. These effects were quantified with meticulous photoluminescence (PL) measurements by Chang et al.,[114] who characterized the Si/Ge heterojunctions of a crystalline, dislocation-free nanowire. Three main peaks at 0.96, 1.02, and 1.08 eV were detected and could be attributed to the radiative transitions within the Si/Ge NW heterojunctions. The higher energy peak was 20 meV red-shifted and strongly broadened compared to the *c*-Si PL spectrum indicating significant strain in the wires, confirmed also by Raman spectra analysis (see ref 115 for a theoretical study of strain effects on core−shell nanowires). While the peaks at 0.96 and 1.08 eV did not change their positions with temperature and excitation energy, the peak at 1.02 eV had a non-monotonic behavior. From this analysis the authors concluded that the strain in Si/Ge NW was induced not only by the lattice mismatch but also by the difference in Si and Ge thermal expansion. These measurements conclusively showed that strain at the Si/Ge junction exists, but does not prevent the growth of dislocation-free interfaces, overcoming the traditional limitation of 2D lattice-mismatched interfaces. Accordingly to what one expects on the basis of the reservoir effect described above, the existence of an alloy transition layer with preferential chemical composition, $x = 0.15-0.2$ close to the Si NW part and $x = 0.5$ close to the Ge NW part, was also revealed.

The present strong interest toward devices based on core/shell SiGe nanowires started after the first observation of hole gas accumulation by Lu et al.[100] in 2005. Following the approach described in ref 87, these authors reported the growth of undoped core/shell nanowires with sharp Ge/Si interface and without dislocations and discussed their transport properties in top- and back-gated FET devices, prepared with lithographically patterned Ni source/drain electrodes. Their room temperature electrical transport measurements in a back-gated device 10-nm core diameter NW with S/D separation of 10 nm, clearly showed a *p*-type depletion mode behavior of the current I versus the source-drain applied voltage V_{SD}. This was explained in terms of hole accumulation in the Ge core, due to the type-II valence band offset between Ge and Si regions (see also ref 116 and the related discussion in section 4.1.5). Indeed, differently from pristine Si and Ge nanowires, a substantial current has been measured at zero gate voltage V_g in the Ge/Si core/shell NW and a clear current decrease is observed changing the gate voltage V_g from −10 to +10 V.

Furthermore Coulomb blockade oscillations have been observed in low temperature transport measurements for those Ge/Si core/shell devices, obtained without annealing at high temperature, which result to have a Si-shell region acting as a tunnel barrier. The differential conductance $G = dI/dV_{SD}$ plotted versus V_g and V_{SD} shows the typical diamonds structures, as expected for transport in single-electron transistors. The scaling of the gate capacitance C_g with the channel length L shows a linear behavior and the experimental data are well fitted by a cylinder-on-plane model with $C_g = (2\pi\varepsilon\varepsilon_0 L)/(\cosh^{-1}(h/r))$ (where h is oxide thickness, ε the dielectric constant, and r the radius of the Ge core), indicating that the barrier is formed at the contacts and that the number of scattering centers is not significant. Ballistic transport trough a 1D subband, due to the confinement of carriers in the radial direction, is further demonstrated by measuring a G versus V_g plateau close to $2e^2/\hbar$ at 4.7 K, which slightly decreases increasing the temperature. Corresponding measurements in top-gated devices, support transport by multiple subbands. Then it is possible to conclude that in these one-dimensional devices, in a different way from planar 2D hole gas devices, the phonon backscattering is strongly reduced and consequently the transport remains ballistic even at room temperature demonstrating that the mean free path exceeds the channel length of several hundred of nanometers.

In a more recent work Lauhon and collaborators[117] reported the direct detection of hole accumulation in Ge-core/Si-shell nanowires by the analysis of Raman spectra. The observed asymmetric line-shape of the Raman peak at around 300 cm^{-1} is well described by a Fano resonance of the F_{2g} phonon mode and the free holes accumulated in the Ge core region. Corresponding measurements in *i*-Ge nanowires rule out other mechanisms responsible for the asymmetric shape like confinement broadening, disorder or inhomogeneity broadening due to laser heating. Although the degree of asymmetry depends on the local hole concentration and the electromagnetic field enhancement, which result rather inhomogeneous, the NW volume contributing to the asymmetry has been estimated, resulting to be around 35% and, by numerical solving the Poisson equation, an average hole concentration of about 5.5×10^{19} cm^{-3} has been obtained. The calculated

dx.doi.org/10.1021/cr400261y | *Chem. Rev.* 2014, 114, 1371−1412

Raman enhancement relative to the bulk, well fits the experimental data. Moreover the observed Raman enhancement by increasing the excitation laser wavelength is again well explained by assuming the Fano origin of the broadening.

A further evidence of hole accumulation in ⟨110⟩-oriented Ge/Si core/shell NWs epitaxially grown on a Si(111) substrate was provided in ref 118 by high resolution electron microscopy (HREM), EDX spectroscopy, high-angle annular dark field (HAADF), and off-axis electron holography measurements (see Figure 10a). The overall width of the studied nanowire was

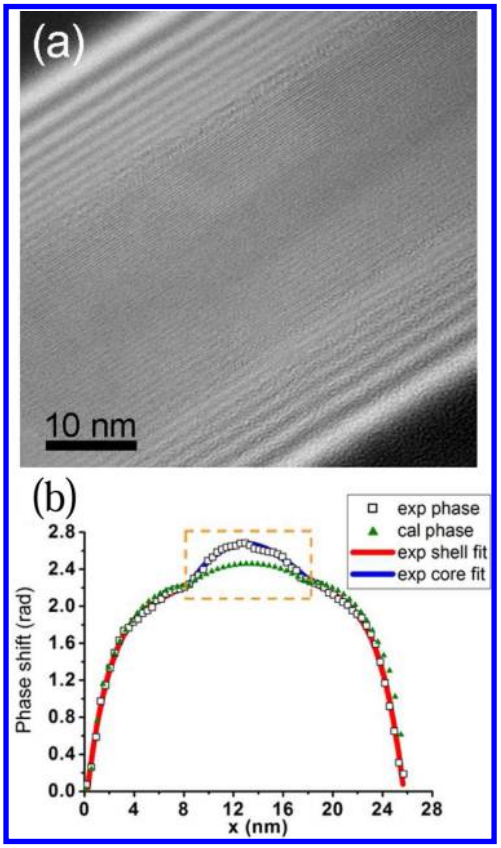

Figure 10. Electron hologram of the Ge-core/Si-shell NW as observed by HAADF measurements of ref 118 (top panel). Experimental and calculated phase-shifts extracted by HAAF data, together with core and shell region contributions, as fitted with polynomial (bottom panel). Adapted and reprinted with permission from ref 118. Copyright 2011 American Chemical Society.

estimated by HREM ad HAADF images to be about 26 nm, while that of the core region around 8.7 nm. Using the projected thickness along the electron beam direction, as extracted by HAADF data, the experimental phase shifts from the corresponding electron holography measurements were then extracted. A comparison with the calculated phase shifts obtained using a simplified coaxial cylindrical core/shell model was also done. The phase-shift was defined as $\phi(r) = C_E(V_{MIP}(r) + \Delta V(r))t(r)$ with C_E the interaction constant, $V_{MPI}(r)$ the mean inner electrostatic potential (considering a nanostructure this was taken to a larger value than in bulk), $\Delta V(r)$ the potential due to accumulation of positive or negative charges and $t(r)$ the projected thickness along the electron beam direction. The positive phase difference between the experimental and expected phase shifts, as shown in Figure 10b, suggests a possible accumulation of holes in the Ge core region. A value of about $0.4/nm^3$ hole accumulation in the core region is estimated, which is in reasonably good agreement with that obtained in ref 100 and extracted by the hole mobilities values measured in back-gate Ge NW transistors of ref 119.

The role of the shell composition on the holes confinement and transport, was instead investigated by the group of Tutuc[120] in Ge-core $Si_{1-x}Ge_x$-shell NW field-effect transistors (FETs) with highly doped source/drain (see panels a and b of Figure 11 which show respectively the energy band profile and

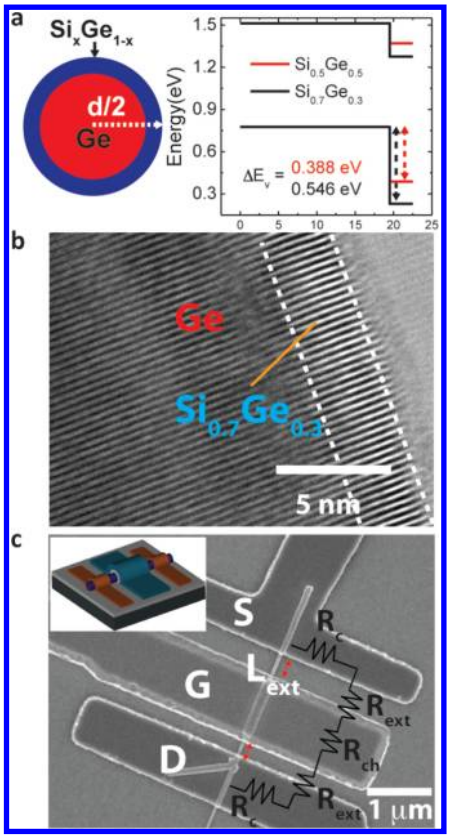

Figure 11. Energy band profile of the core−shell NW with different Si-shell content (a). TEM image of one of the studied NWs (b). SEM image of a representative FET NW (c). See text and the original reference for more details. Reprinted with permission from ref 120. Copyright 2012 American Chemical Society.

the TEM of the core−shell NW). A representative SEM image is shown in Figure 11c, where S,D and G indicate the source, drain, and gate regions; R_c and R_{ch} are the contact and channel resistance, while R_{ext} denotes the resistance of the ungated NW regions of highly doped source and drain. The electrical characteristics $I_d - V_d$ and $I_d - V_g$ have been measured by these authors at different temperatures from 300 to 77 K, in two $Si_{1-x}Ge_x$ nanowires with different diameter and shell composition (d = 45 nm, x = 0.5 and d = 37 nm, x = 0.7, respectively). From the analysis of these curves they extracted the effective hole mobility as $\mu_{eff} = L_g/R_{ch}C_{ox}|V_g - V_t|$ (see panel a of Figure 12), where L_g is the gate length, $C_{ox} = e(dp/dV_g)$ is the capacitance per unit length (p is the total hole density, V_g is the gate voltage) and V_t is the threshold voltage. The plots of μ_{eff} as function of $|V_g - V_t|$, at different temperatures and for the two nanowires, show that a peak at higher gate overdrive occurs for x = 0.7 indicating a larger band-offset at the interface. As shown in panels b and c of

dx.doi.org/10.1021/cr400261y | Chem. Rev. 2014, 114, 1371−1412

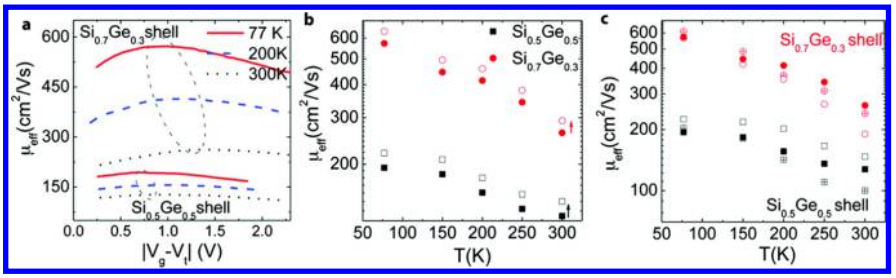

Figure 12. Hole mobility μ_{eff} of Ge/$Si_{0.7}Ge_{0.3}$ and Ge/$Si_{0.5}Ge_{0.5}$ core/shell NWs as function of gate overdrive (a). Peak μ_{eff} as function of T for two different gate lengths, panels b and c. Reprinted with permission from ref 120. Copyright 2012 American Chemical Society.

Figure 12, higher mobilities are obtained in NW FETs with higher Si-shell content at all temperatures and independently of the gate length. By comparison of the Raman spectra, in particular of the Ge−Ge mode, the same group[121] has shown how these core/shell nanowires (the $x = 0.5$ has been analyzed) contain a large amount of strain due to lattice mismatch at the core/shell interface, with respect to pure Ge nanowires. The measured blue-shift of this mode depends on the core and shell thickness and results in good agreement with a theoretical modelization based on a continuum elastic model.

3.1.3. Doped Nanowires. The operation of electronic devices is based on the interaction of adjacent regions of a semiconductor with different, tailor-made conductive properties. The way to design such regions is doping, the controlled addition of impurities able to tune the electronic properties of the host semiconductor. SiGe NWs are no exception and impurity doping is routinely used to modulate their physical and chemical properties to design functional devices.

B and P are the most common impurities used to *p*- and *n*-type dope SiGe NWs. Doping is normally carried out in situ, by the catalytic decomposition of B_2H_4 or PH_3 gas precursors that are mixed with silane and/or germane at growth time. Several groups have demonstrated the controlled coflow of the different precursor gases and the successful achievement of *n*- and *p*-type doping. Already in their pioneering work, Lieber and co-workers reported core−shell SiGe heterostructures in which composition and/or doping were modulated at the nanoscale.[87]

A few years later the doping of $Si_{1-x}Ge_x$ NWs and the electrical characterization of the related devices was reported. Kim et al.[122] first demonstrated the possibility to achieve appropriate *n*- and *p*-type FET transport curves in situ P-doped and B-doped $Si_{1-x}Ge_x$ nanowires, although the estimated mobilities were rather small due to a lack of optimization of the FET design. The device performances were greatly improved by Whang et al.,[123] who engineered a back-gated MOSFET based on phosphorus-doped $Si_{1-x}Ge_x$ nanowire (with diameter around 20 nm) integrated with atomic layer deposition (ALD) HfO_2 and TaN/Ta gate. Both undoped and phosphorus-doped $Si_{1-x}Ge_x$ NW MOSFETs exhibit a p-MOS operation, but higher current $I_{on} \simeq 100$ nA and $I_{on}/I_{off} \simeq 10^5$ are achieved from phosphorus-doped NWs, outlining the effectiveness of doping. The same group[124] explained this behavior with a reduction of the Schottky barrier height due to a thinner depletion width of the doped nanowire.

Micro Raman spectroscopy has been used to study the distribution of Ge composition and of the active acceptors in B-doped $Si_{1-x}Ge_x$ NWs.[125] Due to the Fano resonance caused by B-doping, the Si−Si peaks are much broader and their splitting is less pronounced and then the Ge concentration cannot be estimated from Raman peak wavenumbers. Nevertheless, as seen in Figure 13a, the Ge−Ge Raman peak intensity increases significantly with respect to that of the Si−Si mode moving

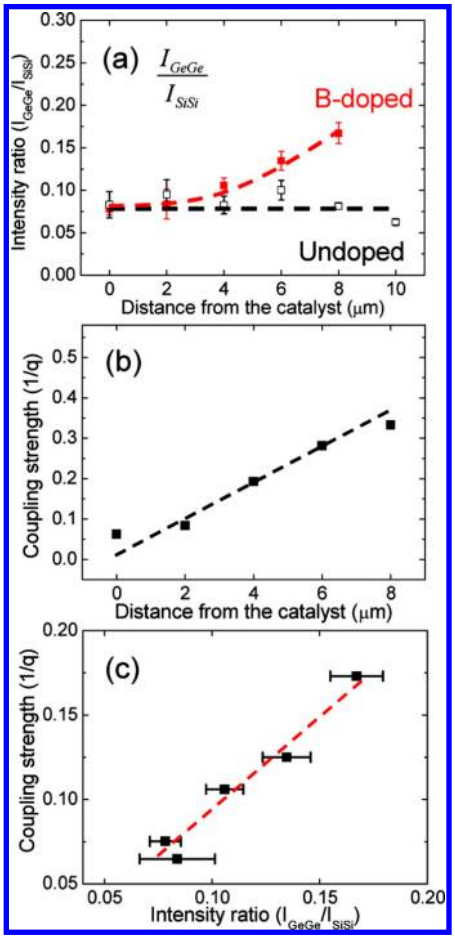

Figure 13. (a) Intensity ratio of Si−Si and Ge−Ge Raman modes as a function of distance from the catalyst. Data of undoped (empty boxes) B-doped (full boxes) SiGe NWs. Coupling strength $(1/q)$ as a function of distance from the catalyst (b) and of the intensity ratio of the Ge−Ge and Si−Si Raman modes (c). Reprinted with permission from ref 125. Copyright 2009 American Chemical Society.

from the catalyst side to the substrate side only in B-doped nanowires. This suggests that B doping not only accelerates the conformal deposition rate, but it also increases the Ge composition of the conformally deposited layer. The Fano resonance, whose asymmetry depends on the doping level, indicates that B atoms are electrical active and mainly located into the substitutional sites. Noticeably, also in the case of doped nanowires, a core−shell structure is revealed, with lower Ge composition in the core, like in nominally undoped

dx.doi.org/10.1021/cr400261y | Chem. Rev. 2014, 114, 1371−1412

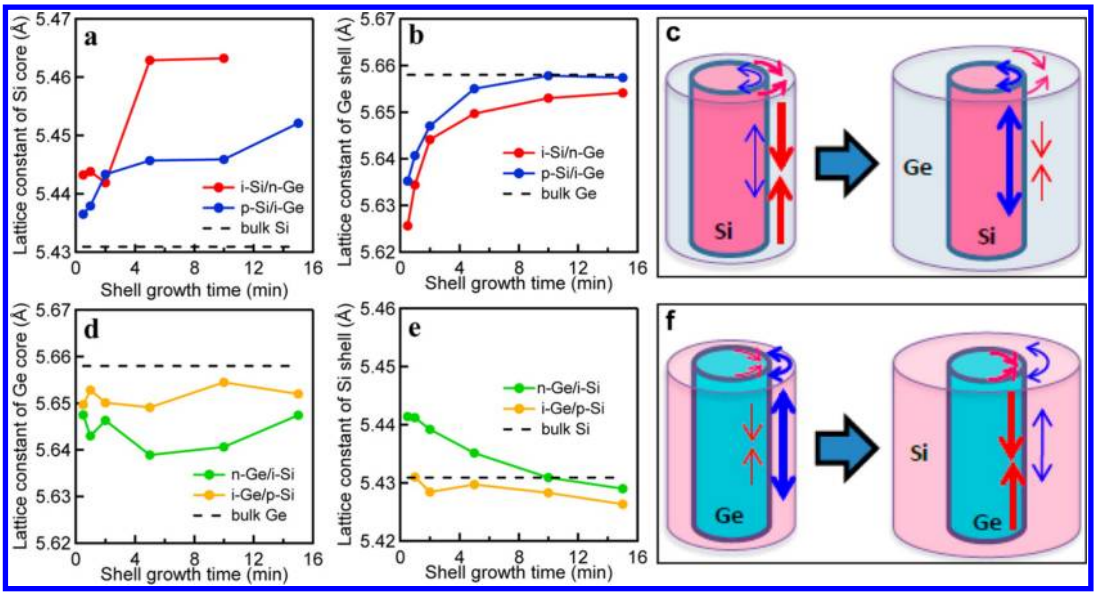

Figure 14. Lattice constant vs shell growth time of (a) the Si core in the *i*-Si/*n*-Ge and *p*-Si/*i*-Ge core−shell NWs, (b) the Ge shell in the *i*-Si/*n*-Ge and *p*-Si/*i*-Ge core−shell NWs, (d) the Ge core in the *n*-Ge/*i*-Si and *i*-Ge/*p*-Si core−shell NWs, and (e) the Si shell in the *n*-Ge/*i*-Si and *i*-Ge/*p*-Si core−shell NWs. Panels c and f illustrate the stress induced by the formation of Si/Ge and Ge/Si core−shell NWs respectively. Reprinted with permission from ref 126. Copyright 2012 American Chemical Society.

$Si_{1-x}Ge_x$ alloy NWs,[109] and with the heavily B-doped region corresponding to higher Ge concentration.

A clear interplay between growth parameters and doping in determining the chemical composition, morphology and electrical properties of $Si_{1-x}Ge_x$ NWs has been analyzed by Givan et al.,[65] as also previously described in section 2.1. Similarly to Si NWs, P-doping induces a reduction of the growth yield, while has a small influence on the growth rate, which is instead strongly increased by B-doping. P insertion increases the Si/Ge ratio with doping level, in comparison with the undoped NW grown under the same conditions; furthermore tapering is observed only in B-doped $Si_{1-x}Ge_x$ nanowires. The *I*/*V* curves of undoped and doped SiGe NWs in a back-gated FET configuration show that the resistivity of B-doped NWs is about 1 order of magnitude smaller than that of nominally undoped SiGe NWs which behave then as *p*-type semiconductors. The electrical transport curves of P-doped NWs show, instead, that they are *n*-type materials.

A systematic analysis of the stress and selective doping in Si/Ge and Ge/Si core/shell nanowires has been performed very recently by Fukata et al.[126] by means of Raman and X-ray diffraction measurements. They investigated four different cases of core−shell geometries, *i*-Si/*n*-Ge, *p*-Si/*i*-Gei, *n*-Ge/*i*-Si, and *i*-Ge/*p*-Si, giving an unprecedented demonstration of the selective doping of the core and shell regions of both Si-core/Ge-shell and Ge-core/Si-shell NWs by detecting the Fano broadening in the optical phonon modes and the presence of P and B local vibrational peaks. The selective doping of core−shell NWs is of paramount importance to improve the carrier mobility and their performances as FET devices. Due to the interface band offset, doped and carrier transport regions are separated, resulting in the suppression of impurity scattering and in improved free carriers mobility, as also corroborated by previous theoretical calculations.[116,127] On top of that, they showed how stress can indeed affect the transport masses and reduce the interband scattering thus playing an important role in improving the carrier mobility. From the X-ray diffraction (XRD) and micro-Raman spectra these authors were able to conclude that Ge (Si)-shell applies tensile (compressive) stress to the Si (Ge)-core, whereas Si (Ge)-core applies compressive (tensile) stress on the Ge (Si)-shell. This is well summarized in Figure 14.

Although in situ doping is by far the most common method for the controlled addition of impurities in SiGe NWs, some exceptions have been reported. Ex situ doping consists in incorporating the dopants into the nanowire at a second stage, after the growth process is over. Nah et al.[128] used low-energy ion implantation to *p*-type dope Ge-core $Si_{1-x}Ge_x$-shell nanowires with B. This approach was chosen in order to avoid some of the shortcomings of in situ doping: (i) at high-doses most of the impurities are incorporated through uncatalyzed conformal growth, so that the doping concentration is proportional to the exposure to the doping agent; (ii) achieving uniform doping concentrations or desired axial doping modulation is difficult. Ion implantation is more challenging in nanowires than in conventional planar devices, because if the implantation damage leads to full amorphization, recrystallization is not always possible. This poses an upper bound to the maximum implant energy and, consequently, to the doping dose. Nevertheless, they successfully obtained doping doses up to 2×10^{20} cm^{-3}, with the doping concentration controlled by the implant dose. Monasterio et al.[129] chose an even less common approach and doped their SiGe NWs by diffusion from a solid source in contact with the sample. They achieved *n*-type doping by incorporating P from a spin-on glass.

3.2. Thermal and Thermoelectric Properties

Due to the next future energy challenge, thermoelectric materials able to convert heat to electrical energy and vice versa are the object of increasing interest by researchers and industries. As we will see in the following, in the last years SiGe nanowires started to play a prominent role among the different systems under investigation to enhance the efficiencies and reduce the costs of the present thermoelectric devices.

dx.doi.org/10.1021/cr400261y | *Chem. Rev.* 2014, 114, 1371−1412

The dimensionless figure of merit $ZT = S^2\sigma T/\kappa$ defines the thermoelectric efficiency, where S is the Seebeck coefficient (which measures the magnitude of an induced thermoelectric voltage ΔV in response to a temperature difference ΔT across that material and is then defined as $S = -\Delta V/\Delta T$), T is the absolute temperature, σ and κ are respectively the electrical and thermal conductivity. The thermal conductivity is the sum of contribution arising from carriers κ_e and lattice thermal vibrations (phonons) κ_l. It is well established that to make thermoelectric devices competitive to other electricity sources it is important to obtain values of ZT of the order of 3−4 at room temperature. Good thermoelectric materials must have small κ to mantain high gradient temperature and at the same time large σ in order to maximize the number of carriers. Reaching this goal is rather than obvious because these quantities are strongly interconnected: indeed metals have both σ and κ_e very high and at the same time the high carrier concentration contributes to reduce S; on the other hand insulators have very high S and low κ but the electrical conductivity is too small to allow high values of ZT. The most efficient thermoelectric materials are, generally, heavily doped semiconductors and moreover superlattices and random alloys show the best performances with respect to pure crystalline materials.

Since 1950 thermoelectric devices based on bismuth tellurides and their solid solutions have been developed for commercial use, reaching $ZT \simeq 1$ at room temperature. Since these materials are rather rare and toxic, much effort has been dedicated to look for alternative semiconducting compounds with reduced costs and improved performances. In this regards, due to their good performances as high-temperature thermoelectric modules for deep-space missions, SiGe alloys received strong attention as possible alternative to tellurides compounds. In particular n-doped SiGe fine grained alloys showed a figure of merit around 1 at 900−950 °C, while for p-type SiGe alloys, used in space-flights runs, ZT remained of the order of 0.5.[130−132] Furthermore, a relatively small thermal conductivity, which is a desired prerequisite for thermoelectric elements, has been measured in $Si_xGe_{1-x}/Si_yGe_{1-y}$ 2D superlattices.[133] Three phonon scattering mechanisms control the heat transport in these superlattices: alloy scattering, interface scattering due to mismatch in acoustic impedance and scattering by defects and dislocations at the interfaces created by the lattice mismatch. While the first mechanism dominates when $|x - y|$ is small, the second process starts to play a role when $|x - y| > 0.3$. Scattering due to dislocations and defects created by large lattice mismatch is instead very important for $|x - y| > 0.6$ but in this regime, although very small κ are measured, their behavior is hardly predictable. Indeed in ref 133 Si/SiGe superlattices with period ranging from 45 to 300 Å show a reduction of κ decreasing the period thickness, while with period of the order of 45 Å, κ approaches the alloy limit. These results indicate that the role of interface in affecting the thermal conductivity is important in Si/Ge alloy superlattices. Instead, in SiGe/SiGe superlattices with period ranging from 100 to 200 Å, no dependence from period thickness is observed. This suggests that in this case the alloy scattering mechanism dominates.

As envisaged by several authors, a promising strategy to greatly enhance ZT is to scale down the material size, taking advantage of confinement effects: these should increase S and σ which depend on the density of states (DOS) and its energy derivative near the Fermi energy and at the same time reduce the thermal conductivity κ, due to an increased phonons scattering rate. In this regard, silicon nanowires[134,135] manifest promising thermoelectric properties, having a thermal conductivity 100 times smaller than bulk silicon which is a very poor thermoelectric material. Then, in the last years, many researchers have focused on SiGe nanowires with the idea to use the advantages of alloy and quantum confinement effects.

This interest has been also motivated by the fact that in nanostructured SiGe alloys an enhanced thermoelectric figure of merit has been measured. For instance Wang et al.[136] reported a value of $ZT = 1.3$ at 900 °C in nanostructured bulk SiGe n-doped alloys with the size of nanocrystallites of the order of 10−20 nm, as measured by TEM images. The origin of the observed improvement of ZT was mainly attributed to the enhanced phonon scattering at the nanograins boundaries which strongly reduces the thermal conductivity without affecting too much the electrical conductivity. This due to the large difference in the mean free path between electrons (5 nm) and phonons (200−300 nm). In the same period Joshi et al.[137] obtained a value of $ZT \simeq 0.95$ at similar temperature, in p-doped alloyed SiGe polycrystalline grains of size ranging from 5 to 50 nm prepared by a dc hot press method. Also in this case the thermal conductivity reduction, due to the increased phonon scattering from the high density nanograin interfaces in the nanocomposite is the main motivation of ZT enhancement.

It is important to point out that in these experiments, like in the great majority of those on nanowires, the main task was to reduce the thermal conductivity. Indeed nanostructuring, done at scales of the order of some tens to few hundreds of nanometers affects much more the thermal than the electrical conductivity, because electrons have much smaller mean free paths then phonons at room temperature. The small thermal conductivities measured in $Si_{1-x}Ge_x$ NWs are then generally explained by the increased phonon scattering due to alloying and surface boundaries: while phonon boundary scattering is frequency independent and mainly affects long-wavelength phonons, alloy scattering is frequency dependent and mainly affects short-wavelength phonons.

Li et al.[138] have synthesized Si/SiGe (111) superlattice nanowires with d = 58 and 83 nm and Ge concentration from 5 to 10%, using a hybrid pulsed laser ablation/chemical vapor deposition method. Their TEM analysis shows high-crystallinity, absence of dislocations, and rather sharp interface. A reduction of thermal conductivity with respect to pure silicon nanowires of similar diameter and also with respect to 2D Si/SiGe superlattice films is observed, with values around 6 W m^{-1} K^{-1} at 300 K. Similarly to 2D superlattice films, a rapid increase of thermal conductivity is measured up to 20 K, while from 20 to 200 K, a slow temperature dependence is observed. Furthermore, κ slightly decreases as the nanowire diameter shrinks down. Finally, the interface scattering is not very significant in these samples because the acoustic impedance mismatch and the number of interfaces are small. From these results, it is possible to conclude that the alloy scattering mechanism in SiGe regions is the main sources of thermal conductivity reduction in these nanowires, while the boundary effects contribute to further decrease κ. The important role of alloying in the reduction of the thermal conductivity has been observed by other authors: Kim et al.[139] in a recent experiment showed that, consistent with the trend observed in bulk alloy,[140] the thermal conductivity of $Si_{1-x}Ge_x$ alloy NWs decreases with an increasing Ge concentration. At similar concentrations the value of thermal conductivities are smaller with respect to the bulk counterparts. Moreover, in agreement

dx.doi.org/10.1021/cr400261y | Chem. Rev. 2014, 114, 1371−1412

with ref 138, they observed that decreasing the NW diameter the thermal conductivity reduction is not as evident like in pure Si NWs. These results confirmed that alloys scattering mechanism is the dominant one in $Si_{1-x}Ge_x$ NWs alloys. More recently Yin et al.[141] studied the influence of Ge concentration, amorphous silicon oxide shell, diameter, and length on the thermal conductivity of SiGe alloy nanowires grown by the VLS method. The diameters ranged from around 32 to 96 nm, the Ge concentration from 9% to 63%, the oxide thickness from 0 to 18 nm and finally the wire length from 1.7 to 6.5 μm. A small influence of the oxide layer was observed and explained in terms of the shortened phonon characteristic lengths, due to the high Ge concentration present in the experimental samples. Similarly a small dependence from the NW length was observed. The thermal conductivities measured from 60 to 450 K were smaller than undoped,[130] *p*-doped[142] and nanostructured[143] bulk alloys and approached the minimum values (around 1−2 W m^{-1} K^{-1} at 300 K) when the nanowire had a diameter of the order of 40−60 nm and with Si:Ge ratios around the unit.

The carrier-phonon scattering of low-frequency modes has been individuated by Martinez et al.[144] as another source of reduction of the thermal conductivity in boron-doped SiGe alloy NWs, with measured values of the order of 1.1 W m^{-1} K^{-1} at 300 K, comparable to bulk silica, and $ZT \simeq 0.18$, more than a factor two smaller than single-crystal alloys. Using a thermoelectric platform produced by photolithography processes, as shown in Figure 15a, and a homemade nanomanipulator, they were able to measure electric and thermal conductivity on suspended wires of two different diameters (100 and 300 nm) and dopants concentration (1.2×10^{19}cm^3 and 3.8×10^{19}cm^3).

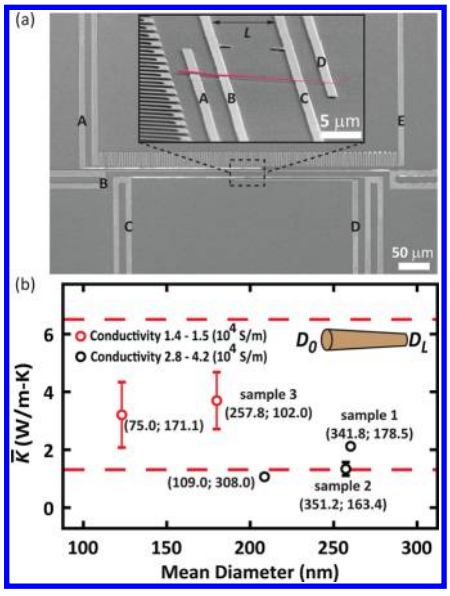

Figure 15. (a) SEM picture of the thermoelectric characterization platform from ref 144. Leads A, B, C, and D are used for 4-probe resistance measurements, and B and C are also used to measure temperature gradient across the nanowire when current is applied to the heater (lead E). (b) Mean thermal conductivity at 300 K for SiGe alloy nanowires versus mean diameter. Numbers in parentheses close to symbols are the diameters of each nanowires measured at lead B and C, respectively. The dashed lines are the thermal conductivities for bulk silica and doped single crystal $Si_{0.6}Ge_{0.4}$ alloy. Reprinted with permission from ref 144. Copyright 2011 American Institute of Physics.

Measurements at room temperature of electrical and thermal conductivity show the largest reduction of κ for the most heavily doped NWs, suggesting that, in addition to boundary and alloy scattering, the carrier-phonon scattering mechanism is present in doped SiGe nanowires. These results are illustrated in Figure 15b. Furthermore, the temperature dependence of κ confirms the role of hole-phonon scattering being a mechanism of increasing importance as T is reduced. Indeed in the most heavily doped samples a strong reduction of κ is observed below room temperature while in less doped nanowires a weak temperature dependence, characteristic of alloy scattering, is observed.

Stimulated by the unusually low thermal conductivity measured by Hochbaum et al.[134] in rough Si nanowires, the role of surface roughness has been also explored in VLS-grown $Si_{1-x}Ge_x$ nanowires with diameters around 200−300 nm.[145] Using this growth method, the authors were able to avoid the presence of nanoscale pores occurring in the case of rough electrolessly etched nanowires and to investigate only the effect of surface roughness. The thermal conductivity of rough $Si_{0.96}Ge_{0.04}$ nanowires is a factor of 4 times smaller than that of corresponding smooth nanowires and also 1 order of magnitude smaller than the bulk alloy, as shown in Figure 16.

Thanks to a new experimental apparatus able to measure thermal conductivities of the order of 0.1 nW m^{-1} K^{-1}, at least

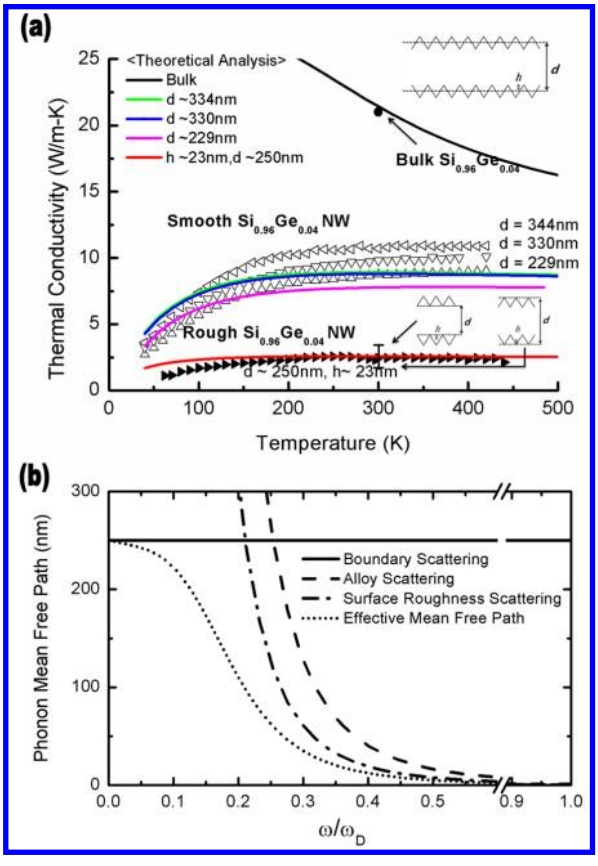

Figure 16. (a) Thermal conductivity of $Si_{0.96}Ge_{0.04}$ crystals in bulk, smooth nanowires, and rough nanowires. Dot and triangular are experimental data from literature; lines: Callaway model (see ref 145 for more details). (b) Phonon mean free path of various scattering mechanisms versus normalized phonon frequency. w_D is the Debye frequency. Reprinted with permission from ref 145. Copyright 2013 Springer-Verlag.

dx.doi.org/10.1021/cr400261y | *Chem. Rev.* 2014, 114, 1371−1412

1 order of magnitude smaller than the traditional measurement sensitivity, Wingert et al.[146] recently measured the thermal conductivity of VLS synthesized small crystalline Ge and Ge/Si core−shell NWs with diameters from 10 to 20 nm, showing that the phonon confinement starts to play a role beyond the diffusive scattering limit when the NW diameter is of the order of the phonon wavelength. Supported by several theoretical simulations,[147] the main reason for the reduction in the thermal conductivity of Ge/Si core/shell NWs was attributed to the altered vibration modes of the phonons that transport heat through the lattice. Indeed the wavelengths of the particles are shortened and compressed at the interface layer between the silicon and the germanium, and this blocks the heat transport to a very large degree. The improved measurement sensitivity was built upon a Wheatstone bridge circuit by employing an on-chip pair resistance for highly sensitive temperature and conductance measurements, able to resolve thermal conductance as low as 10 pW/K. As shown in Figure 17, the

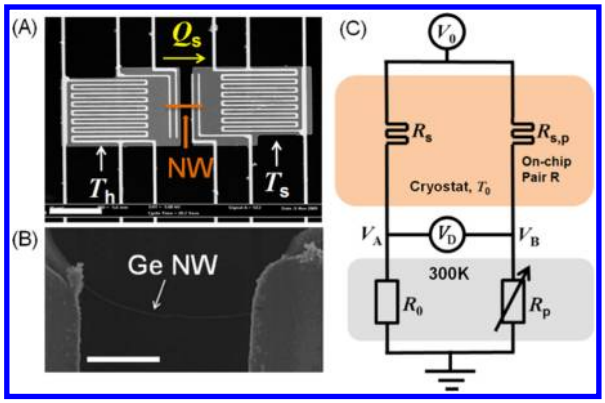

Figure 17. (a) SEM image of the microfabricated device used for single nanowire κ measurement. The device consists of two membranes bridged by a single NW. One of the membranes is heated up (ΔT_h), transferring a small amount of heat flux, Q_s, through the NW, which in turn raises the temperature of the sensing membrane (ΔT_s). Then the thermal conductance G is obtained as $Q_s/(T_h - T_s) = 0.5$. (b) SEM image of a 15 nm Ge NW on the suspended device. (c) The Wheatstone bridge setup for measuring the sensing resistance R_s (see ref 146 for more details). Reprinted with permission from ref 146. Copyright 2011 American Chemical Society.

device consists of two suspended membranes, each integrated with a serpentine Pt coil, serving both as the heaters and resistive thermometers. The measured thermal conductivity of Ge/Si core−shell NWs is of the order of 1−2 W m^{-1} K^{-1} at room temperature and it is rather independent from the temperature, as shown in Figure 18. When the thermal conductivity values of Ge/Si core−shell NWs are compared with those measured in pure Ge NWs, an increase below 220 K is observed while at room and higher temperature, a reduction of about 1 W m^{-1} K^{-1} is found. Furthermore at room temperature κ is lower than the corresponding bulk alloy[132] and also of that measured in larger diameter SiGe alloy nanowires.[139] As shown in the same figure the thermal conductivity in small diameter Ge nanowires shows a linear behavior with T. This trend cannot be explained by a diffusive scattering model,[148] but a quantum confinement effect of the phonon dispersion is invoked and a Boltzmann transport equation model built in this way well explains the experimental findings. The higher values of κ observed at low temperature in core/shell nanowires with respect to pure Ge nanowires can be

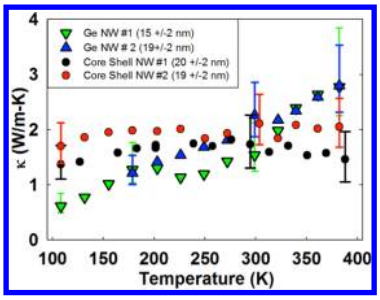

Figure 18. Measured thermal conductivity of pristine Ge NWs and Ge−Si core−shell NWs with diameters ranging from 15 to 20 nm (see ref 146 for the discussion about the error bars). Reprinted with permission from ref 146. Copyright 2011 American Chemical Society.

explained in terms of higher speed velocity sound induced by the Si shell. The opposite trend at high temperature is not clearly explained and could be attributed to the localization of low energy modes at the Si/Ge interface or to the presence of nonpropagating modes at the disordered surface.

As we have seen up to now, apart few examples, the most common strategy to improve the figure of merit ZT is to suppress the lattice component of the thermal conductivity by using the enhanced phonon scattering due to nanostructuring. Despite the theoretical predictions, the increase of the power factor $S^2\sigma$ in low-dimensional systems is more challenging to engineer, because the Seebeck coefficient S and the electrical conductivity σ are highly interdependent.

By simultaneously measuring the thermal conductivity, the electrical conductivity and the thermopower of several $\langle \bar{1}1\bar{1} \rangle$ oriented SiGe NWs with different diameter and Ge concentration (see Figures 19 and 20), Lee et al.[149] reported a large improvement in the figure of merit with respect to a reference bulk material and to Si nanowires. In Figure 19c a value of $ZT \simeq 0.46$ is reached at 450 K. From these measurements the authors concluded that the improvement of ZT was mainly due to the reduction of the thermal conductivity. Figure 20 reports the thermal conductivity as a function of temperature for several nanowires and shows that its reduction is mainly due to surface-boundary scattering for nanowires with diameter over ≃100 nm, while the alloying plays the most important role in suppressing phonon transport for smaller diameters. Differently from thermal conductivities, which show a strong dependence from the nanowire diameter and Ge concentration, the measured electrical conductivities, due to the short electron mean free paths, show a slight dependence as shown in Figure 19a.

In another very recent study Moon et al.[150] presented the first measure of the gate modulated thermoelectric power factor in single Ge/Si core−shell NWs with Ge core diameters ranging from 11 to 25 nm. Their data show that the Seebeck coefficient has a dependence on the carrier concentration similar to that of bulk Ge. This indicates that the quantum confinement effect is not significant for the investigated diameters. Figure 21 illustrates the dependence of the power factor versus carrier concentration, showing that, similar to bulk Ge, also for SiGe NWs there is an optimal carrier concentration for the peak power factor. Interestingly, the highest values are obtained in NWs with with the highest mobility. This suggests the promising possibility of exploiting the high carrier mobility of the hole gas in core−shell Si/Ge NWs for thermoelectric purposes.

dx.doi.org/10.1021/cr400261y | Chem. Rev. 2014, 114, 1371−1412

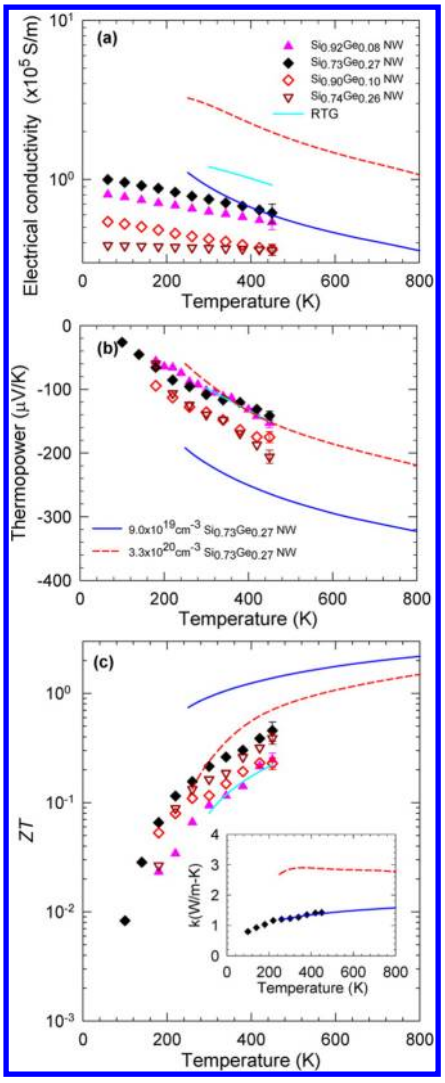

Figure 19. Electrical conductivity (a), thermopower (b), and figure of merit values (c) plotted as function of T for $Si_{0.92}Ge_{0.08}$ (filled pink up triangles), $Si_{0.90}Ge_{0.10}$ (red empty diamonds), $Si_{0.74}Ge_{0.26}$ (empty brown down triangles), and $Si_{0.73}Ge_{0.27}$ (black filled diamonds) with those of a bulk SiGe radio-isotope thermoelectric generator (RTG) as reference values (cyan line). The blue and red dashed curve are the calculated curves obtained with two different carrier densities: 0.9×10^{20} and 3.3×10^{20} cm^{-3}, respectively, for $Si_{0.73}Ge_{0.27}$. The thermal conductivity of one of the wires, as function of *T*, together with the calculated curves are reported in the inset of panel c. Reprinted with permission from ref 149. Copyright 2012 American Chemical Society.

4. THEORETICAL MODELING

In the previous sections we have seen how by bringing together two similar elements, Si and Ge, neighbors in the periodic table, a rich variety of new chemical and physical properties emerge, stimulating both fundamental and application-driven research in nanoscience.[90,92,100,151] SiGe NWs present unique structural, electronic, optical, and transport properties, which are intrinsically associated with their reduced dimensionality. As we have previously pointed out, their physical properties can be modulated not only varying the extrinsic parameters of the wire (like the size of the system or the addition of impurities) but also the intrinsic ones (such as the relative composition of Si and Ge atoms and the geometry of Si/Ge interface).[51] Substituting some of the atoms of a pure Si NW with Ge in random as well as ordered configurations of different

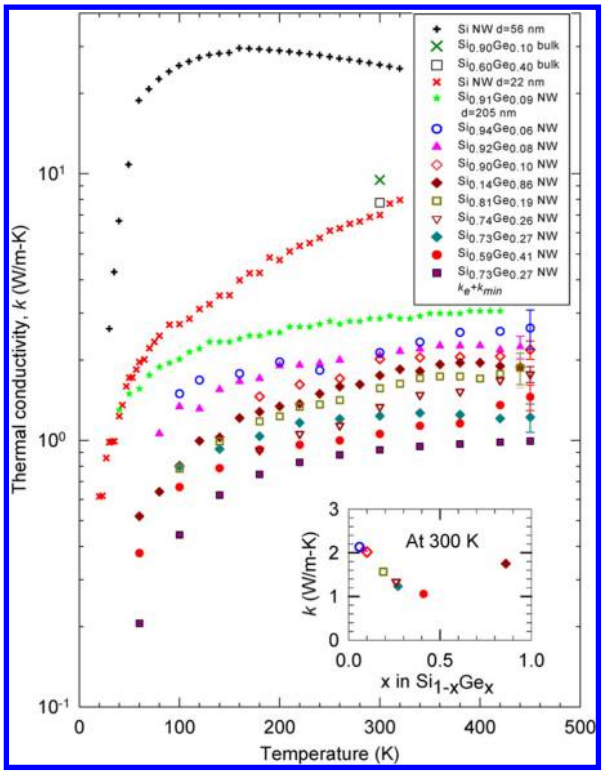

Figure 20. Thermal conductivities of several SiGe nanowires as measured in ref 149 compared with several corresponding values available from the literature for a Si nanowire, $Si_{0.9}Ge_{0.1}$ and $Si_{0.6}Ge_{0.4}$ bulk, a $Si_{0.91}Ge_{0.09}$ nanowire. The inset shows the thermal conductivities as function of Ge concentration at 300 K. Reprinted with permission from ref 149. Copyright 2012 American Chemical Society.

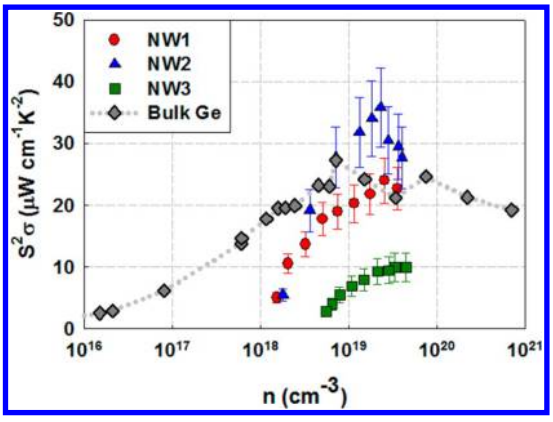

Figure 21. Power factor vs carrier concentration of Ge/Si NWs and bulk p-doped Ge. An optimal carrier concentration for the peak power factor both for nanowires and bulk germanium is visible. The highest values are obtained in nanowires with the highest mobility (NW2). Reprinted with permission from ref 150. Copyright 2013 American Chemical Society.

compositions, strongly affects some fundamental properties such as band gap, effective mass, phonon and electron scattering processes, and excitonic properties. For these reasons, SiGe nanosystems are the target of the most intriguing and exciting technological applications in the field of high performance nanoelectronics (such as FETs and interconnections), thermoelectrics, photovoltaics, superconductivity, and spintronics.

dx.doi.org/10.1021/cr400261y | *Chem. Rev.* 2014, 114, 1371−1412

Nevertheless, it is well-known that the investigation of matter at nanoscale, with experimental techniques, is often complicated by several factors not always well controlled. Moreover, since in these materials the thickness matches length scales of some fundamental quantum mechanical phenomena, their investigation requires clear and deep quantitative understanding of nanoscale phenomena. A significant uncertainty, very often, prevails in discerning the fundamental effect of size-dependent factors, such as quantum confinement, from other factors (shape, composition, local strain, interface states) that affect the main physical and chemical properties. In this context the role of theory, modeling and simulations in the description of SiGe NWs properties is indispensable to give a quantitative description of their unique properties. Today this possibility is becoming tangible, thanks to the recent advances in large-scale and high-performance computing which has made the materials modeling, in the broad sense of theory and simulation in integration with experiments, emerge as a field of research with unique capabilities. The main goal of this section is to review the last progresses in the fundamental understanding of the structural, electronic, optical, and transport properties of SiGe NWs. This will be done by focusing on the main role of theory and modeling in the characterization of these nanomaterials. The following paragraphs will mainly be focused on methods which do not use any empirical adjustable parameters and solve the electronic structure problem *ab initio*, i.e., from first-principles. Though sometimes other computational techniques (e.g., molecular dynamics or Boltzmann theory) have been adopted in the quantitative description of SiGe NWs, currently it is a widespread belief that *ab initio* simulations constitute the most modern and powerful instrument to model and design the properties of this kind of systems.

As it will be clear in the following, a general assessment of the capability of the present theoretical/computational approaches to predict on one side new chemico-physical properties of SiGe NWs and on the other hand to describe and explain the vast panorama of experimental data, cannot be easily given. Indeed most of the atomic models are simplified and the sizes that can be tackled are smaller than the SiGe NWs grown experimentally, whose real complexity (disorder, surface reconstruction, presence of impurities, etc.) cannot be easily taken into account in the simulations due to numerical/computational limits. Further development and implementation of the theoretical approaches, like i.e., the inclusion of many-body effects in the electronic, optical, and transport properties of these nanoscale materials, will improve the quantitative comparison with the experiments. Yet, even the simplified models of SiGe NWs—too small, too clean, too ideal—are often enough to capture the physics underlying an experimental observation or to suggest new directions to look into.

4.1. Electronic Structure

One of the reasons for the enormous scientific interest in confined systems, such as semiconductor nanowires, is the possibility to modify their electronic structure by simply changing their size, as a consequence of the so-called quantum confinement effect (QCE).[3] Indeed in these quasi-one-dimensional materials, the motions of electrons and holes are confined in the radial plane, while charge carriers are free to move along the nanowire's axis. This physical situation is qualitatively well described by quantum-mechanical approaches based on effective mass approximations and particle-in-a-box models:[152] the most simplified situation considers a particle free to move along the wire axis surrounded by impenetrable potential barriers. This confinement quantizes the kinetic energy of the particle, influencing its eigenstate energies as the quantum number n, the effective mass m^* and the width of the potential well d (clearly $d = 2R$, where R is the wire radius) are changed:

$$E_n = \frac{\hbar^2 n^2 \pi^2}{2m^* d^2} \quad (1)$$

In particular one can note that both energy levels and their spacing increase as the confinement is more pronounced (i.e., as d gets smaller). In the case of real systems, such as pure semiconductor nanowires, the confinement of electrons and holes leads to an increase in the electronic energy band gap with decreasing the nanowire diameter. Detailed *ab initio* and semiempirical analysis have shown that size dependence of band gap can be described by an inverse power law $E_g \approx 1/R^a$, where R is the wire radius and the parameter a is between 1 and 2.[153−158]

On the other hand, the idea of combining Si and Ge atoms in random as well as ordered configurations represents a well-established strategy to engineer electronic structure and energy band gap on the basis of the specific needs. In particular in the case of ordered configurations, it is well-known that creating a pseudomorphic junction between Si and Ge results in band discontinuities and creates a band-offset at the interface. Its origin is related to the difference in band-gaps of the two materials and to the consequent charge transfer and dipole induced.[159,160] The value of the offset determines the relative energies of the states in the two constituent materials, and as such controls the quantum well depths, degree of wave function confinement, and the very nature of the heterostructure (i.e., type-I, with holes and electrons confined in the same material, or type-II with confinement in different materials).[161,162] The band offset of Si/Ge systems, like superlattices or bulk heterojunctions, has been an intense object of study in the past.[161−165] These works demonstrated the type-II band-offset character, which means that the valence band maximum (VBM) and the conduction band minimum (CBM) of the system are located on different materials. In particular the VBM is always located on the Ge part, while the CBM is on the Si part, as reported by Van de Walle and Martin.[164,163] Usually, the presence of type-II offset is responsible for a reduction of the band gap of the pure component of the system revealing itself as a crucial tool for band gap engineering. Moreover, its magnitude can be strongly modified by playing with stress, geometry of the interface and composition of the system.

In general one can say that SiGe NWs constitute a prototype system in which both the approaches, size reduction and heterostructuring (or alloying), can be combined, further improving our ability to design and manipulate the electronic structure to satisfy specific demands. However, the physics governing these phenomena at nanoscale strongly changes with respect to bulk. Subject of the next section will be investigating how the QCE can be affected by the presence of a type-II band offset and how this interaction is governed by changing the geometry and composition of the system. Discussion will be mainly dedicated to the most common geometries from an experimental point of view, i.e., radial and axial heterojunctions. Nevertheless, analysis of other geometries and models, though not directly connected with experiments, will be also presented

in view of their relevant contribution to the basic physics governing the properties of these systems.

4.1.1. Quantum Confinement Effect and Band Offset. The physical origin of band offset is related to discontinuities occurring in the valence bands and in the conduction bands when two semiconductors are joined to form an heterojunction.[159,160] When Si and Ge (which have indirect bulk band gap around 1.1 and 0.75 eV, respectively) form an abrupt interface, their band structure line-up in order to accommodate their band gap differences. This process induces offsets both in conduction and valence bands (an example of valence band offsets is shown in Figure 22). Valence and conduction band

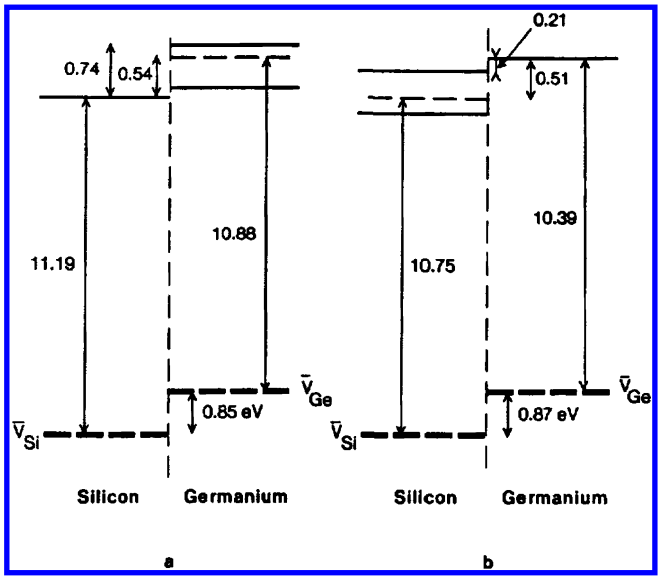

Figure 22. Calculated band-offsets of the Si/Ge interface. Left panel: $a_{\parallel}$ = 5.43 Å (cubic Si, strained Ge); right panel: $a_{\parallel}$ = 5.65 Å (cubic Ge, strained Si) $\bar{V}_{Si}$ and $\bar{V}_{Ge}$ are the average potentials for Si and Ge valence bands, while dashed lines are the weighted averages of band splitting due to strain. Reprinted with permission from ref 163. Copyright 1985 American Vacuum Society.

offsets (VBO and CBO) determine the ability of electrons and holes to pass from one side of the junction to the other one. Calculations of Van de Walle and Martin,[163,164] based on *ab initio* methods, predicted ΔE_v = 0.58 eV and ΔE_c = 0.28 eV for the unstrained junction, in good agreement with experiments. They also pointed out the central role of strain for the evaluation of the offset.

Trying to give a general rule for the determination of the band offset in SiGe NWs is rather hard, because most of the physics strongly depends on the specific geometry considered. However, it is possible to say that when one considers a Si/Ge interface at the nanoscale four main effects should be taken into account: (i) The QCE causes the band gap of Si and Ge zones of the wire to increase as the size of the nanowires is reduced.[166] Since the QCE is stronger in Ge than in Si,[167,168] for the same reduction of diameter, there will be a different effect of the shift of VBM and CBM and hence of the character of the band alignment (type-I or type-II). This fact can be also understood by noting that the exciton energy of Ge is larger than that of Si.[166] (ii) The same observation can be done when varying the composition of the wire (the relative number of Si and Ge atoms). Roughly speaking, changing the composition means also varying the size of Si or Ge zones into the wire at fixed diameter.[169] (iii) Because of the lattice mismatch between Si and Ge (of the order of 4%) the strain can have an influence on the band gap and on the offset. The nature of strain relaxation in nanoscale heterojunctions is quite different from that of bulk ones. In fact, as seen in the previous sections, the reduced dimensionality and small size of NWs allow them to tolerate a relatively large lattice mismatch and corresponding strain without introducing significant defects that could undermine the electrical properties of the material.[170] (iv) The possibility of building different geometry of SiGe interfaces (i.e., axial or radial) changes remarkably the nature of the confined states induces by the offset. Analyzing all these factors at once is quite complicated and most of the studies focus on the effect of the variation of the electronic structure changing a specific parameter (i.e., strain, size, geometry, or composition) and keeping constant the others.[156,169,171−182]

We will start our analysis by considering one of the most common atomic geometries considered at experimental level, that is the core−shell one. As discussed by Nduwimana et al.,[177] the band offset in radial heterojunctions generates an effective potential barrier for electrons and holes moving through the interface, which serves as an additional confinement potential. In their study they proposed a very general quantum mechanical model to study the effect of offsets in SiGe NWs. In particular, the above-mentioned particle-in-a-box-model successfully applied for pure NWs, can be still used by introducing a potential barrier Δ, as shown in the inset of Figure 23. Two configurations are presented, the central well

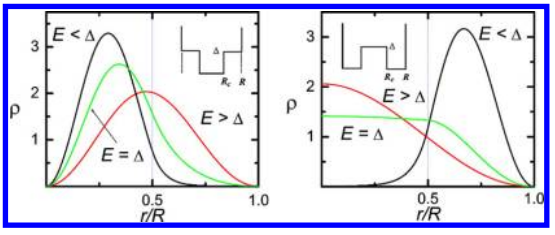

Figure 23. Radial charge distribution for the 1p state in the central well (left) and the 1s state in the central barrier (right) within an effective-mass model. This model involves three parameters: Δ, R_c, R which correspond to the potential barrier, the core radius, and the radius of the nanowire, respectively (see ref 177 for more details). The three curves reported here were obtained for R_c/R = 0.5 and $E = \Delta/5$ (black), $E = \Delta$ (green), and $E = 5\Delta$ (red), respectively. Reprinted with permission from ref 177. Copyright 2008 American Chemical Society.

configuration (left panel) and the central barrier one (right panel); as we will see, they correspond to the case of Si-core/Ge-shell and Ge-core/Si-shell, respectively. The electrons and the holes are confined in the radial plane (but now, because of the offset, they are additionally confined in Si or Ge part of the wire) while they are free to move along the NW axis. Eigenvalues and eigenstates of the system can be found by assuming cylindrical coordinates (r,ϕ,z), supposing the wave function in the form $\Phi(r,\phi,z) = \psi(r)\, e^{i(l\phi+kz)}$ and a radial equation:

$$\frac{\partial^2\psi}{\partial r^2} + \frac{1}{r}\frac{\partial\psi}{\partial r} + \left(\frac{2m^*}{\hbar^2}(E - V(r)) - \frac{l^2}{r^2}\right)\psi = 0 \qquad (2)$$

where m^* is the effective mass and l is the angular momentum, which is quantized. The analytical solution of the model, describes a set of parabolic sub-bands with corresponding values E_{nl} in the zone center. Two considerations can be easily

dx.doi.org/10.1021/cr400261y | Chem. Rev. 2014, 114, 1371−1412

derived: (i) in the case in which there is no barrier and no offset (as in pure Si or Ge NW), $\Delta = 0$ and all the states are unconfined, while (ii) in the case in which $\Delta = \infty$ all the charges are confined in a tube of width $R - R_c$ for the central barrier case of Figure 23 (this situation is still the case of pure Si and Ge NWs).

For general values of Δ, which is the case of core−shell NWs with different diameters and core−shell ratios (i.e., composition), by numerically solving eq 2, it is possible to define confined ($E < \Delta$) and unconfined ($E > \Delta$) states. The plot of two sample case (1p state with central well and 1s state with central barrier) are reported in Figure 23, where it can be seen that the offset localizes electrons in the shell zone in the case of central barrier, while it localizes electrons in the core region in the case of central well.

The validity of the analytical model proposed by Nduwimana et al.[177] has been confirmed by a lot of different *ab initio* calculations, based on density functional theory (DFT),[183,184] on hydrogen passivated core−shell NWs.[169,171−178,180,182] It is worth to note that *ab initio* methods are able to self-consistently account for charge transfer and hence they include automatically in the calculation the built-in electric field that develops at the interface.[183,184] The calculations showed that in core−shell NWs the offset has a type-II character with the VBM on the Ge part of the wire and the CBM on the Si one. Moreover, it has been pointed out that by changing the relative core−shell size and the component of the core or shell the magnitude of the offset can be tuned.

Usually *ab initio* pseudopotential calculations for SiGe superlattices or bulk heterojunctions enabled the band offset to be deduced from the average self-consistent potential.[163,164] The potentials become bulk-like at a short distance from the interface, allowing to align the average bulk potentials on a common energy scale. Band calculations for the bulk materials provided the relative positions of the individual band edges, and thus the actual valence offsets. In the case of core−shell wires, it is worth underlining that, due the very small size of the core and the shell regions (of the order of 1−2 nm), and to the rapidly oscillating nature of the potential, is very hard to define its average value. Therefore alternative methods have been proposed, most of the times using charge density based approaches (with the noticeable exception of Kagimura et al.,[156] who proposed the surface dangling bond energy level as common reference level to predict band offsets among Si, Ge and SiGe NWs). Recently though, Niquet and Delerue[185] demonstrated that the extrapolation of band-offset calculated in bulk interfaces to axial nanowires junctions leads to qualitatively wrong results. Their self-consistent tight-binding calculations showed that, in absence of a homogeneous shell, the band offset is strongly influenced by the nature of the surfaces and the usual picture of square wells and barriers borrowed from bulk materials does not hold.

Yang et al.[176] proposed a quantitative criterion for the band offset estimation of ⟨110⟩ Ge-core/Si-shell and Si-core/Ge-shell with diameters up to 4 nm. They performed DFT calculations in the Local Density Approximation (LDA) in order to investigate the spatial localization of the charge density into the wire. After examining the charge distribution for all the states, they adopted the following criteria for identifying the confined states: the total charge and the average charge density n are calculated both in core and shell regions. Then a state is assigned to be confined in the core if $n^{core} > 4n^{shell}$ and in the shell if $n^{shell} > 4n^{core}$, where n^{shell} (n^{core}) is the charge density localized in the core (shell) region. By applying this method they determine the energy range of confined states and the band offsets. Figure 24 reports the plot of the charge

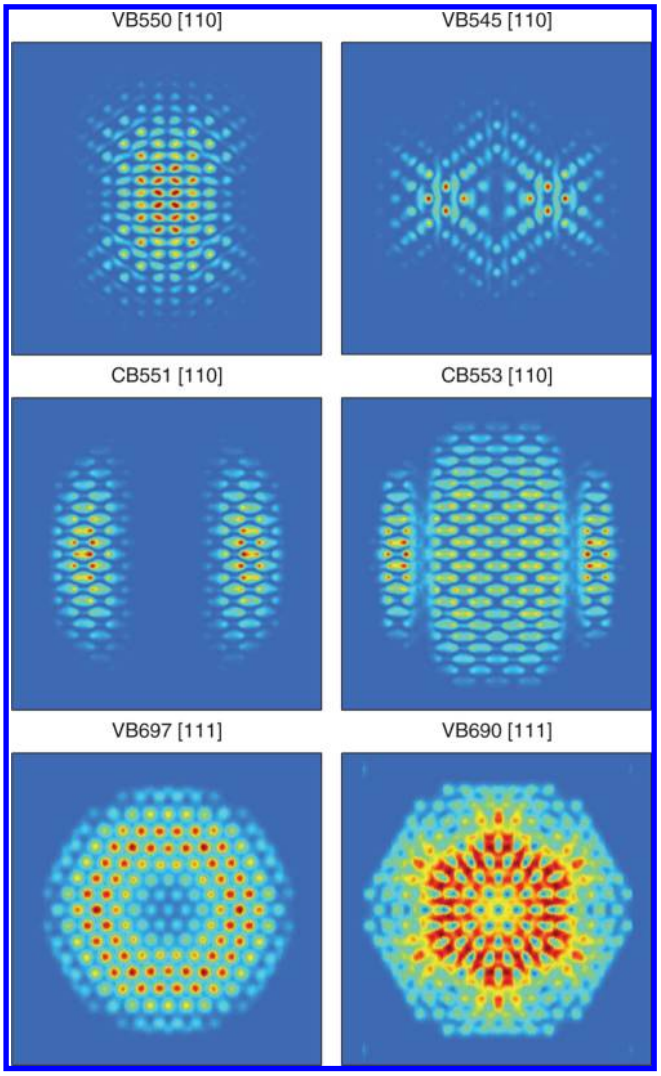

Figure 24. Plot of charge distributions in the cross sections of core−shell NWs. The picture shows four states for a ⟨110⟩ NW containing 62 germanium atoms in the core and 200 silicon atoms in the shell regions. Two states in the valence bands of a ⟨111⟩ NW containing 62 silicon atoms in the core and 264 germanium atoms in the shell region are also shown. Reprinted with permission from ref 176. Copyright 2008 American Physical Society.

distributions in the cross section of ⟨110⟩ wire with 62 Ge atoms in the core and 200 Si atoms in the shell and a ⟨111⟩ wire with 62 Si atoms in the core and 200 Ge atoms in the shell. Interestingly, the authors also reported the dependence of the offsets as a function of the ratio between the core radius R_c and the total radius R for ⟨110⟩ NWs, which defines the composition of the wire. Two conclusions can be drawn from their study: (i) Ge-core/Si-shell NWs have valence states with a significant confinement energy of 0.4 eV while the conduction states offset are 1 order of magnitude smaller. This magnitude for the offset can explain the use of this type of wires for device applications. (ii) The confinement energies, both for Si-core/Ge-shell and Ge-core/Si-shell slightly vary as the size of the core changes.

dx.doi.org/10.1021/cr400261y | *Chem. Rev.* 2014, 114, 1371−1412

Amato et al.,[116] adopting a semiquantitative criterion have given an estimation of the band offset for core−shell NWs with diameter up to 2.4 nm. They performed DFT calculations in the LDA approximation in order to analyze the real-space localization of the wave function. The criterion is quite similar to the one of Yang et al. In the case of VBO for Si-core/Ge-shell NW, one can first note that the VBM is located on Ge-shell of the wire; then all of the valence states at lower energies are plotted until the first one located on the Si-core appears. The difference between the DFT eigenvalues of the corresponding localized states is used to estimate the VBO. The same discussion can be done for CBO. They predict larger offset for both valence and conduction bands with respect to results of Yang et al.,[176] because of the different size of the considered wires and to the fact that at diameter less than 3 nm the QCE is very strong both for Si and Ge.

A qualitative criterion based on the analysis of wave function localization was also used by Liu et al.[178] for ⟨112⟩ Ge-core/Si-shell and Ge-core/Si-shell NWs. Their DFT results were a further confirmation that the type-II staggered band alignment is a general property of core−shell NWs which does not depend from the specific crystallographic orientation.

The general tendency of SiGe NWs to have a type-II offset has clearly been pointed out by Amato et al.[171,172] by considering different types of Si/Ge interfaces in nanowires. For all of the geometries presented in Figure 25 they plotted

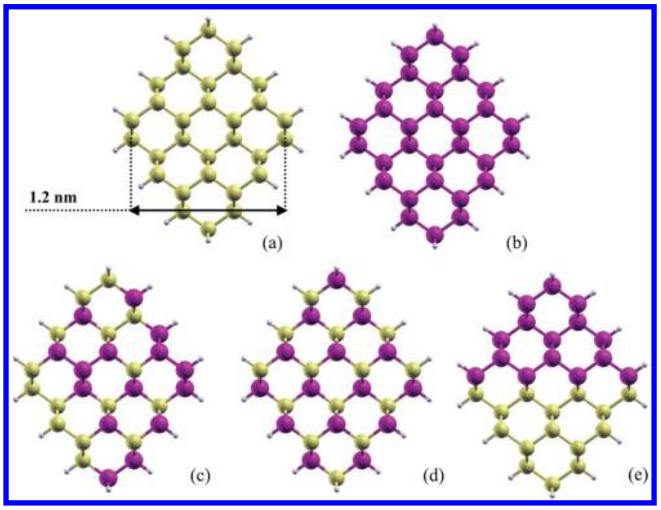

Figure 25. Top view of (a) Ge, (b) Si, and (c) SiGe random, (d) mixed, (e) abrupt nanowires with d = 1.6 nm and x_{Ge} = 0.5. Yellow/light gray spheres represent Si atoms, magenta/dark gray spheres Ge atoms, while the small white spheres are H atoms used to saturate the dangling bonds. Reprinted with permission from ref 171. Copyright 2009 American Physical Society.

the wave function localization obtained by DFT calculations and they always found that the VBM is on Ge and the CBM on Si. In the case of random alloyed NWs this effect can be recognized by a certain tendency of valence (conduction) states to be localized into the Ge (Si) regions along the wire. Also Pekoz et al.[179] obtained the same results for triangular shaped NWs. A noticeable exception to this type-II localization was underlined by Akman et al.[186] which investigated hydrogen passivated SiGe axial nanojunctions by means of *ab initio* calculations. Their results showed that by varying the length of the Si or Ge zones along the wire's axis, the offset can be changed from type-II to type-I thus modifying the localization of electrons and holes. Recently, Amato et al.,[187] by performing transport calculations on the same geometry, confirmed these findings, while a path to type-I/II band alignment transition in core−shell SiGe NWs was discussed by Kim et al.[188]

We conclude this section observing that the type-II band offset is responsible for a reduction of the band gap with respect to the pure Si and pure Ge NWs. For this reason some studies defined a reduced QCE in the case of SiGe NWs with such offset:[171,172] this means that for the same reduction of diameter, the opening of the bulk band gap due the confinement is less pronounced with respect to the pure cases. However, for the investigation of the reduced QCE and its dependence on the size of the system, one has to take into account the specific geometry considered as it will be shown in the next paragraph.

4.1.2. Size Effects. The ability to control the electronic and optical response of nanowires by changing their size is of crucial importance for nanodevices. For this reason in the case of pure Si and Ge NWs a lot of studies have been focused on the analysis of the dependence of the energy band gap on the wire's diameter. The state-of-the-art of *ab initio* calculations on this topic has established that the size dependence of band gap can be described by an inverse power law $E_g \sim 1/R^a$, with the parameter a being between 1 and 2.[153−158]

The aim of carrying out this type of study also in case of SiGe NWs is more complicated since in this case, for a fixed geometry, the electronic structure is strongly affected by the presence of the type-II band offset, whose magnitude in turn depends on the size reduction and on the relative composition of Si and Ge atoms. In order to get a deep insight in this aspect, one should keep fixed the composition of the wire and, for different geometries, analyze the effect of the reduction of diameter.

This was done by Amato et al.[171] which considered the geometries presented in Figure 25 which have the same composition (x_{Ge} = 0.5) but different distributions of the atoms. For the mixed SiGe NWs, they distinguish three different types of structures, with the same composition, the same geometry, but different distribution of the two types of atoms. The first one is random SiGe NWs (random NWs), where the distribution of the two type of atoms in the lattice unit cell is completely random, see Figure 25c; the second one is mixed SiGe NWs (mixed NWs), in which a type of atom is bonded in a tetrahedral geometry with four atoms of the other type, see Figure 25d; and the last one is half SiGe NWs (abrupt NWs), where one-half of cross section of the NW is made up of Si and the other half is made up of Ge atoms, see Figure 25e. They calculated the DFT energy band gap as a function of the diameter for wires up to 1.6 nm. Their most interesting result is that the abrupt NWs show a strongly reduced QCE, which appears to be more pronounced increasing the diameter of the wire. This property is absent in mixed and random NWs, which have energy band gap very close to those obtained for pure Si and Ge NWs, even if they have the same composition of the abrupt NWs (x_{Si} = 0.5 and x_{Ge} = 0.5). Therefore, this effect must be related to the geometry of the NW, in particular, to the configuration of the atoms in the unit cell and to the presence of a clear interface between Si and Ge regions. Indeed their analysis of wave function localization confirm that in the wires with an abrupt interface present a type-II band offset which reduces the band gap of the pure NWs. To further investigate the physical origin of the size dependence, they evaluated the entity of QCE for pure Si and pure Ge calculating the energy variation of the VBM, ΔE_v, and of the CBM, ΔE_c, with respect

dx.doi.org/10.1021/cr400261y | *Chem. Rev.* 2014, 114, 1371−1412

to their values in the largest NWs. They showed that the confinement effects are stronger in Ge than in Si and that, while Ge tends to confine both valence and conduction states, in Si one can note confinement mainly for valence states.[167,168] Reducing the diameter in abrupt NWs, the VBM tends to be more shifted down for the Si than for the Ge ($\Delta E_v^{Si} > \Delta E_v^{Ge}$), so finally the edge of the valence band will be localized on the Ge region of the wire; whereas in the case of the CBM an opposite behavior is observed, the shift is more pronounced for Ge than for Si ($\Delta E_c^{Ge} > \Delta E_c^{Si}$); thus, the edge of the wire's conduction band will be localized on the Si region. This is the reason why, also at very small diameters, type-II offset is preserved in NWs with an abrupt interface and one can observe the reduced QCE.

As regards as the core−shell geometry, Musin et al.,[169] by calculating the dependence of energy band gap on the number of atoms in ⟨110⟩ SiGe core−shell NWs, proposed the following formula:

$$E_g(N) = E_g(\infty) + \frac{A}{N} \quad (3)$$

where A is an adjustable parameter and $E_g(\infty)$ is the bulk limit value of the energy band gap corresponding to the nanowires with an infinite diameter ($N \rightarrow \infty$). The number N is the sum of atoms both in core and shell and it is directly related to the radial size of nanowires. Since the considered nanowires has an approximately cylindrical shape, this equation leads to an inverse square relation $E_g \approx 1/R^2$ in accordance with experimental observations of quantum size effects in 1-D system. This model has been demonstrated to be valid for ultrathin nanowires with diameter up to 1 nm.

4.1.3. Alloying and Interface Effects. The most innovative degree of freedom in SiGe NWs properties with respect to the pure NWs is the possibility to change the electronic structure by varying the relative composition of the wire. As we have seen in section 2, SiGe NWs can be grown in a wide range of different values of composition and hence this tunability can be fundamental in designing their properties. Of course the appropriate variation has to be chosen on the particular geometry we consider. We start our analysis by considering the most common experimental geometries.

As discussed by Musin et al.,[169] for core−shell NWs, there are two distinct ways to explore the composition dependent properties. The first one, more conventional, consists in changing numbers of core (N_{core}) and shell (N_{shell}) atoms in the unit cell keeping the total number of atoms $N = N_{core} + N_{shell}$ fixed. This method offers the possibility to cover the whole range of composition which has as limiting case the pure Si and Ge NWs ($x = 0$ and 1). In this approach the diameter is fixed. The second method is to fix the number of the core atoms and increase the number of shell atoms from $N_{shell} = 0$ to $N \rightarrow \infty$. Clearly, in this way the diameter of the wire is changed and the results obtained cannot be related to a pure compositional effect. The results of their calculations are reported in Figures 26 and 27, which show how the compositional variation of the energy gaps is nonlinear for all nanowires (both Si-core/Ge-shell and Ge-core/Si-shell), the shape of all the curves is similar, and they all have minima around 0.2 and 0.5. This nonlinear behavior has been ascribed to the simultaneous variation of both core and shell size when the composition of the system is changed. As a matter of fact, Amato et al.[172] and Pekoz et al.[179] have reproduced a similar trend but for ⟨110⟩ core−shell NWs. All of these results are in qualitative agreement with previous experimental studies on

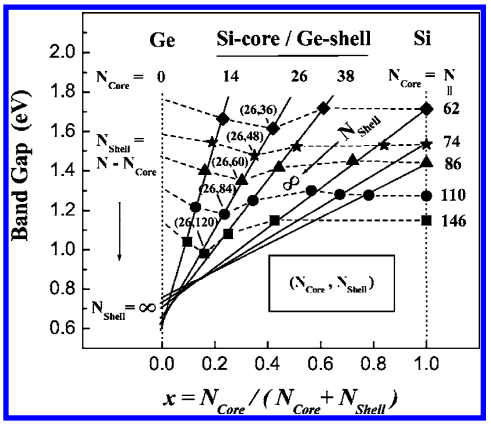

Figure 26. Electronic direct gap E_g as a function of composition x (dashed lines) for Si-core/Ge-shell NWs with different number of atoms N (62 (diamonds), 74 (stars), 86 (triangles), 110 (circles), and 146 (squares)) in the unit cell. Solid lines are the linear fits of the calculated E_g values using $E_g(N_{Core},x) = (N_{Core},0) + k(N_{Core})x$ (see ref 169 for more details) for nanowires with N_{Core} = 14, 26, 38, 62, 74, and 86 and $N_{Shell} = N - N_{Core}$. In parentheses: Numbers of core and shell atoms for nanowire with N_{Core} = 26. Dotted lines denote the end points for N_{Core} = 0 and N_{Shell} = 0 corresponding to the pure Ge and Si structures, respectively. Reprinted with permission from ref 169. Copyright 2009 American Physical Society.

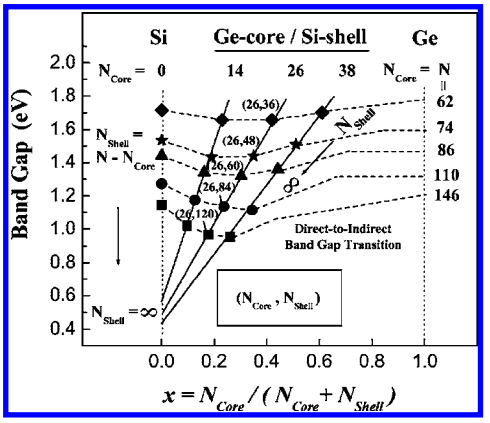

Figure 27. As in Figure 26, but for Ge-core/Si-shell NWs. Reprinted with permission from ref 169. Copyright 2009 American Physical Society.

alloyed nanocrystals in which the possibility to change the electronic and optical response without varying the size of the system was pointed out.[189] Musin et al.[169] also showed that increasing the shell thickness by keeping fixed the number of the atoms in the core leads to a substantial decrease of the energy band gap as indicated by solid lines in Figures 26 and 27. Surprisingly in this case the decreasing of the band gap has a linear dependence on the composition.

Amato et al.[172] tried to generalize the scaling properties of band gap with composition extending the analysis to other geometries, as abrupt and random NWs (see Figure 25). Their most interesting result showed that in abrupt NWs (in which the composition variation is obtained by preserving the abrupt interface) the $E_g(x)$ has a perfectly parabolic trend and can be interpolated with the following analytical formula:

$$E_g(x_{Ge}) = 0.98292 - 1.3508x_{Ge} + 1.3478x_{Ge}^2 \quad (4)$$

The reduction of the band gap increasing the composition for this configuration is the strongest observed among all the

dx.doi.org/10.1021/cr400261y | Chem. Rev. 2014, 114, 1371−1412

considered geometries. The authors ascribed the origin of this property to the very similar band gap values of Si and Ge NWs and to the strong symmetry of the system which can preserve the existence of a noticeable type-II band offset also when the relative size of Ge and Si zones is changed.

4.1.4. Strain Effects. For bulk SiGe alloys and for SiGe superlattices it has been demonstrated that strain effects, altering the intrinsic interatomic distances, modify the energy levels.[163−165] In fact it is well-known that strain has two main effects on the band structure of a SiGe system both for valence and conduction states: hydrostatic strain shifts the energetic position of a band, while uniaxial or biaxial strain splits degenerate bands. Furthermore, strain can strongly affect the values and magnitude of band offsets, effective masses and mobility. For all these reasons the strain has always been considered as a powerful tool to modulate electronic features of a material in device engineering.[161,162]

More in general, for SiGe systems strain originates from two sources:[161,162] (i) an intrinsic one, related to the lattice mismatch between Si and Ge which is about 4%, and (ii) an extrinsic one connected to the presence of a substrate, to the growth method or to an intentional applied deformation.

At the nanoscale, the increase of the surface−volume ratio exerts a strong influence on the structural properties of the wires. Indeed the reduced dimensionality and the small size of the systems allow to relax larger amounts of strain with respect to the bulk junctions without introducing dislocations or other defects that could influence the electrical behavior. This was confirmed by the experimental growth of axial SiGe nanojunctions in which the lattice mismatch is partially relieved at the interface by lateral displacement of atoms.[114] In core−shell NWs both theoretical and experimental studies confirm that the full 4% lattice mismatch can be accommodated without the creation of dislocations by periodic modulation of the shell thickness. In particular for Si-core/Ge-shell experiments show that the Ge shell is fully crystallized for low-temperature growth, with compressed Ge core and tensile strained Si shell.[87] While for Ge-core/Si-shell, amorphous Si shell is formed and crystallized with thermal annealing.[87]

The debate on the role of strain in determining and modifying the electronic structure of SiGe NWs has been vivid in the last years. Several *ab initio* calculations[170,173−175,178,180,182] on the effect of intrinsic and extrinsic strain on the electronic band gap, band offset and carrier localizations have been performed.

The first attempt to analyze the structural properties and intrinsic strain of core−shell SiGe NWs has been carried out by Musin et al.[173] which performed DFT simulations to analyze the dependence of the lattice parameter on the composition of the wire for diameters up to 1.7 nm. Their results showed that structural parameters of the wire *c* (axial parameter) and *d* (diameter) have a nonlinear composition dependence for both Si core and Ge core NWs. Nevertheless, the deviation from the linear behavior (represented by the Vegard's law for binary bulk alloys[190,191]) is of the order of hundredths of Å and hence negligible (as confirmed by other theoretical simulations, in particular those of Amato et al.[172] and Yang et al.[176]).

Peng and Logan[175] studied the effect of increasing the diameter on the axial lattice constant of core−shell NWs giving a quantitative estimation of the produced intrinsic strain. Their findings, in good agreement with experiments and with results of Musin et al.,[173] confirmed that the Si composition is always in tensile strain (i.e., positive strain) while the Ge composition is in compressive strain (i.e., negative strain). Moreover they showed that by applying sufficient external tensile strain (around 2.8%) along the axis of Si-core/Ge-shell NWs a transformation of direct band gap to indirect one can be obtained.

A meaningful example of band offset engineering by applying external strain is reported by Huang and Yang,[182] who performed DFT-LDA calculations to investigate mechanisms controlling the band offset by axial external strain in ⟨110⟩ core−shell NWs. They considered applied strains varying from −3% to +5% and diameters up to 3.7 nm. The procedure they used to estimate the offset is the same described by Yang et al.[176] Their main result is reported in Figure 28. As one can see

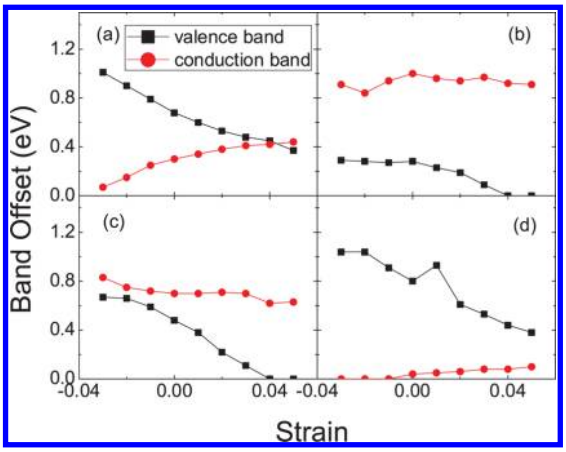

Figure 28. Variation in band offsets of four typical Si/Ge core−shell NWs under different strain conditions. (a) A Si-core/Ge-shell NW with core diameter of 1.2 nm and shell diameter of 2.5 nm. (b) A Si-core/Ge-shell NW with core diameter of 1.7 nm and shell diameter of 2.5 nm. (c) A Ge-core/Si-shell NW with core diameter of 1.3 nm and shell diameter of 2.5 nm. (d) A Ge-core/Si-shell NW with core diameter of 1.8 nm and shell diameter of 2.5 nm. Reprinted with permission from ref 182. Copyright 2011 American Institute of Physics.

from the figure, both for Ge-core and Si-core NWs, applying strain can strongly modify the values of the valence band offsets, while the conduction band offsets are not sensitive to the applied strain. These results suggest that core−shell NWs should be preferred to pure NWs for photovoltaic applications, because the efficiency of the e−h pair separation, determined by the offset, can be modulated by the strain. The authors explain the physical mechanism of this effect supposing two main sources: (i) The first one is the different response of Ge and Si state energy to the applied strain, so that the band alignment can be varied. Interestingly, when the applied tensile strain is greater than 4%, the energy shifts make the offset zero. (ii) The second one is related to the fact that strain can change the nature of a state, transforming a core state into a shell one and vice versa. In this way a confined state can become nonconfined eliminating its contribution to the band offset.

4.1.5. Addition of Impurities. The understanding of doping at the nanoscale represents one of the main topic for the design and development of SiGe nanowire-based devices. As we will see further on in section 5, for NWs applications the possibility of modifying electronic properties of the material by introducing impurities is of paramount importance and its full understanding requires a microscopic picture of basic mechanisms.

dx.doi.org/10.1021/cr400261y | *Chem. Rev.* 2014, 114, 1371−1412

Experimentally it has been clearly demonstrated that, with the current growth methods (such as vapor−liquid−solid growth) it is possible to incorporate III and V group impurities into the wire and to obtain both *n*-type, *p*-type, and codoped SiGe wires. Nevertheless, it has not yet been clarified how the electrical properties of the wire, e.g., the mobility, depend on the impurity carrier concentration and through which mechanisms.

The intentional addition of impurities has the general purpose of tuning the number of free charges into the semiconductor, hence controlling the wire conductivity. In Si, Ge or SiGe bulk this goal is fulfilled by incorporating very small amounts of selected additives, usually boron or phosphorus atoms, to them (generally no more than a few parts per million). These impurities increase the number of electrons or holes and therefore the mobility of the material.

On the other hand the doping process at nanoscale, as shown for pure Si and Ge NWs, is particularly inefficient when the diameter is reduced, as a consequence of surface segregation of the impurities, quantum confinement, and dielectric mismatch effects.[192−196] These phenomena creates several problems about the real applications of these types of materials for electronic devices. Theoretical studies on doped SiGe NWs are still very few to give a whole overview of the basic mechanism of addition of impurities in this kind of systems. Nevertheless, in this section we aim to review some of them trying to point out possible future perspectives in this field.

A contribution to the understanding of the doping in SiGe core−shell NWs has been given by Amato et al.[116] The results of their *ab initio* DFT calculations on core−shell SiGe NWs (with diameter of 2.4 nm) gave the first theoretical proof of hole accumulation in core−shell NWs (previously found in experiments[100]) as well as a successful strategy to overcome impurity deactivation in nanostructures. As we have already seen, in core−shell NWs the band offset between the two materials causes a localization of the valence states on Ge and of conduction states on Si. As a consequence of this property, with particular doping conditions, a one-dimensional electron (hole) gas at the band edge can be created and the carrier density can be uniquely controlled by the impurity concentration without no need of thermal activation. As showed in Figure 29, in the case of a Ge-core/Si-shell wire with a P impurity into the core, the impurity level falls inside the conduction band, yielding an electron at its bottom. This result is related to the type-II band-offset that develops at the Si/Ge interface. In a pure Ge NW of the same size of the core, the impurity level would have been deep into the band gap and very difficult to activate at typical device temperatures. In this case instead, analyzing the wave function localization, the authors found that the bottom of conduction band is on Si-shell, which are below the impurity and all the Ge-core states; it means that the impurity does not need to be thermally activated. This indicates the formation of a one-dimensional electron gas that can have relevant importance for device applications. The other interesting case is the configuration with a B atom into the Si shell of a Ge-core/Si-shell NW. The impurity level is deep into the valence states: the valence band is made by germanium-core states at higher energy than the boron state and we have the formation of one-dimensional hole gas. These conclusions can be generalized to Si-core/Ge-shell NWs as well.[197] The findings of Amato et al.[116] are in qualitative agreement with two experimental studies in which the existence of hole accumulation in intrinsic Ge-core/*p*-type

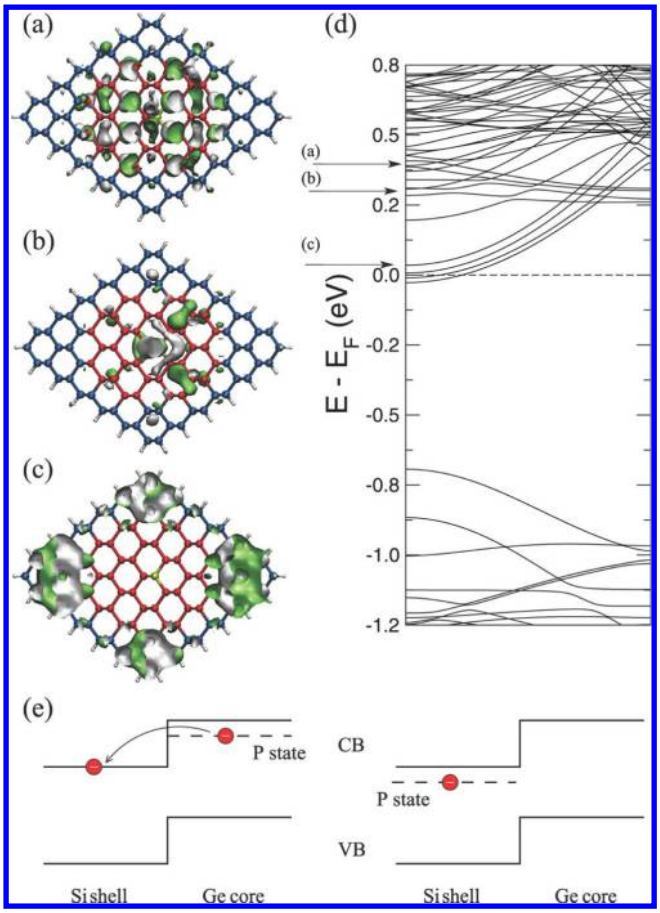

Figure 29. Band structure of a Ge-core/Si-shell NW with P doping in the Ge-core (d); labeled arrows indicate the states whose real-space distribution is shown in panels a−c. Lateral panels show the shell character of the bottom of the conduction band (c), the impurity state, 0.34 eV above the band-edge (b), and the lowest energy Ge-core state (a). A qualitative model of the band offset (not in scale) for P-doping of a Ge/Si core−shell NW is shown below (e). Doping of the Ge core yields an electron at the bottom of the conduction band localized in the Si-shell (left-hand side), whereas doping of the Si-shell is similar to the case of an all-Si NW (right-hand side). Reprinted with permission from ref 116. Copyright 2011 American Chemical Society.

Si-shell has been demonstrated.[117,118] Up to now no experimental studies have demonstrated the existence of an electron accumulation. Probably, this can be explained through the reduction of conduction band offset at the experimental diameter considered.

Another noticeable work on this topic has been done by Park et al.,[198] who reported results of DFT calculations for the stability of donor-pair defects in SiGe alloyed NWs oriented along the ⟨111⟩ direction, doped with P atoms and with diameters up to 30 Å. They found that it is energetically favorable for P dopants to create nearest-neighbor donor-pair defects when the diameter is below a critical value, suggesting an additional deactivation factor for small diameters SiGe NWs. Moreover, they demonstrated that this stability is increased when the composition of Ge atoms is increased, indicating that, to have electrical active NWs, the impurity concentration in experiments cannot be the same for all of the range of composition.

4.1.6. Electronic Transport. The electrical conductivity of different types of SiGe NWs has been mostly studied in structures that have been proposed for thermoelectric

dx.doi.org/10.1021/cr400261y | *Chem. Rev.* 2014, 114, 1371−1412

applications. These works are much less abundant than those purely focused on thermal transport, due to the implicit assumption that the electrical conductivity can ultimately be tuned by adjusting the concentration of dopants. This hypothesis is often an oversimplification, however, especially in view of the difficulties connected with nanoscale doping discussed here (sections 3.1.3 and 4.1.5) and elsewhere.[3,192]

SiGe superlattices are amenable to electrical conductivity modulation, in principle, but it is only with nanowires that defect-free interfaces can be obtained, thanks to the lateral release of the strain deriving from the lattice mismatch. Shi et al.[199] performed DFT calculations of a few representative SiGe superlattices where the thickness of the Ge segment was varied, calculating the ballistic conductance with non-equilibrium Green's functions (NEGF) within the Landauer formalism. They calculated the thermal power factor, $P = S^2G$, where S and G are the Seebeck coefficient and the conductance, respectively, showing that there exist energies of the incoming carriers that maximize it. More in general, and similar to previous reports based on semiclassical Boltzmann transport theory,[200] they showed that ZT can be increased by tuning the superlattice periodicity. Arbitrary long nanowires were considered by Shelley and Mostofi[201] thanks to a method that allowed them constructing the Hamiltonian by assembling building blocks obtained from the smaller segments.[202−204] With this setup they could look into a broader class of superlattices, some of which are only locally periodic (see also the discussion in section 4.2.1).

The interest of core−shell nanowires for thermoelectric application derives directly from the confinement determined by the band-offset, as nicely shown by Markussen:[205] charge carriers can be confined in the core and flow ballistically, while phonons are scattered at the rough shell surface. Things get even better, because holes and electrons suffer only minor impurity scattering and mobilities are consequently high.[127] As already discussed, this happens because the dopants carriers are located in a different region than where the charge carriers that they provide flow, i.e., a confined hole in the Ge core comes from an acceptor in the Si shell.[116]

An attempt at bridging the single-impurity case considered by Lee et al.[127] and the works on superlattice was carried out by Amato et al.,[187] who studied how the conductance vary by moving from a single impurity, to an alloyed $Si_{1-x}Ge_x$ segment of increasing x, and finally to an all-Ge segment inclusion in a scattering region sandwiched by semi-infinite Si NWs. The interesting conclusion is that, at already relatively modest Ge concentrations, the alloyed segment scatters carriers like abrupt inclusions of an all-Ge NW segment; thus, interface scattering, rather than a collection of point defect scattering is the dominant mechanism. It follows that, for thermoelectrics applications, the exact value of the Ge content can be chosen to minimize the heat conductivity without caring too much about its effect on the electrical transport.

4.1.7. Optical Properties. The possibility of design the electronic structure of SiGe NWs by playing with intrinsic and extrinsic parameters offers also a useful and straightforward tool to modulate their optical response. Though still in its infancy if compared to the modeling of the electronic properties, in the last years, the theoretical description of the elementary optical excitations in SiGe NWs has been starting to play a key role in particular in view of the envisaged technological applications. The interest in the use of SiGe NWs as building-blocks for optical and opto-electronic devices is 2-fold: from one-side, by offering the possibility to obtain direct band gaps and strong oscillator strengths, these materials are potential candidates for new generation light emission devices:[2,4,206,207] on the other side, thanks to the strong charge separation and to the improved absorption in the visible spectrum, SiGe NWs are expected to play a role in the future photovoltaics.[1,5,37,208] However, it is important to point out that at small dimensions, as in the case of electronic structure, also optical properties change dramatically with respect to bulk systems. This is particularly true in the case of SiGe NWs, where beyond size effects also geometry, alloying and strain can strongly influence optical absorption and emission properties. Most commonly DFT based methods used for structural energies are formally inadequate to describe electronic excitations, for which many-body perturbation theory methods (namely GW approximation and Bethe-Salpeter approaches[209,210]) are more appropriate. Up to now very few works have investigated the dielectric response of SiGe NWs adopting the appropriate methodology[171,211] and basic questions such as the right estimation of carrier lifetimes, electron−hole interactions, electron addition or removal energies, and correct description of spectroscopic experiments, are still largely unanswered and a lot of work has to be done.

As regards as the application of SiGe NWs in light emitting devices, a first theoretical contribution has been given by Migas and Borisenko,[174] who, by applying DFT based methods, gave an estimation of the optical response in such kind of systems. In fact they showed that ⟨100⟩ SiGe mixed NWs either with Si or Ge dimers can display a direct gap and a noticeable oscillator strength of the first direct transition. Recently, a remarkable work in this direction has been done by Zhang et al.,[212] who, by adopting a combination of a genetic algorithm and a semiempirical pseudopotential Hamiltonian, were able to analyze thousands of possible coaxial core/multishell SiGe configurations in order to find the ones that are formally direct in the momentum space but, at the same time, present a strong oscillator strength. Their main results showed that (i) the presence of a Ge core always produces a strong band gap transition and assumes particular importance for ⟨100⟩ and ⟨111⟩ oriented NWs (that have a direct band gap) and (ii) the core-multishell configuration can offer optical transition that can be more than an order of magnitude bigger than pure Si, pure Ge and core/single shell NWs.

On the other hand, SiGe NWs present the optimal combination of optical properties required by photovoltaic applications. For example, Amato et al.[171] have demonstrated, by employing *ab initio* calculations with the inclusion of many body effects, that a strong electron−hole separation can be obtained in SiGe NWs with a sharp interface between Si and Ge, direct consequence of the type II band offset. In addition, different works[174,179,213] in which the optical absorption is evaluated at the single-particle level, have pointed out that the introduction of Ge atoms into a pure Si NW is responsible for a red shift of the first absorption peak remnant of the direct absorption peak of the bulk Ge. This red shift causes a strong absorption in the solar spectra. The rule is quite general and has been demonstrated to be valid, with appropriate modifications, for different types of geometries (random, core−shell, mixed and triangular shaped SiGe NWs) and different crystallographic directions. In some cases, also an improved quantum yield with respect to pure wires has been observed, confirming the great potential of these materials for high efficiency photovoltaic devices.

dx.doi.org/10.1021/cr400261y | *Chem. Rev.* 2014, 114, 1371−1412

4.2. Phonons and Thermal Conductivity

4.2.1. Breakdown of Fourier's Law at Nanoscale. Usually, in semiconductors the heat conduction is mainly due to the contribution of phonons while the influence of electrons and photons in the process is negligible. The standard macroscopic approach to describe heat transport is the well-known Fourier's law, which states that the heat flux density in the material is proportional to temperature gradient as reported in the following equation:

$$J = -k\nabla T \tag{5}$$

the quantity κ is the lattice thermal conductivity of the material and it is an intrinsic property. Equation 5 is a diffusive equation in which the thermal conductivity, which is a function of the temperature, is independent of the size and geometry.[214] The efficacy of the application of Fourier's law in the description of thermal processes from a macroscopic point of view is enormous, and for this reason, it represents the starting point in describing heat conduction in new and unknown materials. Indeed Debye and Boltzmann-Peierls approaches,[215,216] which are the more rigorous and complete theories based on the Fourier's law, represent standard methods for theoretical prediction of thermal properties in bulk semiconductors.

However, at small length scales, as in the case of nanowires, nanodots, and superlattices, the validity of eq 5 is not any more guaranteed for several reasons: first of all, as clearly pointed out by Liu and co-workers,[214] up to now a rigorous proof for Fourier's law from a microscopic Hamiltonian dynamics is still lacking; second, when the size of the system is comparable to the phonon characteristic lengths, out-of-equilibrium and quantum phenomena (i.e., coherence resonance or ballistic effects) are dominant and must be taken into account; finally, in the quantum regime the possibility to manipulate both phononic and thermal properties by changing the size of the system provides a wide offer of new materials which present specific properties and do not obey to the general macroscopic rules of the Fourier's law; in particular, now the thermal conductivity cannot be defined as intrinsic property of the material[217] (i.e., it is not any more independent from the size and geometry of the system).

For the above reasons, in the last years it is starting to be common belief that Fourier's law and the Boltzmann-Peierls theories suffer of noticeable limitations, in particular in describing lattice dynamics of systems in which quantum effects are dominant, such as the case of SiGe nanowires. Among the attempts to go beyond the Boltzmann theory, the idea of combining atomistic non-equilibrium Green's function (NEGF) method with Landauer formalism to calculate transmission coefficients[218,219] is receiving an enormous interest since it explains well thermal properties when systems under considerations are smaller than the mean free paths of phonons. Nevertheless, NEGF based methods are exact in the harmonic approximation (or at very low temperatures when anharmonicity is small) and if the ballistic approximation is valid. When phonon−phonon interactions have to be incorporated, numerical methods based on molecular dynamics (MD)[220−223] seem to be more appropriated. Furthermore, MD significant limitation to be entirely classical seems to be overcome by novel methods such as Car−Parrinello MD (CPMD)[220,224] or quantum thermal bath MD.[225] Other ways to include anharmonic effects are based on combination of DFT calculations with Boltzmann formalism in a multiscale strategy, which has been used to describe thermal conductivity of several materials (Si, Ge, or diamond) successfully.[226−228]

4.2.2. Numerical Simulations of Thermal Properties. The great interest in the thermal properties of SiGe NWs is related to the possibility of engineering phonon dispersion and thermal conductivity by playing on some parameters of the system (see section 3.2). In the last decades a lot of theoretical and experimental works, mainly focused on the nanostructuring of existing thermoelectric materials, have shown a strong reduction of thermal conductivity (if compared with bulk values) when the dimensions of the system are at the nanometer scale. For instance, it has been demonstrated that pure Si NWs possess a 100-fold improved thermoelectric performance over bulk Si near room temperature due a drastic reduction of thermal conduction, while charge transport remains unaltered.[134,135] This reduction is mainly caused by the strong phonon boundary scattering in NWs and, accordingly, it has been shown that the effect is more pronounced decreasing the diameter of the wire. Other works,[229] devoted to the discovery of high thermal materials for electronics, have demonstrated how periodic arrangements of atoms of two different materials in the form of a superlattice can yield thermal conductivities higher than the two constituent materials.

These effects can be greatly enhanced in SiGe NWs by building structures with different interfaces or compositions. In fact, it is expected that the significant difference in the mass between Si or Ge or the presence of interfaces offers the possibility of engineering phonon scattering and heat conduction. In the case of SiGe NWs most of the theoretical works[147,199−201,205,230] have the design of the high-efficiency thermoelectric materials as main objective and, hence, are focused on the estimation of the figure of merit ZT by studying both thermal and electronic transport. However, in this section we will try to review all of the theoretical aspects of thermal conduction in such materials and to deduce rules as general as possible. In this context theoretical atomistic simulations are fundamental for the comprehension of heat conduction at nanoscale since they can complement the experimental difficulties of controlling and measuring heat flux in such nanoscale systems.[214]

As it has been pointed out in section 2, the possibility of synthesizing SiGe NWs with different geometries, interfaces and compositions offers a wide choice on the tunability of the phonon transport. However, superlattice and core−shell SiGe NWs have been the object of most of the theoretical investigation due their very promising performances as high efficiency thermoelectric materials. Although at this stage it is rather hard to define a general trend for the dependence of thermal properties on the extrinsic and intrinsic parameters of the system, it is possible to say that, irrespective of the geometry of the wire (i.e., superlattice or core−shell), the thermal conductivity of a SiGe NW can be modulated by playing on the following parameters: (i) the relative of length of Si and Ge regions, which can change the relative magnitude of competing contributions to the heat conduction from the thermal vibrations (since Si and Ge atoms have different masses their contributions to the overall thermal conductivity are not the same); (ii) the cross-section width, i.e., the diameter of the wire, which, being comparable to the mean free path of phonons, can be critical in determining the entity of phonon boundary scattering and hence the propagation of heat in the wire; (iii) the temperature that, as in the case of bulk systems,

modulate the magnitude of atomic displacements strongly influencing the energy transport associated to vibrations.

$Si_{1-x}Ge_x$ alloy NWs received comparatively less attention, though it is worth mentioning the work of Whang and Mingo,[231] who calculated the thermal conductivity as a function of the Ge concentration in wires of different diameter, and that of Chan et al.[232]

SiGe Superlattice NWs. SiGe superlattice NWs are made of Si and Ge NW segments periodically stacked one upon the other to form a single crystalline nanowire. A model system for this kind of wires is shown in Figure 30. As we discuss below, the

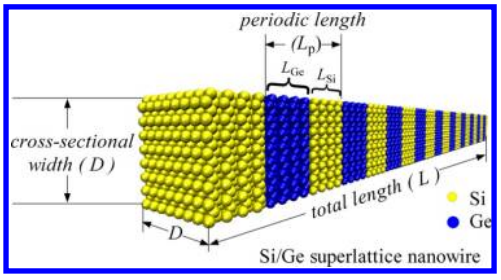

Figure 30. Side and cross-sectional view of the Si/Ge core−shell nanowire with 9 × 9 × 302 unit cells of Si (yellow) core covered by 1 unit cell of Ge (blue). Reprinted with permission from ref 147. Copyright 2011 American Chemical Society.

thermal transport properties of these systems are strongly related to the individual layer thickness in the superlattice (periodic length), the wire diameter (or the cross-sectional width), and the temperature.[233,234]

A first simple model to calculate the thermal conductivity of SiGe superlattice NWs has been provided by Dames and Chen[235] extending the photon-net radiation method and the Schuster-Schwarzschild approximation to dispersive acoustic phonons in a gray medium. The model builds upon the basic idea that, since current experimental techniques are not able to perfectly reproduce sufficiently uniform surfaces and interfaces for coherent interference and quantum conductance, thermal transport in superlattice NWs can be considered as mainly dominated by scattering of incoherent phonons. Although this model completely neglects the effects of confinement on the phonon dispersions (which is instead fundamental at small diameters), it is very useful to qualitative understand basic mechanism and sources of scattering in SiGe superlattice NWs. Three main assumptions characterizes the model: (i) in real superlattices, at temperatures above few Kelvin, phonon coherence cannot be observed and transport is due to incoherent phonons (this statement is supported by experimental observations[236,237]); (ii) the phonon dispersion is three-dimensional and not confined; (iii) the scattering is diffuse and not specular. Figure 31 depicts very well all the sources of scattering in this model system.

In a SiGe superlattice there are three different types of thermal resistance: the first one is the volumetric resistance, R_V, which is due to defects, impurities, grain boundaries and other phonons (see Figure 31); the second is the transmission resistance, R_T, which is related to phonon boundary scattering at the interface with the other material; finally, the space resistance, R_S, is originated by the scattering of phonons with the sidewalls of the wire. The authors consider the three mechanisms completely decoupled, applying a simple Matthiessen's rule and deriving three effective independent mean

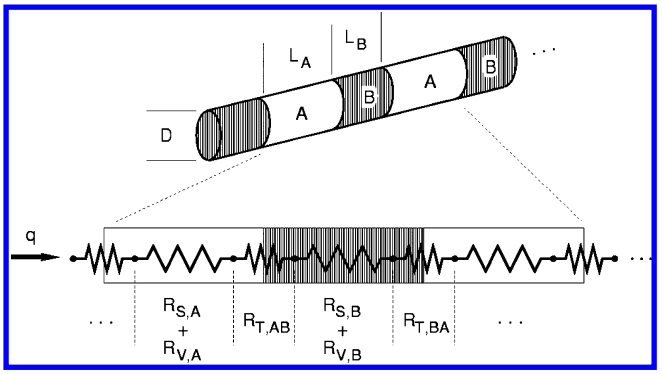

Figure 31. Schematic figure of a model superlattice nanowire, with L = segment lengths and R = thermal resistances, where period is $L_A + L_B$, $R_{T,AB}$ = intersegment transmission resistance, R_V = volumetric/bulk scattering resistance. R_S = intrasegment space resistance, including reflection and reradiation from the cylinder sidewalls. Reprinted with permission from ref 235. Copyright 2002 American Institute of Physics.

free paths. Further analytical details and assumptions of the model can be found in ref 235. Here we stress on the fact that the proposed model works well for the description of diffusive scattering until the quantum coherence effects become dominant. In fact, their results concerning the dependence of the thermal conductivity κ on the Si or Ge segment length ($L = L_{Si} = L_{Ge}$) and the diameter D show that it decreases with decreasing wire diameter, segment length and intersegment transmission. Furthermore, they point out how it is possible to recognize three distinct regimes of scattering reported in the Figure 32.

In the small diameter regime [panel a of Figure 32] the dominant scattering mechanism is due to the sidewalls of the wire; in the short segment regime [panel b of Figure 32] the thermal resistance of the Si/Ge interface plays the major role while in the bulk regime [panel c of Figure 32] both the diameter and the segment length are much larger than the mean free path of the bulk phonons and, hence, nanostructuring is not any more relevant. These results, beyond their fundamental contribution to the understanding sources of scattering in superlattice NWs, are in fair agreement with experimental data[138] for $Si/Si_{0.9}Ge_{0.1}$ superlattice nanowires of 58 and 83 nm in the temperature range 30−150 K.

As mentioned above, the main limit of the discussed model is its inadequacy to describe coherence resonance and quantum confinement effects at small diameters. However, several studies[147,199,201] in literature have filled this gap, by studying the thermal behavior of ultrathin nanowires taking into account quantum effects.

The most noticeable work has been done by Hu and Poulikakos,[233] who have performed nonequilibrium molecular dynamics calculations to investigate the dependence of thermal conductivity of ⟨100⟩ SiGe superlattice NWs on the periodic length, on the diameter and on the temperature. Their main result is the nonmonotonic behavior of κ when the periodic length of the superlattice is varied (see Figure 33a, which reports a comparison between pure Si NWs, SiGe superlattice NWs and random alloyed wires).

First, one can notice that in a Si/Ge superlattice NW the thermal conductivity is strongly reduced (of nearly 92%) with respect to a pure Si NW. To further investigate the difference between the three types of wires (pure, superlattice, and random alloyed), the authors fixed the periodic length in the

dx.doi.org/10.1021/cr400261y | Chem. Rev. 2014, 114, 1371−1412

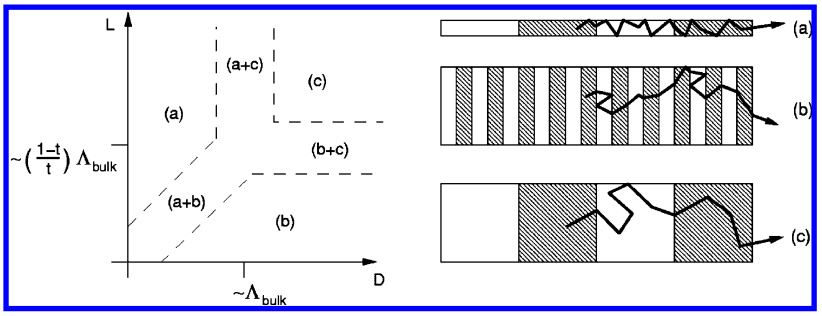

Figure 32. Map of the classical scattering mechanisms in the wire of Figure 31 as discussed by Dames and Chen:[235] (a) diameter limited, (b) superlattice limited, and (c) volumetric/bulk limited. Reprinted with permission from ref 235. Copyright 2002 American Institute of Physics.

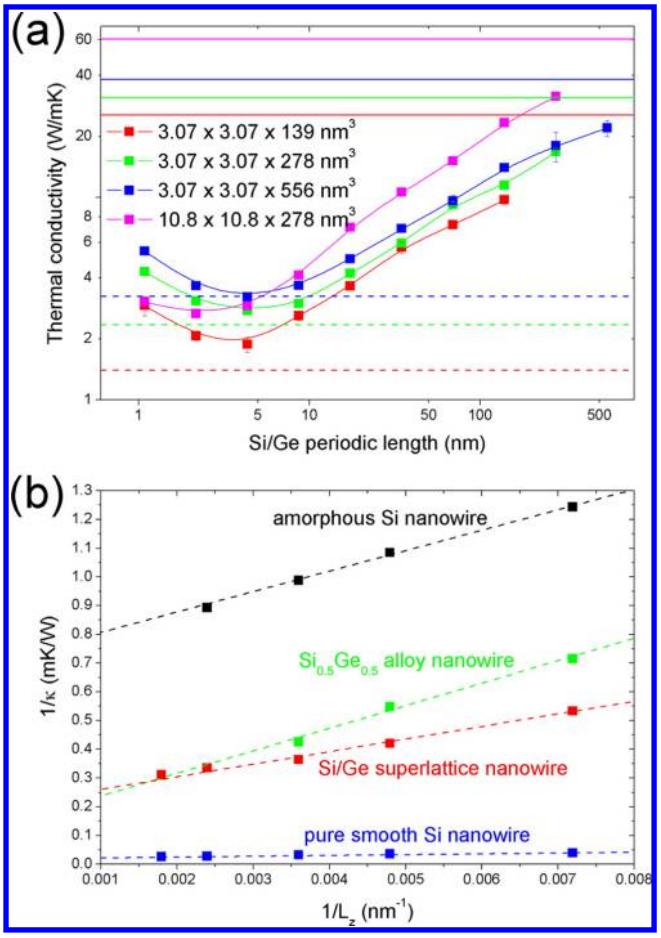

Figure 33. (a) Periodic length dependence of the thermal conductivity of Si/Ge superlattice nanowires for different total lengths. The solid and dashed lines indicate the thermal conductivity of pure smooth Si nanowires and $Si_{0.5}Ge_{0.5}$ alloy nanowires with same length and cross-section width (red, 139 nm; green, 278 nm with 3.07 × 3.07 nm^2 cross-section; blue, 556 nm; magenta, 278 nm with 10.8 × 10.8 nm^2 cross-section). (b) Length dependence of $1/\kappa$ on $1/L$ for smooth Si nanowire, Si/Ge superlattice nanowire, $Si_{0.5}Ge_{0.5}$ alloy nanowire, and fully amorphous Si nanowire. Reprinted with permission from ref 233. Copyright 2012 American Chemical Society.

superlattice to 4.34 nm and calculated the thermal conductivity as a function of the total length of wire L (see Figure 33b). Then they compared the results with fully amorphous Si NW, pure Si NW, and random alloyed SiGe NWs. They fitted the obtained data and present a very useful equation to estimate the effects of heterostructuring on the thermal conductivity of wires with small periodic length:

$$\frac{1}{\kappa} = \frac{1}{\kappa_{\infty}^{NW}}\left(\frac{l_{NW}}{L_Z} + 1\right) \quad (6)$$

where K_{∞}^{NW} is the thermal conductivity of an infinitely long NW and l_{NW} is the mean free path in the NW. The values of K_{∞}^{NW} for pure Si NW, random alloyed SiGe, and SiGe superlattice NWs and fully amorphous Si NW are 45.3, 6.03, 4.44, and 1.35 W m^{-1} K^{-1}, respectively, indicating that the more the system is heterostructured, the more the thermal conductivity is reduced. In order to explain the unusual nonmonotonic behavior of thermal conductance when the periodic length of the wire is varied, the authors adopted two different arguments. First, to describe why κ decrease with respect to the pure wire in SiGe superlattice NWs, they computed phonon dispersion curves for all the systems considered. They found that the phonon velocity is drastically reduced in SiGe NW with respect to pure wires. This velocity reduction, aided by the phonon interface and boundary scattering, hinders heat conduction. Surprisingly, the curve of Figure 33 presents a minimum because, at small periodic lengths, coherence effects become dominant and cancel the interface effects. In fact, as explained in the normal-mode analysis, at the shortest periodic length considered, the phonon modes of interface and inner regions participate with the same contribution to the thermal transport. In other words, there is a constructive interference phenomena between oscillations of atoms in the surface and in the core of the wire which suppresses the interface scattering and facilitates the thermal transport along the wire. The superlattice NW behaves as a new material with its own phonon dispersion caused by phonon waves propagation through the whole structure. This very interesting result has been recently confirmed by Shi et al.,[199] who, by combining density functional theory calculations and nonequilibrium Green's Function simulations for ⟨100⟩ SiGe superlattice NWs, found the same nonmonotonic behavior for the thermal conductance dependence on the periodic length.

Another interesting aspect of the work of Hu and Poulikakos[233] is the study of the dependence of κ as a function of the cross-section width (diameter) of the wire (see Figure 34b). Again, the superlattice NW presents the lowest thermal conductivity if compared with pristine NWs. Furthermore, at fixed periodic length of 4.34 nm, the thermal conductivity is a nonmonotonic function of the diameter of the wire (see Figure 34a). The authors tried to explain this unexpected result in this way: the first decrease of the thermal conductance can be explained, according to the Boltzmann equation, with the calculated reduction of heat capacity. However, this explanation is not valid for ultrathin wires (for which κ increases). As shown by the vibrational density of states calculation, at small

dx.doi.org/10.1021/cr400261y | Chem. Rev. 2014, 114, 1371−1412

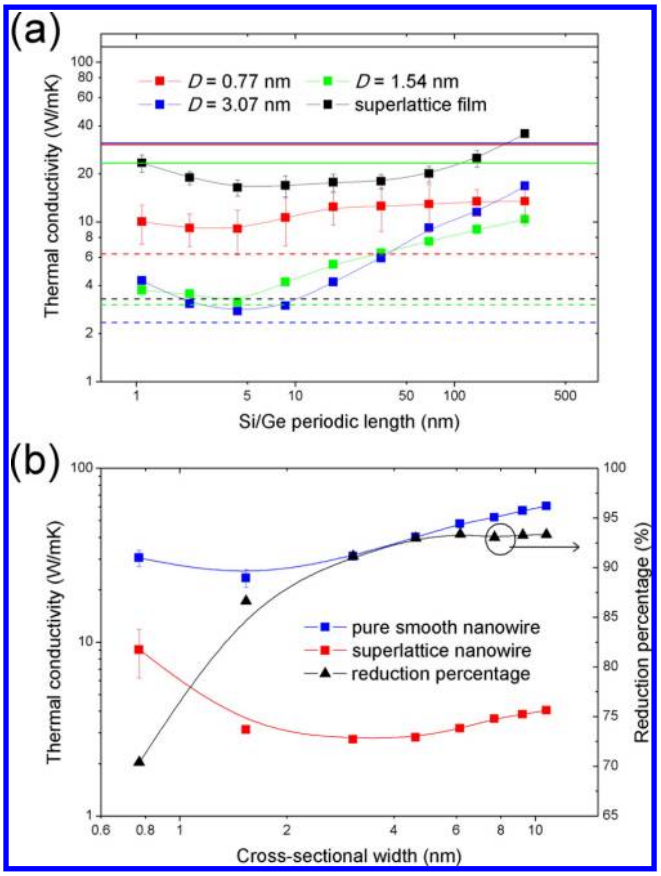

Figure 34. (a) Thermal conductivity of Si/Ge superlattice nanowires with different diameter D as a function of the Si/Ge periodic length at T = 300 K. The solid and dashed lines represent the thermal conductivity of pure smooth Si nanowires and $Si_{0.5}Ge_{0.5}$ alloy nanowires with the same length, respectively. (b) Thermal conductivity of Si/Ge superlattice nanowires with fixed periodic length of 4.34 nm as a function of wire cross-sectional width. The right axis shows the percent reduction in thermal conductivity of Si/Ge superlattice nanowires relative to that of pure smooth Si nanowires. All nanowires in a and b have the same length of 278 nm. Reprinted with permission from ref 233. Copyright 2012 American Chemical Society.

diameters long-wavelength surface modes become predominant because the surface-volume ratio strongly increases. As a consequence of this enhancement, the heat conduction will be facilitated since low frequency phonons conduct heat more efficiently. In the last part of the work the authors analyzed the dependence of thermal conductivity on the temperature in the range 50−650 K. They found that for SiGe superlattice NWs, due the presence of nonpropagating vibrational modes, the increasing of the temperature has only a negligible effect on the heat conduction which remains constant all over the considered range.

A remarkable contribution to the understanding of thermal conduction in the coherent regime for SiGe superlattice NWs is due to the work of Shelley and Mostofi.[201] By using a combination of *ab initio* simulations, interatomic potentials, and Landauer-Büttiker approach, they evaluated the thermal transport for axial SiGe heterostructures. Their aim was to understand which is the effect of introducing Ge layers in a pure Si NWs along the growth direction. Interestingly, they showed that introducing only a single Ge layer into a pure Si NWs can reduce the thermal conductivity of 5 orders of magnitude for the ⟨111⟩ direction of the corresponding pristine wire while the reduction is of four orders for ⟨110⟩ and ⟨112⟩ directions. Then, they considered much longer Si wires with many Ge layers along their axis. In contrast with the above-mentioned works, here the authors do not consider only a perfect ordered superlattice but three different distributions of Ge layers: (i) random, (ii) periodic, and (iii) Fibonacci chain,[238] each with ten Ge layers along the axis of the wire. They evaluated the thermal conductivity both in the ohmic and the coherent regimes. Their results confirmed the strong reduction of thermal conduction when the heterostructure is created and an enhancement of this effect when the disorder is increased (periodic to Fibonacci to random); moreover the entity of reduction is larger when the ohmic regime is considered.

SiGe Core−Shell NWs. As mentioned several times in this review, after the first experimental work on the synthesis of SiGe core−shell NWs,[87] these materials have attracted an enormous interest from a technological point of view, in particular in the field of nanoelectronics, nanophotonics, and thermoelectrics. The latter, which aims to engineer phonon and electronic transport in the wire, is the origin of the great interest in the thermal transport of this new class of materials. As pointed out in the first section, core−shell NWs are radial heterostructures which are made up by two coaxial cylinders of different materials. The presence of at least one dimension of the order of the phonon mean free path and of interface between Si and Ge offer the right conditions to modulate phonon scattering and, hence, heat conduction. In particular, as we will see, the deposition of a Ge or Si coating on the top of a pure Si or Ge NW can strongly modify normal modes of the system[239] and give rise to unusual coherent resonance effects.

A first detailed simulation investigation of thermal processes in core−shell NWs has been performed by Hu and co-workers.[147] They presented results from molecular dynamics of phonon propagation in Si-core/Ge-shell NWs with diameters up to 7.7 nm and oriented along the ⟨100⟩ crystallographic direction. They analyzed to what extent the dimension of the shell, the diameter, and the length of the wire can affect thermal conduction.

From Figure 35a it is clear that the addition of the Ge shells and, hence, the creation of a core−shell geometry lowers substantially the phonon transport with respect to the pure Si NWs. Also the calculated thermal conductivity of only the core is really lower than the one of the pure wire (see Figure 35b). The curve of Figure 35 is slightly nonmonotonic since as the number of Ge shells is increased the value of κ increases as a consequence of the larger contribution of the Ge part of the wire to the overall heat conduction. Very interestingly, this pronounced thermal conductivity reduction, which is very promising for thermoelectrics, is preserved also if the cross-section width and length of the wire are varied. The authors clearly explained the origin of these findings by calculating the vibrational density of states of Si surface atoms. In particular, they showed that when a Ge layer is added on the surface of a pure Si NW there is a suppression of low frequency vibrational modes of the Si surface atoms. While oscillations of Si core atoms are not modified by the presence of Ge atoms, in the case of Si surface atoms the bonds with the heavier Ge atoms strongly depress low frequency vibrational modes. It is well-known that low frequency modes are very delocalized and hence their contribution to heat conduction is very large. For this reason, suppressing these modes by adding Ge layers is the main cause of thermal conduction reduction with respect to the

dx.doi.org/10.1021/cr400261y | *Chem. Rev.* 2014, 114, 1371−1412

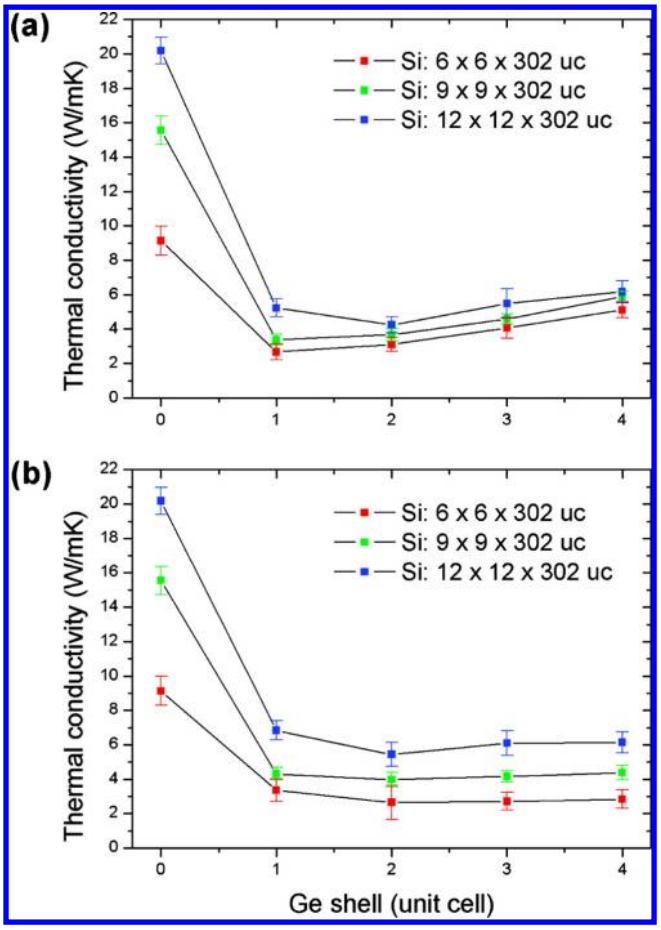

Figure 35. (a) Overall thermal conductivity of the Si-core/Ge-shell nanowire as a function of the number of layers in the Ge shell for different cross-sectional areas of the Si core. (b) Thermal conductivity of only the Si core in the core−shell structure, plotted as in panel a. Reprinted with permission from ref 147. Copyright 2011 American Chemical Society.

pure system. Finally, the authors demonstrated that another contribution to the thermal conductivity reduction comes from the depression of high frequency phonons which usually can carry heat in core−shell structure.

All of the above-mentioned effects have been further highlighted in the works of Chen and co-workers,[240,241] who have investigated the nature of coherent resonance in Ge-core/Si-shell NWs. By using molecular dynamics simulations, they have shown that the depression of thermal conduction is due to the strong localization of longitudinal phonon modes which comes out from a coherent resonance effect between longitudinal and transversal vibrational modes. In a pure nanowire, all of the atoms have the same mass and the atoms in the same cross-section plane have the same sound velocity and the longitudinal and transversal modes are completely decoupled. On the other hand, in a SiGe core−shell NW, atoms on the same cross-section have different masses and, consequently, different sound velocity in the longitudinal direction. This induces a stretching of the atoms belonging to the Si/Ge interface and a coupling between longitudinal and transversal oscillations. Since the lateral dimension of the wire is of the order of mean free path of phonons, transversal modes are quantized and nonpropagating. Therefore, the coupling between longitudinal and transversal modes creates a resonance effect which makes atoms oscillate with an almost close frequency. The nonpropagating nature of transversal modes will be transferred to the longitudinal ones, strongly depressing the overall heat conduction in the material. This effect plays a major role under a critical values of shell thickness (that, in agreement with the work of Hu and co-workers, is nearly two layers[147]); after this critical value, the heat conduction in the wire increases as a consequence of the reduced surface scattering induced by the larger Ge region.

Another way to manipulate the thermal conduction in Ge-core/Si-shell NWs is playing with the roughness of the surface by introducing disorder. In fact, it is expected that the surface disorder can have an influence on the phonon boundary scattering. Chen et al.[240] have demonstrated that the introduction of an imperfect interface does not change the qualitative dependence of thermal conductivity on coating thickness, but it strongly enhances the magnitude of the reduction of κ as compared to pure NWs. This means that the coherence mechanism of κ reduction is still valid when the Si/Ge interface is irregular. Markussen,[205] by using atomistic calculation based on semiempirical methods and Green's function theory, demonstrated the same phenomena, stressing on the role of surface disorder to further reduce phonon transmission. To understand the basic mechanism governing this effect, Chen et al.[240] analyzed the normal modes distribution for such kind of wires and found that the further reduction in thermal conductivity as compared to pristine Ge-core/Si-shell NWs is due to a strong localization of optical phonons, as pointed out in Figure 36. Beyond the sole interest for SiGe NWs, these findings are essential to understand the role of coating and surface roughness on the experimental thermal conductivity measured in pure NWs.

The effect of cross-section width (diameter) has been also investigated. Hu et al.,[242] on the basis of nonequilibrium molecular dynamics, found that, in contrast to the behavior for pure Si and Ge NWs, for core−shell NWs the decreasing of diameter leads to a minimum and a crossover in the thermal conductivity estimation. The origin of this behavior, which differs from the monotonic one of pure NWs, is ascribed to changes in relative magnitude of competing contributions to the heat conduction from the thermal vibrations in the core center vs the shell surface, as core diameter changes. The same authors also found an unusual constant dependence of κ from the temperature.[242] This trend, that was found also in the case of SiGe superlattice NWs,[233] can be explained observing that the presence of nonpropagating vibrational modes is not influenced by the temperature and hence heat conduction in these wires is mainly due to diffusive modes.

5. DEVICES AND APPLICATIONS

The potential of SiGe NWs as building blocks for next generation technological devices is enormous thanks to their remarkable electronic, thermal, and optical features. Moreover, as already stated at the end of the section on the chemical and physical properties, they offer the unique opportunity to be implemented on a semiconductor infrastructure which is easily integrated with current CMOS technology.[104,105] However, despite some preliminary ongoing innovations and breakthroughs, there is no doubt that research in this field is still in a premature state and further challenges have to be overcome before SiGe nanowires are implemented in a high-end product. At this stage it seems that the great potential of these nanostructures can be exploited in the following applied research fields: (i) nanoelectronics, (ii) energy conversion, and

dx.doi.org/10.1021/cr400261y | Chem. Rev. 2014, 114, 1371−1412

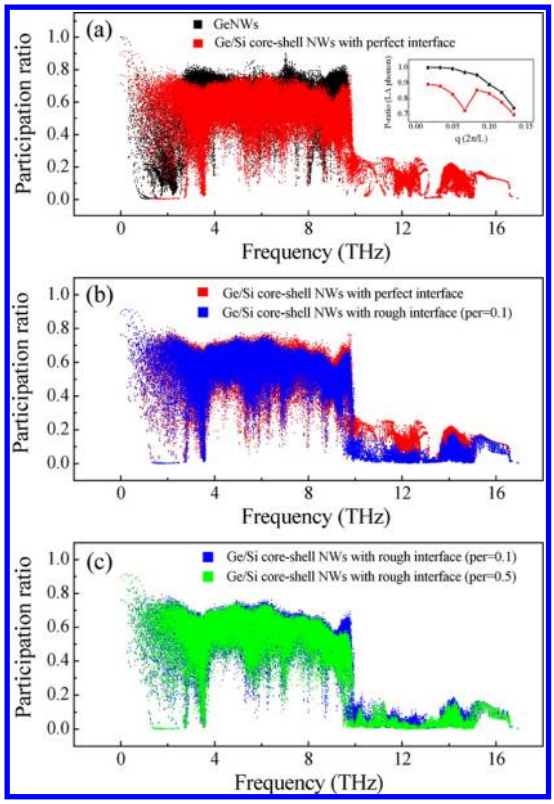

Figure 36. Participation ratio for different phonon modes in Ge NWs before and after coating. The black, red, blue, and green colors denote respectively participation ratio in Ge NWs, Ge-core/Si-shell NWs with perfect interface, Ge-core/Si-shell NWs with 10% interface roughness, and Ge-core/Si-shell NWs with 50% interface roughness. Calculated results for ⟨100⟩ Ge NWs with D_{Ge} = 5.64 nm and Ge-core/Si-shell NWs with $D_{coating}$ = 0.54 nm are shown. The inset in panel a shows the polarization-resolved participation ratio (p-ratio) for the longitudinal acoustic (LA) phonon near the Brillouin zone center in Ge NWs (black) and Ge-core/Si-shell NWs with perfect interface (red). Reprinted with permission from ref 240. Copyright 2012 American Chemical Society.

(iii) spintronics. The first field, i.e., nanoelectronics, is the one in which the most concrete results have been reached. The possibility to fabricate transistors, the building blocks of electronics, using SiGe NWs as channel material has been clearly demonstrated.[90,123,123,243,244] The use of a SiGe NW in comparison to a pure Si wire has allowed the manufacture of transistors with improved performance thanks to the increased mobility (an increment of the order 40% with respect to a pure Si wire) due to the presence of the hole gas.[90] It is expected that silicon−germanium transistors will soon be used in digital as well as analog circuits to improve wireless communications, low power electronics, and high performing computing.[104] Moreover, such improving of device performances will certainly play a significant role in the application of NW field effect transistors for the detection and quantification of biological and chemical species in medicine and biology (a field in which the use of pure NWs has been already demonstrated to be fundamental, see for example ref 245). Finally, these promising results in terms of electronic performance will be certainly combined with the already demonstrated compatibility of SiGe NWs with hippocampal neurons in order to fabricate nanowire-based neuron devices,[246] including coupling nanowire transistors to neurons and probing neurons with vertical nanowire array. This will pave the way to future developments in the field of biomedicine.[245] As regards as the applications of SiGe NWs in the field of energy conversion, we can state that two fields will take great advantage by the use of this material, namely thermoelectrics and photovoltaics. Unfortunately, up to now, there are no studies demonstrating the fabrication of a thermoelectric or photovoltaic device based on a SiGe NW. However, supported by the huge numbers of studies concerning the application of pure NWs in these fields,[37,208] we can assess that SiGe NWs will strongly contribute to further improvements. In particular, in the case of thermoelectrics, as we have seen in the previous sections, the reduction in thermal conductivity (if compared with bulk values) observed in pure Si NW,[37] can be really enhanced in SiGe NWs by building structures with different interfaces or compositions. In fact it is expected that the significant difference in the mass or the presence of interfaces offer the possibility of engineering phonon scattering, while the similar electronic structure allows expecting a limited degradation of the electrical conductivity. On the other hand, though only with simulations, it has been demonstrated that the development of NW-based solar cell devices below some tens of nanometers, where confinement effects are important, can be exploited by the using coaxial Ge-core/Si-shell nanowires, thanks to their high doping efficiency consequence of the type-II band offset at the SiGe NWs.[116] Finally, another field in which the application of SiGe NWs can be envisaged is the spintronics, i.e., the spin-based data storage and manipulation technology. It is well-known that the research in this field is carried out on a 2-fold perspective, i.e., discovering new fundamental science and developing innovative technological devices. As we will see in the last paragraph, up to now SiGe NWs have been used as a platform for fundamental studies on spin manipulation and domain dynamics, though no example of a spintronic SiGe device has been yet fabricated.

5.1. High-Performance Nanoelectronic Components

In this section we will review the most recent advances in electronic devices based on SiGe nanowires. The most common solution is using a nanowire-based system as the channel of a field effect transistor (FET). The systems discussed in section 2 can all provide potential advantages for the design of efficient devices, though for different reasons. The interest in alloy NWs, for instance, derives from the use of a material with enhanced properties, such as a tunable band gap. Core−shell NWs, on the other hand, are expected to outperform conventional Si or Ge channel FET mostly due to a design reason: the shell effectively confine carriers in the core, thus reducing surface scattering and increasing the mobility.

5.1.1. $Si_{1-x}Ge_x$ Alloy Nanowire Transistor. $Si_{1-x}Ge_x$ alloy NWs are interesting as material for FET channels mainly because adding some Ge to a Si NW should lead to an increase in the mobility, which is larger in Ge than in Si for both electron and holes.

The first $Si_{1-x}Ge_x$ alloy nanowire FET was reported by Kim et al.[243] They successfully obtained *n*- and *p*-type $Si_{0.5}Ge_{0.5}$ devices, by in situ doping with PH_3 and B_2H_6 the 40 nm alloy nanowire. The gate voltage V_g was applied through the degenerate Si substrate across the SiO_2. Resistivities of 17.4 and 9.27 Ω cm at V_g were extracted from the linear $I-V$ curves, for the *p*- and the *n*-type FET, respectively. The modeling of

dx.doi.org/10.1021/cr400261y | Chem. Rev. 2014, 114, 1371−1412

the nanowire as a cylindrical capacitor leads to estimate mobilities of 6.07×10^{-1} and 2.09 cm^2/V.

Shortly after, Whang et al.[123] reported a similar MOSFET structure ($Si_{1-x}Ge_x$ NW of 20 nm diameter, in situ doping with PH_3) with I_{on}/I_{off} ratio of 10^4 and a low gate leakage current of 10^{-11} A. A remarkable novelty in this device was the use of a high-κ HfO_2 grown by atomic layer deposition (ALD) as a gate dielectric, which results in a better control of the gate, especially when the oxide thickness is reduced up to 5 nm.[124]

The role of alloying on the mobility of SiGe alloy NWs was studied by Seong et al.[244] in $Si_{1-x}Ge_x$ wire of increasing Ge concentration ($0 < x < 0.3$). The mobility was estimated in a particularly careful way, accounting for the non-negligible contact resistance and measuring the effective channel length that is shortened upon contact silicidation. They reached the surprising conclusion that both the hole mobility and the I_{on}/I_{off} ratio decrease with Ge content. Carrier mobility in these $Si_{1-x}Ge_x$ FET turned out to be dominated by interface Ge−O and Si−O−Ge bonds that act as surface traps, as shown by photoemission experiments.

These results showed that the assumption that SiGe alloy NWs should have higher mobility than Si NWs, based on the fact that bulk Ge has higher carrier mobility than Si, was at least oversimplified. A more complex scenario emerges, highlighting the role surface trap levels and their dependence on the Ge concentration. As a matter of fact, none of the FET based on $Si_{1-x}Ge_x$ alloy NWs to date[54,65,123,124,243,247−249] has convincingly shown larger mobilities with respect to Si NW FET.[250,251]

Besides the promise of increased mobilities, a promise yet to be fulfilled, another great advantage of SiGe alloy NWs is that their band gap can be tuned by controlling the composition of the alloy. A tunable band gap, though not within a tremendously large energy window (E_{gap} = 0.75 and 1.1 eV for Ge and Si, respectively, in the absence of strong confinement effects), would be of utter interest for optoelectronic applications. The band gap has indeed been successfully modulated by controlling the Ge concentration in $Si_{1-x}Ge_x$ NWs.[51,92,244]

Recently, Kim et al.[112] fabricated a multiterminal contacted ⟨110⟩ SiGe NW where the Ge composition varied continuously by ∼4.5% per 1 μm along the NW axis. Each of the 3.7 μm nanowire segments obtained could then be measured as the channel of a given Ge compositions (within an axial variation of 15%). This setup grants access to five segments of $Si_{1-x}Ge_x$ NW of increasing Ge content ($0 < x < 1$) with a single measurement and permitted to show that both the dark conductivity, the photoconductivity and the photoconductive gain vary by up to 2 orders of magnitude due to the modulation of the band gap and surface-state density.

The modulability of the band gap, however, can also be exploited in electronic applications. Dayeh et al.[111] demonstrated a FET device based on a heterostructured NW, rather than a compositionally graded system, where the difference in the band gap of the Si and Ge side was used to tune the Schottky barrier heights. In this way they managed to avoiding ambipolar transport, which resulted in high on-currents of 50 $\mu A/\mu m$ and I_{on}/I_{off} ratio of 10^7. A similar idea was proposed by Jiang et al.,[252] this time with $Si_{1-x}Ge_x$ alloy NWs, where hole backscattering in the channel was minimized by playing with the relative Ge concentration of the channel and the source and drain contacts. In another axial heterojunction structure, this time between $Si/Si_{1-x}Ge_x$ rather than Si/Ge, Das Kanugo et al.[253] measured the I/V characteristic of a nominally undoped nanowire, finding a significantly low resistivity with respect to the nominal carriers concentration. This behavior was attributed to the presence of surface states which, like in pure Si and Ge NWs, can enhance the surface conductivity.

A Si/Ge axial heterojunction is also behind the efficient implementation of a tunneling field-effect transistor (TFET). In tunneling devices the gate voltage modulates the band-to-band tunneling injection of carriers, leading in principle to sharper switching and operating at lower bias. The performance of Si and Ge TFETs are limited by their ambipolar response where tunneling can occur at both the source-channel and drain-channel junction. This problem is normally obviated by reducing the symmetry of the device by doping or by gate alignment asymmetry. Le et al.[254] designed a TFET based on a Si/Ge NWs, reporting a suppression of ambipolar conduction with a very low I_{off} and a I_{on}/I_{off} ratio of 5 decades of current. Additionally, they showed that the same device can also operate as an efficient MOSFET. An example of TFET based on SiGe core−shell nanowires can be found in ref 255.

5.1.2. Si-Shell Ge-Core Nanowire Transistor. Unoptimized devices based on core−shell Si/Ge NWs had already been reported to be comparable to carbon nanotube FET,[87] but it was the observation of a one-dimensional hole-gas (see section 3) that opened up the way to a new class of nanowire-based devices.[100] This physical property of Si/Ge interfaces lead to a true milestone in nanowire devices, achieved by the same group 1 year later, by optimizing the device structure previously used. Xiang et al.[90] greatly increased the control over the gate coupling high-κ dielectrics (HfO_2 and ZrO_2) with a gate-all-around (GAA) geometry with metal top electrodes. The device obtained behaved like a p-type depletion mode FET and exhibited a peak transconductance g_m of 26 μS and a maximum drain current $I_{d(max)}$ of 35 μA, substantially outperforming single semiconductor NW-based FETs.[119,250] The estimated hole mobility of 730 $cm^2\ V^{-1}\ s^{-1}$ was more than 1 order of magnitude larger than state-of-the-art MOSFET and more than twice that of Ge and strained Si/Ge heterostructures PMOS devices.

The reproducibility of this device concept was demonstrated by the fabrication of FET with channel lengths varying from 170 nm to 1 μm, all of them exhibiting a high-performance behavior. The intrinsic switching delays τ, which provides an upper boundary to the frequency operation of the transistor, of these devices was up to three times shorter than planar devices with comparable channel lengths, thus envisaging the use of these Si/Ge FETs as high-frequency devices.

Carrier mobility is a common device metric to quantify the performances of electron devices, and most of the works reviewed in this section are no exception. Nevertheless, in strongly nanoscaled systems mobility is not well-defined, and it has been suggested that comparison against a device ballistic limit is more suitable. Following this approach, some of the properties of the device of ref 90 were compared to the results of simulations based on a semiclassical, ballistic transport model and a tight-binding description of the electronic structure.[256] This analysis demonstrated that the experimental device works between 60 and 85% of the ballistic limit. The simulation yielded additional insight into the device operation, showing that only 14−18 modes participate to the carrier transport and that an estimated 5 nm diameter ⟨110⟩ Ge core is required to observe true one-dimensional transport.

Nah et al.[257] produced the definitive smoking gun on the role of band-offset to achieve such extraordinary hole mobilities.

dx.doi.org/10.1021/cr400261y | Chem. Rev. 2014, 114, 1371−1412

Instead of building their FET device upon a Ge-core/Si-shell NW, they used a $Si_{1-x}Ge_x$ -shell, still wrapped around a Ge core. We have discussed several times how, by controlling the alloy composition, the electronic properties can be modulated. The valence band-offset is no exception and Nah et al. showed that it can be reduced from 0.55 to 0.4 eV by increasing the Ge content from $x = 0.3$ to 0.5.[258] The alloy shells were 3 nm thick and the only parameter varied was their composition. The higher mobilities were systematically observed in the FETs that had shells with lower Ge content, i.e., a larger valence band-offset. Also, the electrical measurements showed that the peak mobilities of $Si_{0.7}Ge_{0.3}$-Ge occurred at higher gate overdrives than with $Si_{0.5}Ge_{0.5}$-Ge FETs: a picture again consistent with a larger band-offset of the Si-rich shells, which thus requires higher gate biases to induce holes in the shell. These results proved to be robust and were confirmed in other device structures where the gate length or the shell thickness were varied. Similar core−shell devices had been previously used by the same group to study the effect of high-doping to reduce the series and contact resistance at the source and drain.[259] A detailed study of the scaling properties of these core−shell devices was reported one year later by the same authors.[260]

In a more recent work Zhao et al.[102] carried out a systematic study of the effect of the shell morphology and doping on the transport characteristic of a SiGe core−shell FET. *n*-type dopants cannot be activated if the Si shell is amorphous and their device exhibited a *p*-type behavior due to the dominant conduction of the nominally undoped Ge core. On the other hand, *n*-type conduction is recovered when the doped Si shell is synthesized at 600 °C, a growth condition that was shown to promote a single-crystalline structure.

5.2. From Quantum Transport to Superconductivity: SiGe Nanowires As Platforms for Fundamental Physics Studies

In this section we review those cases where SiGe NWs have been used to address fundamental physics topic, rather than to implement (nano)electronic devices. Specifically, we will discuss the role of SiGe NWs in (i) quantum transport in nanowire-quantum dots hybrid systems, (ii) quantum computing and spintronics, and (iii) superconductivity.

The growth of quantum dots with controlled shape and distribution has provided the ideal test-beds for several fundamental quantum transport studies. These quantum dots are either grown on substrates by the Stranski-Krastanow method[261,262] or embedded into a nanowire as short axial inclusion, typically of a III−V material into another III−V nanowire host.[76,263,264] As discussed previously in section 2.3, it is much more challenging to obtain sharp interfaces in group IV semiconducting nanowires and it would not be as easy as in III−V systems to observe the signature of quantum transport phenomena.

An effective workaround to these limitations consists in defining the quantum dots electrostatically. Roddaro et al.[265] patterned three metal gates on top of a SiGe core−shell NW: the two external gates are biased close to pinch-off and define the quantum dot, while the inner gate is used to modulate transport conditions. This setup allowed single level Coulomb blockade measurements to be performed where spin doublets are found to become sequentially filled by holes. The same concept was previously used by Hu et al.,[266] who defined two quantum dots by depleting the high mobility hole gas of a Ge-core/Si-shell NW.[100] Five gates are needed here: three create the barriers required to define the dots and two control the energy level of each dot. The middle barrier is also used to modulate the coupling between the two quantum dots.

Since the proposal of Kane,[267] great efforts have been devoted to the implementation of quantum computing within the realm of solid-state electronics. Group-IV elements are much better suited than III−V systems for quantum computing applications because the host nuclei (spin $I = 0$) are not a source of decoherence for the electron spins.[268−270] Using nanowires to implement Kane's original idea, where donor spins are used as qubits, could provide additional benefits such as deeper impurity states and a larger hyperfine interaction.[271] All of these considerations triggered a noticeable interest in exploring the use of SiGe NWs for quantum computing applications. These studies are highly intertwined with the broader field of spintronics, the developing of electronic devices that make use of the electron spin as well as the electron charge. The use of a controlled and strong spin−orbit interaction is the key to realize these spintronic devices. Ge-core/Si-shell NWs not only show high hole mobility and strong quantum confinement effects, but also possess low nuclear spin densities and consequently the promising possibility of long spin coherence times. Thus, recently, a large spin−orbit interaction of the Rashba type has been theoretically predicted for the hole states in SiGe NWs.[272] The Rashba effect is the spin splitting of electron energy levels without external magnetic field as a result of enhanced spin−orbit coupling in the material. In bulk solids it is connected with a lack of inversion symmetry of the crystal potential. In low-dimensional structures, this effect can be superimposed by an inversion asymmetry of the confinement potential. Thus, two components, that is material related spin−orbit coupling and quantum confinement, may contribute to the total spin splitting.[273]

From the experimental point of view Hao et al.[274] have investigated the temperature, back gate dependences of phase coherent length, spin−orbit relaxation time, and background conductance of individual undoped Ge/Si core/shell NWs with an average Ge core of 10 nm and a Si shell of 2 nm. They have observed one-dimensional weak antilocalization of holes in presence of strong spin−orbit coupling. In particular it was possible to show that the spin−orbit coupling strength, obtained taking into account the Rashba effect, can be modulated by more than five fold with an external field.

Another possible spin qubit device based on Ge-core/Si-shell NWs has been proposed by Hu et al.[275] and is shown in Figure 37. They demonstrated state preparation, pulsed gate control, and charge-sensing readout of hole spins confined on a double quantum dot, defined by barriers in the nanowire. Large spin-relaxation times, up to 0.6 ms, at zero magnetic field are measured, showing the potential for coherent spintronics.

Other opportunities to develop interesting devices based on SiGe NWs are given by the possibility to couple the low-dimensionality of these systems with superconducting phenomena. Nanoscale superconductor/semiconductor hybrid devices were fabricated by Xiang et al.[276] using undoped Ge-core/Si-shell NWs contacted by superconducting leads. A mesoscopic Josephson junction is obtained that show tunable dissipationless supercurrents and clear signatures of multiple Andreev reflections.

6. CONCLUSIONS AND PERSPECTIVES

Semiconductors are the most important materials in our modern technology-based world. In particular, in the last two decades, semiconductor nanostructures have become one of the

dx.doi.org/10.1021/cr400261y | *Chem. Rev.* 2014, 114, 1371−1412

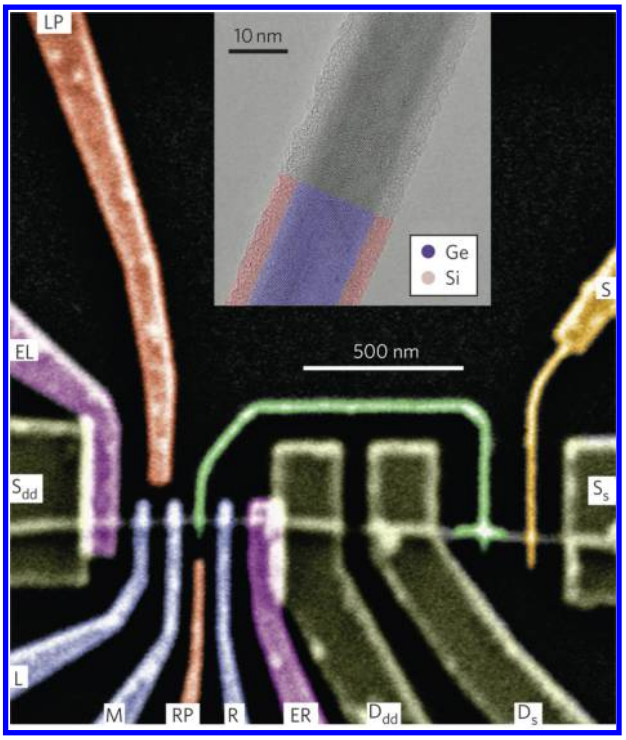

Figure 37. Scanning electron micrograph of a Ge-core/Si-shell nanowire contacted by four palladium electrodes (Sdd, Ddd, Ss, Ds, gray) and covered by a HfO2 gate dielectric layer. A TEM image of the core−shell wire is shown in the inset. Reprinted with permission from ref 275. Copyright 2012 Nature Publishing Group.

most rapidly developing area within the nanoscience research community. Among the different semiconductor nanostructures, SiGe nanowires, that can be manipulated through size reduction, geometry variation, and alloying, are considered one of the key developments for next generation technologies, due to their ease of processing, unique properties, and compatibility with the existent silicon based microelectronics industry. In this review we have thoroughly discussed the major advances in the synthesis of SiGe nanowires, their experimental and theoretical characterization and the progresses done in device applications.

The different employed growth techniques for SiGe nanowires, their morphology and structural properties were discussed in details (section 2). SiGe NWs are truly products of this new millennium: the first nanoscopic SiGe alloy NWs were produced in 2000 using laser-assisted catalytic growth.[41] Significant progresses toward a precise control of the NWs composition were subsequently made in chemical vapor deposition using an appropriate gas inlet ratio in an optimum temperature range[49] or tuning the total growth pressure.[52] Long and straight, without significant tapering, SiGe NWs were obtained through the use of additional gases, other than the usual precursors.[58,59] Regarding the morphology both axial and radial heterostructures have been reported so far. When laser ablation and CVD techniques were combined, axially modulated SiGe NWs of different diameters were produced.[68] A better control of the interface sharpness, of the order of 1 nm, has been then reached combining VLS and VSS growth.[78] Indeed an atomically abrupt interface has been reported in 2013.[84] Such abrupt heterojunctions are required to improve functionalities in both electronic and optoelectronic devices. Radial heterostructures (SiGe and GeSi core−shell NWs) were first reported in 2002.[87] A problem here is the control of strain relaxation. Dislocation free Ge-core/Si-shell NWs with different orientations and diameters[99] have been obtained altering the surface energies involved. In the case of Si-core/Ge-shell NWs smooth and uniform coaxial wires have, instead, been obtained only for core diameters below a certain threshold.[87,103]

The relation between growth parameters, shape, homogeneity, crystallinity of the synthesized SiGe nanowires and their chemical and physical properties has been discussed in detail in section 3. In evidence, here, were (i) the ability to tune the NWs optical gap by intrinsic alloy and extrinsic size effects,[51] (ii) the possibility to modulate the conductivity of an alloy nanowire along its axis,[112] (iii) the observation of hole gas accumulation in SiGe and GeSi core/shell NWs,[100,117,118] and, regarding the thermoelectric properties, (iv) the large improvement in the figure of merit, for SiGe NWs with different diameter and Ge concentration, with respect to bulk materials and to Si nanowires.[149]

The rapid developing theoretical studies, that includes the most advanced *ab initio* techniques, of the structural, electronic, optical and transport properties of the SiGe NWs have been highlighted in section 4, reviewing in particular the role of composition, size, geometry and strain. The presented results confirm the widespread belief that *ab initio* approaches constitute a unique and very powerful instrument to control and design the properties of novel materials and devices with an accuracy that complements experimental observations.

Finally, in section 5, we have presented recent advances in SiGe nanowires based devices, ranging from nanoelectronics, for example regarding FET and MOSFET components[54,65,123,124,243,247−249] to thermoelectrics,[146,149,150] quantum computing,[275] spintronics,[274] and superconductivity.[276]

It is clear that SiGe nanowires will play an important role in the next generation of advanced miniaturized devices; nevertheless, in order to have success, there is, on the theoretical side, the necessity to further develop and implement computational approaches (for example through a full inclusion of many-body effects in the determination of the physical properties of these nanoscale materials), and, on the experimental side, the need to have growth techniques with high processing resolution and efficiency. In fact an accurate control of size, composition, crystallinity, band gap engineering, and doping features will be the key factor toward the integration of SiGe nanowires, with their unique electronic, optical, and transport properties, into the current technologies. In this respect many breakthroughs should be expected in the near future, in particular through increasing common effort between experimentalists and theorists.

AUTHOR INFORMATION

Corresponding Authors

*E-mail: michele.amato@u-psud.fr.
*E-mail: maurizia.palummo@roma2.infn.it.
*E-mail: rrurali@icmab.es.
*E-mail: stefano.ossicini@unimore.it.

Notes

The authors declare no competing financial interest.

Biographies

Michele Amato is Assistant Professor at Institut d'Electronique Fondamentale of Université Paris-Sud. In 2007 he received a M.Sc. degree in Materials Engineering at Università Federico II, Naples, Italy, with a thesis entitled *Theoretical Study of Metal-Graphene Interactions for Applications in Nanoelectronics*. In 2011 he received his Ph.D. in Physics at the Ph.D. School in *Nano and Physical Sciences* of Università di Modena e Reggio Emilia, Italy, with a thesis entitled *Structural, electronic and optical properties of SiGe nanowires: Ab initio results*. He was a visiting scientist at Institut de Ciència de Materials de Barcelona from 2009 to 2011. In January 2012 he moved to Paris to working at Laboratoire de Physiques des Solides of Université Paris Sud. In March 2013 he was awarded a Marie Curie Intra-European Fellowship to work as a Senior Researcher at École Polytechnique in Paris. His research is devoted to the application of computational modeling to outstanding problems and issues in materials science, using *ab initio* quantum mechanical theory and codes, with a particular focus on nanoscience. He has contributed to 11 publications in high impact journals and presented his work at several international conferences and workshops.

Maurizia Palummo, after a stage in experimental Condensed Matter Physics during her Master Degree, since 1991 has worked in the field of *ab initio* calculations of the structural and electronic properties of materials. In particular during her Ph.D. she worked with Dr. Lucia Reining (Ecole Polytechnique, Palaiseau, France) performing pioneering GW calculations on wide-band gap materials. A member of the European Theoretical Spectroscopy Facility, she is an expert in the most modern theories and computational tools of *ab initio* electronic structure calculations (density functional theory and many-body perturbation theory methods). The main focus of her present research is on the calculation of electronic and optical properties of surfaces, nanostructures, and organic molecules. She has been co-organizer of several international conferences and some of the Nanowires workshop series. She was a visiting scientist in the group of Prof. J. Grossman at the DSME of the Massachusetts Institute of Technology (Cambridge, MA) during summer 2012. The author of more than 80 articles in international scientific journals, since 2004 she has been a researcher at the Department of Physics at the Università di Roma, Tor Vergata, Italy.

Riccardo Rurali graduated in Electrical Engineering from the Politecnico di Milano in 1996. After working for two years at ABB Industrial Systems, between Milan, Italy and Västerås, Sweden, he obtained his Ph.D. in 2003 at the Centro Nacional de Micorelectrónica in Barcelona, Spain, where he worked on the theoretical modeling of defects in silicon carbide. He was then a postdoc fellow at the group led by Prof. Nicolás Lorente at the Université Paul Sabatier in Toulouse, France, working on surface science related topics. He returned to Barcelona in 2006 to join the group of Computational Nanoelectronics lead by Prof. Jordi Suñé at the Universitat Autònoma de Barcelona, whose research topics are the simulation and modeling of emerging electronic devices. He is now a tenured scientist at the Institut de Ciència de Materials de Barcelona (ICMAB-CSIC) where he works on the theoretical modeling of the structural and electronic properties of semiconducting nanowires and of different nanoscale systems. In 2008 he initiated and has been the co-organizer since then of the Nanowires workshop series, which has gathered more than 400 researchers from all over the world throughout its six editions.

Stefano Ossicini, after graduating (1976) in Physics at the Università di Roma La Sapienza, was active as postdoctoral associate and assistant in the Department of Physics of the Università di Roma La Sapienza, the Department of Theoretical Physics of the Freie Universitäet in Berlin, the Department of Physics of the Università della Calabria, Italy, and finally the Università di Modena e Reggio Emilia, where he is now Full Professor in the Department of Science and Methods of Engineering. His group is one of the leading theoretical groups in the field of semiconductor surfaces, interfaces, and nanosystems. He is the author

of more than 150 articles in international scientific journals and more than 20 chapters of books. He is the author of several books, in particular (with L. Pavesi and F. Priolo) *Light Emitting Silicon for Microphotonics* (Springer Verlag 2003, 2009) and (with V. N. Borisenko) *What is What in the Nanoworld* (Wiley-VCH 2004, 2008, 2012).

ACKNOWLEDGMENTS

We thank Uri Givan, Jeff Drucker, and Alexis Potié for providing data of their works, all those who granted permission for using figures of their original works, and Jie Chen for critically reading the manuscript. Funding of the Spanish Ministerio de Economía y Competitividad under Contract No. FIS2012-37549-C05-05 is greatly acknowledged. We would like to thank all the participants to the CECAM workshop "Theory, Simulation and Modelling of SiGe Nanostructures: from Nanoelectronics to Renewable Energy", that we organized in Lausanne (Switzerland) for their inspiring presentations and for the constructive discussions. Funding for this workshop by CECAM, ESF, and Ψ_k is greatly acknowledged.

REFERENCES

(1) Conibeer, G. *Mater. Today* **2007**, *10*, 42.
(2) Daldosso, N.; Pavesi, L. *Laser Photonics Rev.* **2009**, *3*, 508.
(3) Rurali, R. *Rev. Mod. Phys.* **2010**, *82*, 427.
(4) Khriachtchev, L.; Ossicini, S.; Iacona, F.; Gourbilleau, F. *Int. J. Photoenergy* **2012**, *2012*, 1.
(5) Govoni, M.; Marri, I.; Ossicini, S. *Nat. Photonics* **2012**, *6*, 672.
(6) Abstreiter, G. *Thin Solid Films* **1989**, *183*, 1.
(7) Gnutzmann, U.; Clausecker, K. *Appl. Phys* **1974**, *3*, 9.
(8) Kasper, E.; Herzog, H.-J.; Kibbel, H. *Appl. Phys.* **1975**, *8*, 199.
(9) Bean, J. C.; Feldman, L. C.; Fiory, A. T.; Nakahara, S.; Robinson, I. K. *J. Vac. Sci. Technol. A* **1984**, *2*, 436.
(10) Kasper, E.; Herzog, H.-J.; Jorke, H.; Abstreiter, G. *Superlattices Microstruct.* **1987**, *3*, 141.
(11) Terashima, K.; Tajima, M.; Tatsumi, T. *Appl. Phys. Lett.* **1990**, *57*, 1925.
(12) Sturm, J.; Manoharan, H.; Lenchyshyn, L. C.; Thewalt, M. L. W.; Roweel, N. L.; Noël, J. P.; Houghton, D. C. *Phys. Rev. Lett.* **1991**, *66*, 1362.
(13) Whall, T. E.; Parker, E. H. C. *J. Mater. Sci.: Mater. Electron.* **1995**, *6*, 249.
(14) Patton, G. L.; Comfort, J. H.; Meyerson, B. S.; Crabbé, E. F.; Scilla, G. J.; de Frésart, E.; Stork, J. M. C.; Sun, J. Y.-C.; Harame, D. L.; Burghartz, J. N. *IEEE Electron Device Lett.* **1990**, *11*, 171.
(15) Lin, T. L.; Maserjian, J. *Appl. Phys. Lett.* **1990**, *57*, 1422.
(16) Xie, Y.-H.; Monroe, D.; Fitzgerald, E.; Silverman, P.; Thiel, F.; Watson, G. *Appl. Phys. Lett.* **1993**, *63*, 2263.
(17) Dingle, R.; Störmer, H. L.; Gossard, A. C.; Wiegmann, W. *Appl. Phys. Lett.* **1978**, *33*, 665.
(18) König, U.; Schäffler, F. *IEEE Electron Device Lett.* **1993**, *14*, 205.
(19) Schäffler, F. *Thin Solid Films* **1997**, *12*, 1515.
(20) Whall, T. E.; Parker, E. H. C. *Thin Sol. Films* **2000**, *369*, 297.
(21) Paul, D. J. *Semicond. Sci. Technol.* **2004**, *9*, R75.
(22) Lee, M. L.; Fitzgerald, E. A.; Bulsara, M. T.; Currie, M. T.; Lochtefeld, A. *J. Appl. Phys.* **2005**, *97*, 011101.
(23) Brunner, K. *Rep. Prog. Phys.* **2002**, *65*, 27.
(24) Berbezier, I.; Ronda, A. *Surf. Sci. Rep.* **2009**, *64*, 47.
(25) Aqua, J.-N.; Berbezier, I.; Favre, L.; Frisch, T.; Ronda, A. *Phys. Rep.* **2013**, *522*, 52.
(26) Hobbs, R. G.; Petkov, N.; Holmes, J. D. *Chem. Mater.* **2012**, *24*, 1975.
(27) Singh, N.; Buddharaju, K.; Manhas, S.; Agarwal, A.; Rustagi, S.; Lo, G.; Balasubramanian, N.; Kwong, D.-L. *IEEE Trans. Electron Devices* **2008**, *55*, 3107.
(28) Frucci, G.; Di Gaspare, L.; Evangelisti, F.; Giovine, E.; Notargiacomo, A.; Piazza, V.; Beltram, F. *Phys. Rev. B* **2010**, *81*, 195311.
(29) Notargiacomo, A.; Gaspare, L. D.; Scappucci, G.; Mariottini, G.; Evangelisti, F.; Giovine, E.; Leoni, R. *Appl. Phys. Lett.* **2003**, *83*, 302.
(30) Kanjanachuchai, S.; Thornton, T. J.; Fernández, J. M.; Ahmed, H. *Semicond. Sci. Technol.* **2001**, *16*, 72.
(31) Giovine, E.; Notargiacomo, A.; Gaspare, L. D.; Palange, E.; Evangelisti, F.; Leoni, R.; Castellano, G.; Torrioli, G.; Foglietti, V. *Nanotechnology* **2001**, *12*, 132.
(32) van Veen, R. G.; Verbruggen, A. H.; van der Drift, E.; Schäffler, F.; Radelaar, S. *Semicond. Sci. Technol.* **1999**, *14*, 508.
(33) van Veen, R. G.; Verbruggen, A. H.; van der Drift, E.; Schäffler, F.; Radelaar, S. *Phys. Rev. B* **2000**, *61*, 7545.
(34) Lu, W.; Lieber, C. M. *J. Phys. D: Appl. Phys.* **2006**, *39*, R387.
(35) Fan, H. J.; Werner, P.; Zacharias, M. *Small* **2006**, *2*, 700.
(36) Schmidt, V.; Wittemann, J. V.; Gösele, U. *Chem. Rev.* **2010**, *110*, 361.
(37) Hochbaum, A. I.; Yang, P. *Chem. Rev.* **2010**, *110*, 527.
(38) Collins, G.; Holmes, J. D. *J. Mater. Chem.* **2011**, *21*, 11052.
(39) Wagner, R. S.; Ellis, W. C. *Appl. Phys. Lett.* **1964**, *4*, 89.
(40) Morales, A. M.; Lieber, C. M. *Science* **1998**, *279*, 208.
(41) Duan, X.; Lieber, C. M. *Adv. Mater.* **2000**, *12*, 298.
(42) Wang, N.; Tang, Y. H.; Zhang, Y. F.; Lee, C. S.; Lee, S. T. *Phys. Rev. B* **1998**, *58*, R16024.
(43) Holmes, J. D.; Johnston, K. P.; Doty, R. C.; Korgel, B. A. *Science* **2000**, *287*, 1471.
(44) Geyer, N.; Huang, Z.; Fuhrmann, B.; Grimm, S.; Reiche, M.; Nguyen-Duc, T.-K.; de Boor, J.; Leipner, H. S.; Werner, P.; Gösele, U. *Nano Lett.* **2009**, *9*, 3106.
(45) Schmidt, V.; Wittemann, J. V.; Senz, S.; Gösele, U. *Adv. Mater.* **2009**, *21*, 2681.
(46) Wang, N.; Cai, Y.; Zhang, R. *Mater. Sci. Eng. R* **2008**, *60*, 1.
(47) Wolfsteller, A.; Geyer, N.; Nguyen-Duc, T.-K.; Kanungo, P. D.; Zakharov, N.; Reiche, M.; Erfurth, W.; Blumtritt, H.; Kalem, S.; Werner, P.; Gösele, U. *Thin Solid Films* **2010**, *518*, 2555.
(48) Non-VLS alloy SiGe NWs were previously reported. The nanowires were formed by pulsed UV laser induced epitaxy of Ge NWs deposited on a Si substrate.[277]
(49) Lew, K.-K.; Pan, L.; Dickey, E.; Redwing, J. *Adv. Mater.* **2003**, *15*, 2073.
(50) Lew, K.-K.; Pan, L.; Dickey, E. C.; Redwing, J. M. *J. Mater. Res.* **2006**, *21*, 2876.
(51) Yang, J.-E.; Jin, C.-B.; Kim, C.-J.; Jo, M.-H. *Nano Lett.* **2006**, *6*, 2679.
(52) Givan, U.; Patolsky, F. *Nano Lett.* **2009**, *9*, 1775.
(53) Dailey, E.; Madras, P.; Drucker, J. *Appl. Phys. Lett.* **2010**, *97*, 143106.
(54) Qi, C.; Goncher, G.; Solanki, R.; Jordan, J. *Nanotechnology* **2007**, *18*, 075302.
(55) Potie, A.; Baron, T.; Dhalluin, F.; Rosaz, G.; Salem, B.; Latu-Romain, L.; Kogelschatz, M.; Gentile, P.; Oehler, F.; Montes, L.; Kreisel, J.; Roussel, H. *Nanoscale Res. Lett.* **2011**, *6*, 187.
(56) Kawashima, T.; Imamura, G.; Fujii, M.; Hayashi, S.; Saitoh, T.; Komori, K. *J. Appl. Phys.* **2007**, *102*, 124307.
(57) Lu, Q.; Adu, K. W.; Gutierrez, H. R.; Chen, G.; Lew, K.-K.; Nimmatoori, P.; Zhang, X.; Dickey, E. C.; Redwing, J. M.; Eklund, P. C. *J. Phys. Chem. C* **2008**, *112*, 3209.
(58) Potié, A.; Baron, T.; Latu-Romain, L.; Rosaz, G.; Salem, B.; Montès, L.; Gentile, P.; Kreisel, J.; Roussel, H. *J. Appl. Phys.* **2011**, *110*, 024311.
(59) Lee, W.-J.; Ma, J. W.; Bae, J. M.; Park, S. H.; Cho, M.-H.; Ahn, J. P. *CrystEngComm* **2011**, *13*, 5204.
(60) Zhuang, X.; Ning, C. Z.; Pan, A. *Adv. Mater.* **2012**, *24*, 13.
(61) Ben-Ishai, M.; Patolsky, F. *Nano Lett.* **2012**, *12*, 1121.
(62) Kim, I.; Lee, K.-Y.; Kim, U.; Park, Y.-H.; Park, T.-E.; Choi, H.-J. *Nanoscale Res. Lett.* **2010**, *5*, 1535.
(63) Zhang, X.; Lew, K.-K.; Nimmatoori, P.; Redwing, J. M.; Dickey, E. C. *Nano Lett.* **2007**, *7*, 3241.

(64) Ma, J. W.; Lee, W. J.; Bae, J. M.; Jeong, K. S.; Kang, Y. S.; Cho, M. H.; Seo, J. H.; Ahn, J. P.; Chung, K. B.; Song, J. Y. *Nano Lett.* **2013**, *13*, 1118.
(65) Givan, U.; Kwiat, M.; Patolsky, F. *J. Phys. Chem. C* **2010**, *114*, 4331.
(66) Other defects, such as twin boundaries and kinks, can also be found,[278] though they are not specific of SiGe heterostructures and are also rather common in single-phase nanowires.
(67) Vincent, L.; Boukhicha, R.; Cherkashin, N.; Reboh, S.; Patriarche, G.; Renard, C.; Yam, V.; Fossard, F.; Bouchier, D. *Nanotechnology* **2012**, *23*, 395701.
(68) Wu, Y.; Fan, R.; Yang, P. *Nano Lett.* **2002**, *2*, 83.
(69) Early reports of micrometer-sized Ge whiskers on top of Si whiskers date back to 1971.[279]
(70) Redwing, J. M.; Lew, K.-K.; Bogart, T. E.; Pan, L.; Dickey, E. C.; Carim, A. H.; Wang, Y.; Cabassi, M. A.; Mayer, T. S. *Proc. SPIE* **2004**, *5361*, 52.
(71) Mouchet, C.; Latu-Romain, L.; Cayron, C.; Rouviere, E.; Celle, C.; Simonato, J.-P. *Nanotechnology* **2008**, *19*, 335603.
(72) Dujardin, R.; Poydenot, V.; Devillers, T.; Favre-Nicolin, V.; Gentile, P.; Barski, A. *Appl. Phys. Lett.* **2006**, *89*, 153129.
(73) Zakharov, N.; Werner, P.; Gerth, G.; Schubert, L.; Sokolov, L.; Gösele, U. *J. Cryst. Growth* **2006**, *290*, 6.
(74) Clark, T. E.; Nimmatoori, P.; Lew, K.-K.; Pan, L.; Redwing, J. M.; Dickey, E. C. *Nano Lett.* **2008**, *8*, 1246.
(75) Li, N.; Tan, T. Y.; Gösele, U. *Appl. Phys. A: Mater. Sci. Process.* **2008**, *90*, 591.
(76) Björk, M. T.; Ohlsson, B. J.; Thelander, C.; Persson, A. I.; Deppert, K.; Wallenberg, L. R.; Samuelson, L. *Appl. Phys. Lett.* **2002**, *81*, 4458.
(77) Eisenhawer, B.; Sivakov, V.; Berger, A.; Christiansen, S. *Nanotechnology* **2011**, *22*, 305604.
(78) Wen, C.-Y.; Reuter, M. C.; Bruley, J.; Tersoff, J.; Kodambaka, S.; Stach, E. A.; Ross, F. M. *Science* **2009**, *326*, 1247.
(79) Wang, Y.; Schmidt, V.; Senz, S.; Gösele, U. *Nat. Nanotechnol.* **2006**, *1*, 186.
(80) Kodambaka, S.; Tersoff, J.; Reuter, M. C.; Ross, F. M. *Science* **2007**, *316*, 729.
(81) Chou, Y.-C.; Wen, C.-Y.; Reuter, M. C.; Su, D.; Stach, E. A.; Ross, F. M. *ACS Nano* **2012**, *6*, 6407.
(82) Perea, D. E.; Li, N.; Dickerson, R. M.; Misra, A.; Picraux, S. T. *Nano Lett.* **2011**, *11*, 3117.
(83) Monasterio, M.; Rodríguez, A.; Rodríguez, T.; Ballesteros, C. *MRS Proc.* **2012**, *1408*, 111080.
(84) Geaney, H.; Mullane, E.; Ramasse, Q. M.; Ryan, K. M. *Nano Lett.* **0**, *0*, null.
(85) Geaney, H.; Dickinson, C.; Barrett, C. A.; Ryan, K. M. *Chem. Mater.* **2011**, *23*, 4838.
(86) Geaney, H.; Kennedy, T.; Dickinson, C.; Mullane, E.; Singh, A.; Laffir, F.; Ryan, K. M. *Chem. Mater.* **2012**, *24*, 2204.
(87) Lauhon, L. J.; Gudiksen, M. S.; Wang, D.; Lieber, C. M. *Nature* **2002**, *420*, 57.
(88) At variance with the two-step growth process, common to all the cases discussed in this Section, some reports exist where SiGe core−shell nanowires with very diffuse interfaces were grown in a single-step process.[280,281]
(89) Dayeh, S. A.; Tang, W.; Boioli, F.; Kavanagh, K. L.; Zheng, H.; Wang, J.; Mack, N. H.; Swadener, G.; Huang, J. Y.; Miglio, L.; Tu, K.-N.; Picraux, S. T. *Nano Lett.* **2103**, *13*, 1869.
(90) Xiang, J.; Lu, W.; Hu, Y.; Wu, Y.; Yan, H.; Lieber, C. M. *Nature* **2006**, *441*, 489.
(91) Goldthorpe, I. A.; Marshall, A. F.; McIntyre, P. C. *Nano Lett.* **2008**, *8*, 4081.
(92) Dayeh, S. A.; Mack, N. H.; Huang, J. Y.; Picraux, S. T. *Appl. Phys. Lett.* **2011**, *99*, 023102.
(93) Dayeh, S. A.; Gin, A. V.; Picraux, S. T. *Appl. Phys. Lett.* **2011**, *98*, 163112.
(94) Gutkin, M. Y.; Ovid'ko, I. A.; Sheinerman, A. G. *J. Phys.: Condens. Matter* **2000**, *12*, 5391.
(95) Ovid'ko, I. A.; Sheinerman, A. G. *Philos. Mag.* **2004**, *84*, 2103.
(96) Kolesnikova, A. L.; Romanov, A. E. *Philos. Mag. Lett.* **2004**, *84*, 501.
(97) Liang, Y.; Nix, W. D.; Griffin, P. B.; Plummer, J. D. *J. Appl. Phys.* **2005**, *97*, 043519.
(98) Schmidt, V.; McIntyre, P. C.; Gösele, U. *Phys. Rev. B* **2008**, *77*, 235302.
(99) Goldthorpe, I. A.; Marshall, A. F.; McIntyre, P. C. *Nano Lett.* **2009**, *9*, 3715.
(100) Lu, W.; Xiang, J.; Timko, B. P.; Wu, Y.; Lieber, C. M. *Proc. Natl. Acad. Sci. U.S.A.* **2005**, *102*, 10046.
(101) Cao, Y. Y.; Ouyang, G.; Wang, C. X.; Yang, G. W. *Nano Lett.* **2013**, *13*, 436.
(102) Zhao, Y.; Smith, J. T.; Appenzeller, J.; Yang, C. *Nano Lett.* **2011**, *11*, 1406.
(103) Pan, L.; Lew, K.-K.; Redwing, J. M.; Dickey, E. C. *Nano Lett.* **2005**, *5*, 1081.
(104) Palacios, T. *Nature* **2012**, *481*, 152.
(105) Thelander, C.; Agarwal, P.; Brongersma, S.; Eymery, J.; Feiner, L.; Forchel, A.; Scheffler, M.; Riess, W.; Ohlsson, B.; Gösele, U.; Samuelson, L. *Mater. Today* **2006**, *9*, 28.
(106) Dhara, S.; Sengupta, S.; Solanki, H. S.; Maurya, A.; R., A. P.; Gokhale, M. R.; Bhattacharya, A.; Deshmukh, M. M. *Appl. Phys. Lett.* **2011**, *99*, 173101.
(107) Ren, R.; Cheng, W. P. Y. *Phys. Rev. B* **2004**, *69*, 235327.
(108) Kawashima, T.; Imamura, G.; Fujii, M.; Hayashi, S.; Saitoh, T.; Komori, K. *J. Appl. Phys.* **2007**, *102*, 124307.
(109) Nishimura, C.; Imamura, G.; Fujii, M.; Kawashima, T.; Saitoh, T.; Hayashi, S. *Appl. Phys. Lett.* **2008**, *93*, 203101.
(110) Yang, J.-E.; Park, W.-H.; Kim, C.-J.; Kim, Z. H.; Jo, M.-H. *Appl. Phys. Lett.* **2008**, *92*, 263111.
(111) Dayeh, S. A.; Dickerson, R. M.; Picraux, S. T. *Appl. Phys. Lett.* **2011**, *99*, 113105.
(112) Kim, C.-J.; Lee, H.-S.; Cho, Y.-J.; Yang, J.-E.; Lee, R. R.; Lee, J. K.; Jo, M.-H. *Adv. Mater.* **2011**, *23*, 1025.
(113) He, J. H.; Wu, W. W.; Lee, S. W.; Chen, L. J.; Chueh, Y. L.; Chou, L. J. *Appl. Phys. Lett.* **2005**, *86*, 263109.
(114) Chang, H.-Y.; Tsybeskov, L.; Sharma, S.; Kamins, T. I.; Wu, X.; Lockwood, D. J. *Appl. Phys. Lett.* **2009**, *95*, 133120.
(115) Menéndez, J.; Singh, R.; Drucker, J. *Ann. Phys. (Berlin)* **2011**, *523*, 145.
(116) Amato, M.; Ossicini, S.; Rurali, R. *Nano Lett.* **2011**, *11*, 594.
(117) Zhang, S.; Lopez, F. J.; Hyun, J. K.; Lauhon, L. J. *Nano Lett.* **2010**, *10*, 4483.
(118) Li, L.; Smith, D. J.; Dailey, E.; Madras, P.; Drucker, J.; McCartney, M. R. *Nano Lett.* **2011**, *11*, 493.
(119) Wang, D.; Wang, Q.; Javey, A.; Tu, R.; Dai, H.; Kim, H.; McIntyre, P. C.; Krishnamohan, T.; Saraswat, K. C. *Appl. Phys. Lett.* **2003**, *83*, 2432.
(120) Nah, J.; Dillen, D. C.; Varahramyan, K. M.; Banerjee, S. K.; Tutuc, E. *Nano Lett.* **2012**, *12*, 108.
(121) Dillen, D. C.; Varahramyan, K. M.; Corbet, C. M.; Tutuc, E. *Phys. Rev. B* **2012**, *86*, 045311.
(122) Kim, C.-J.; Yang, J.-E.; Lee, H.-S.; Jang, H. M.; Jo, M.-H.; Park, W.-H.; Kim, Z. H.; Maeng, S. *Appl. Phys. Lett.* **2007**, *91*, 033104.
(123) Whang, S. J.; Lee, S. J.; Yang, W. F.; Cho, B. J.; Kwong, D. L. *Appl. Phys. Lett.* **2007**, *91*, 072105.
(124) Yang, W. F.; Lee, S. J.; Liang, G. C.; Whang, S. J.; Kwong, D. L. *Nanotechnology* **2008**, *19*, 225203.
(125) Nishimura, C.; Imamura, G.; Fujii, M.; Kawashima, T.; Saitoh, T.; Hayashi, S. *J. Phys. Chem. C* **2009**, *113*, 5467.
(126) Fukata, N.; Mitome, M.; Sekiguchi, T.; Bando, Y.; Kirkham, M.; Hong, J.-I.; Wang, Z. L.; Snyder, R. L. *ACS Nano* **2012**, *6*, 8887.
(127) Lee, H.; Choi, H. J. *Nano Lett.* **2010**, *10*, 2207.
(128) Nah, J.; Varahramyan, K.; Liu, E.-S.; Banerjee, S. K.; Tutuc, E. *Appl. Phys. Lett.* **2008**, *93*, 203108.
(129) Monasterio, M.; Rodríguez, A.; Rodríguez, T.; Ballesteros, C. *MRS Proc.* **2012**, *1408*, 111052.

(130) Dismukes, J. P.; Ekstrom, L.; Steigmeier, E. F.; Kudman, I.; Beers, D. S. *J. Appl. Phys.* **1964**, *35*, 2899.
(131) Rowe, D. M.; Shukla, V. S.; Savvides, N. *Nature* **1981**, *290*, 765.
(132) Rowe, D. M.; Shukla, V. S. *J. Appl. Phys.* **1981**, *52*, 7421.
(133) Huxtable, S. T.; Abramson, A. R.; Tien, C.-L.; Majumdar, A.; LaBounty, C.; Fan, X.; Zeng, G.; Bowers, J. E.; Shakouri, A.; Croke, E. T. *Appl. Phys. Lett.* **2002**, *80*, 1737.
(134) Hochbaum, A. I.; Chen, R.; Delgado, R. D.; Liang, W.; Garnett, E. C.; Najarian, M.; Majumdar, A.; Yang, P. *Nature* **2008**, *451*, 163.
(135) Boukai, A. I.; Bunimovich, Y.; Tahir-Kheli, J.; Yu, J.-K.; Goddard, W. A., III; Heath, J. R. *Nature* **2008**, *451*, 168.
(136) Wang, X. W.; Lee, H.; Lan, Y. C.; Zhu, G. H.; Joshi, G.; Wang, D. Z.; Yang, J.; Muto, A. J.; Tang, M. Y.; Klatsky, J.; Song, S.; Dresselhaus, M. S.; Chen, G.; Ren, Z. F. *Appl. Phys. Lett.* **2008**, *93*, 193121.
(137) Joshi, G.; Lee, H.; Lan, Y.; Wang, X.; Zhu, G.; Wang, D.; Gould, R. W.; Cuff, D. C.; Tang, M. Y.; Dresselhaus, M. S.; Chen, G.; Ren, Z. *Nano Lett.* **2008**, *8*, 4670.
(138) Li, D.; Wu, Y.; Fan, R.; Yang, P.; Majumdar, A. *Appl. Phys. Lett.* **2003**, *83*, 3186.
(139) Kim, H.; Kim, I.; Choi, H.-J.; Kim, W. *Appl. Phys. Lett.* **2010**, *96*, 233106.
(140) Vining, C. B.; Laskow, W.; Hanson, J. O.; der Beck, R. R. V.; Gorsuch, P. D. *J. Appl. Phys.* **1991**, *69*, 4333.
(141) Yin, L.; Lee, E. K.; Lee, J. W.; Whang, D.; Choi, B. L.; Yu, C. *Appl. Phys. Lett.* **2012**, *101*, 043114.
(142) Stöhr, H.; Klemm, W. *Z. Anorg. Allg. Chem.* **1939**, *241*, 305.
(143) Zhu, G. H.; Lee, H.; Lan, Y. C.; Wang, X. W.; Joshi, G.; Wang, D. Z.; Yang, J.; Vashaee, D.; Guilbert, H.; Pillitteri, A.; Dresselhaus, M. S.; Chen, G.; Ren, Z. F. *Phys. Rev. Lett.* **2009**, *102*, 196803.
(144) Martinez, J. A.; Provencio, P. P.; Picraux, S. T.; Sullivan, J. P.; Swartzentruber, B. S. *J. Appl. Phys.* **2011**, *110*, 074317.
(145) Kim, H.; Park, Y.-H.; Kim, I.; Kim, J.; Choi, H.-J.; Kim, W. *Appl. Phys. A: Mater. Sci. Process.* **2011**, *104*, 23.
(146) Wingert, M. C.; Chen, Z. C. Y.; Dechaumphai, E.; Moon, J.; Kim, J.-H.; Xiang, J.; Chen, R. *Nano Lett.* **2011**, *11*, 5507.
(147) Hu, M.; Giapis, K. P.; Goicochea, J. V.; Zhang, X.; Poulikakos, D. *Nano Lett.* **2011**, *11*, 618.
(148) Related to nondiffusive thermal transport, very recently, Hsiao et al.[282] reported ballistic heat transport at room temperature persisting over 8.3 μm in SiGe NWs with different structures and alloy concentrations.
(149) Lee, E. K.; Yin, L.; Lee, Y.; Lee, J. W.; Lee, S. J.; Lee, J.; Cha, S. N.; Whang, D.; Hwang, G. S.; Hippalgaonkar, K.; Majumdar, A.; Yu, C.; Choi, B. L.; Kim, J. M.; Kim, K. *Nano Lett.* **2012**, *12*, 2918.
(150) Moon, J.; Kim, J.-H.; Chen, Z. C.; Xiang, J.; Chen, R. *Nano Lett.* **2013**, *13*, 1196.
(151) Nam, S.; Jiang, X.; Xiong, Q.; Ham, D.; Lieber, C. M. *Proc. Natl. Acad. Sci. U.S.A.* **2009**, *106*, 21035.
(152) Bransden, B.; Joachain, C. *Quantum Mechanics*; Benjamin Cummings: Upper Saddle River, NJ, 2000.
(153) Beckman, S. P.; Han, J.; Chelikowsky, J. R. *Phys. Rev. B* **2006**, *74*, 165314.
(154) Kholod, A. N.; Shaposhnikov, V. L.; Sobolev, N.; Borisenko, V. E.; D'Avitaya, F. A.; Ossicini, S. *Phys. Rev. B* **2004**, *70*, 035317.
(155) Bruno, M.; Palummo, M.; Marini, A.; Del Sole, R.; Olevano, V.; Kholod, A. N.; Ossicini, S. *Phys. Rev. B* **2005**, *72*, 153310.
(156) Kagimura, R.; Nunes, R. W.; Chacham, H. *Phys. Rev. Lett.* **2007**, *98*, 026801.
(157) Bruno, M.; Palummo, M.; Marini, A.; Del Sole, R.; Ossicini, S. *Phys. Rev. Lett.* **2007**, *98*, 036807.
(158) Rurali, R.; Aradi, B.; Frauenheim, T.; Gali, A. *Phys. Rev. B* **2007**, *76*, 113303.
(159) Peressi, M.; Binggeli, N.; Baldereschi, A. *J. Phys. D: Appl. Phys.* **1998**, *31*, 1273.
(160) Zunger, A. *Curr. Opin. Solid State Mater. Sci.* **1998**, *3*, 32.
(161) Kasper, E.; Lyutovich, K. *Properties of Silicon Germanium and SiGe:Carbide*; IET: Edison, NJ, 2000.
(162) Suresh, C. J.; Willander, M. *Silicon-Germanium Strained Layers and Heterostructures*; Academic Press, Inc.: New York, 2003.
(163) Van de Walle, C. G.; Martin, R. M. *J. Vac. Sci. Technol. A* **1985**, *3*, 1256.
(164) Van de Walle, C. G.; Martin, R. M. *Phys. Rev. B* **1986**, *34*, 5621.
(165) Ciraci, S.; Batra, I. P. *Phys. Rev. B* **1988**, *38*, 1835.
(166) Hill, N. A.; Pokrant, S.; Hill, A. J. *J. Phys. Chem. B* **1999**, *103*, 3156.
(167) van Buuren, T.; Dinh, L. N.; Chase, L. L.; Siekhaus, W. J.; Terminello, L. J. *Phys. Rev. Lett.* **1998**, *80*, 3803.
(168) Bostedt, C.; van Buuren, T.; Willey, T. M.; Franco, N.; Terminello, L. J.; Heske, C.; Möller, T. *Appl. Phys. Lett.* **2004**, *84*, 4056.
(169) Musin, R. N.; Wang, X.-Q. *Phys. Rev. B* **2006**, *74*, 165308.
(170) Nduwimana, A.; Wang, X.-Q. *J. Phys. Chem. C* **2010**, *114*, 9702.
(171) Amato, M.; Palummo, M.; Ossicini, S. *Phys. Rev. B* **2009**, *79*, 201302(R).
(172) Amato, M.; Palummo, M.; Ossicini, S. *Phys. Rev. B* **2009**, *80*, 235333.
(173) Musin, R. N.; Wang, X.-Q. *Phys. Rev. B* **2005**, *71*, 155318.
(174) Migas, D. B.; Borisenko, V. E. *Phys. Rev. B* **2007**, *76*, 035440.
(175) Peng, X.; Logan, P. *Appl. Phys. Lett.* **2010**, *96*, 143119.
(176) Yang, L.; Musin, R. N.; Wang, X.-Q.; Chou, M. Y. *Phys. Rev. B* **2008**, *77*, 195325.
(177) Nduwimana, A.; Musin, R. N.; Smith, A. M.; Wang, X.-Q. *Nano Lett.* **2008**, *8*, 3341.
(178) Liu, N.; Li, Y.-R.; Lu, N.; Yao, Y.-X.; Fang, X.-W.; Wang, C.-Z.; Ho, K.-M. *J. Phys. D Appl. Phys* **2010**, *43*, 275404.
(179) Peköz, R.; Malcıoğlu, O. B.; Raty, J.-Y. *Phys. Rev. B* **2011**, *83*, 035317.
(180) Peng, X.; Tang, F.; Logan, P. *J. Phys.-Condens. Mater.* **2011**, *23*, 115502.
(181) Peelaers, H.; Partoens, B.; Peeters, F. M. *Phys. Rev. B* **2010**, *82*, 113411.
(182) Huang, S.; Yang, L. *Appl. Phys. Lett.* **2011**, *98*, 093114.
(183) Hohenberg, P.; Kohn, W. *Phys. Rev.* **1964**, *136*, B864.
(184) Kohn, W.; Sham, L. J. *Phys. Rev.* **1965**, *140*, A1133.
(185) Niquet, Y.-M.; Delerue, C. *Phys. Rev. B* **2011**, *84*, 075478.
(186) Akman, N.; Durgun, E.; Cahangirov, S.; Ciraci, S. *Phys. Rev. B* **2007**, *76*, 245427.
(187) Amato, M.; Ossicini, S.; Rurali, R. *Nano Lett.* **2012**, *12*, 2717.
(188) Kim, J.; Lee, J. H.; Hong, K.-H. *J. Phys. Chem. Lett.* **2013**, *4*, 121.
(189) Bailey, R. E.; Nie, S. *J. Am. Chem. Soc.* **2003**, *125*, 7100.
(190) Denton, A. R.; Ashcroft, N. W. *Phys. Rev. A* **1991**, *43*, 3161.
(191) Vegard, L. *Z. Phys.* **1921**, 17.
(192) Diarra, M.; Niquet, Y.-M.; Delerue, C.; Allan, G. *Phys. Rev. B* **2007**, *75*, 045301.
(193) Niquet, Y. M.; Genovese, L.; Delerue, C.; Deutsch, T. *Phys. Rev. B* **2010**, *81*, 161301.
(194) Björk, M. T.; Schmid, H.; Knoch, J.; Riel, H.; Riess, W. *Nat. Nanotechnol.* **2008**, *4*, 103.
(195) Calderón, M. J.; Verduijn, J.; Lansbergen, G. P.; Tettamanzi, G. C.; Rogge, S.; Koiller, B. *Phys. Rev. B* **2010**, *82*, 075317.
(196) Koren, E.; Berkovitch, N.; Rosenwaks, Y. *Nano Lett.* **2010**, *10*, 1163.
(197) Amato, M.; Rurali, R.; Ossicini, S. *J. Comput. Electron.* **2012**, *11*, 272.
(198) Park, J.-S.; Ryu, B.; Chang, K. J. *J. Phys. Chem. C* **2011**, *115*, 10345.
(199) Shi, L.; Jiang, J.; Zhang, G.; Li, B. *Appl. Phys. Lett.* **2012**, *101*, 233114.
(200) Chen, X.; Wang, Z.; Ma, Y. *J. Phys. Chem. C* **2011**, *115*, 20696.
(201) Shelley, M.; Mostofi, A. A. *Europhys. Lett.* **2011**, *94*, 67001.
(202) Markussen, T.; Rurali, R.; Brandbyge, M.; Jauho, A.-P. *Phys. Rev. B* **2006**, *74*, 245313.
(203) Markussen, T.; Rurali, R.; Jauho, A.-P.; Brandbyge, M. *Phys. Rev. Lett.* **2007**, *99*, 076803.

(204) Shelley, M.; Poilvert, N.; Mostofi, A. A.; Marzari, N. *Comput. Phys. Commun.* **2011**, *182*, 2174.
(205) Markussen, T. *Nano Lett.* **2012**, *12*, 4698.
(206) Soref, R. A. *Proc. IEEE* **1993**, *81*, 1687.
(207) Pearsall, T. P.; Bevk, J.; Feldman, L. C.; Bonar, J. M.; Mannaerts, J. P.; Ourmazd, A. *Phys. Rev. Lett.* **1987**, *58*, 729.
(208) Dasgupta, N.; Yang, P. *Front. Phys.* **2013**, 14.
(209) Onida, G.; Reining, L.; Rubio, A. *Rev. Mod. Phys.* **2002**, *74*, 601.
(210) Hanke, W.; Sham, L. J. *Phys. Rev. B* **1980**, *21*, 4656.
(211) Palummo, M.; Amato, M.; Ossicini, S. *Phys. Rev. B* **2010**, *82*, 073305.
(212) Zhang, L.; d'Avezac, M.; Luo, J.-W.; Zunger, A. *Nano Lett.* **2012**, *12*, 984.
(213) Zhang, Y.; Xiang, G.; Gu, G.; Li, R.; He, D.; Zhang, X. *J. Phys. Chem. C* **2012**, *116*, 17934.
(214) Liu, S.; Xu, X.; Xie, R.; Zhang, G.; Li, B. *Eur. Phys. J. B* **2012**, *85*, 1.
(215) Carruthers, P. *Rev. Mod. Phys.* **1961**, *33*, 92.
(216) Peierls, R. E. *Quantum Theory of Solids*; Oxford University Press: Oxford, U.K., 1955.
(217) Li, B.; Wang, J. *Phys. Rev. Lett.* **2003**, *91*, 044301.
(218) Nikolić, B. K.; Saha, K. K.; Markussen, T.; Thygesen, K. S. *J. Comput. Electron.* **2012**, *11*, 78.
(219) Calzolari, A.; Jayasekera, T.; Kim, K. W.; Nardelli, M. B. *J. Phys.: Condens. Matter* **2012**, *24*, 492204.
(220) Car, R.; Parrinello, M. *Phys. Rev. Lett.* **1985**, *55*, 2471.
(221) Schelling, P. K.; Phillpot, S. R.; Keblinski, P. *Phys. Rev. B* **2002**, *65*, 144306.
(222) McGaughey, A. J. H.; Kaviany, M. *Phys. Rev. B* **2004**, *69*, 094303.
(223) McGaughey, A. J. H.; Kaviany, M. *Adv. Heat Transfer* **2006**, *39*, 169.
(224) Marx, D.; Hutter, J. *Ab Initio Molecular Dynamics: Basic Theory and Advanced Methods*; Cambridge University Press: New York, 2009.
(225) Dammak, H.; Chalopin, Y.; Laroche, M.; Hayoun, M.; Greffet, J.-J. *Phys. Rev. Lett.* **2009**, *103*, 190601.
(226) Broido, D. A.; Malorny, M.; Birner, G.; Mingo, N.; Stewart, D. A. *Appl. Phys. Lett.* **2007**, *91*, 231922.
(227) Ward, A.; Broido, D. A. *Phys. Rev. B* **2010**, *81*, 085205.
(228) Ward, A.; Broido, D. A.; Stewart, D. A.; Deinzer, G. *Phys. Rev. B* **2009**, *80*, 125203.
(229) Garg, J.; Bonini, N.; Marzari, N. *Nano Lett.* **2011**, *11*, 5135.
(230) Chen, X.; Wang, Y.; Ma, Y. *J. Phys. Chem. C* **2010**, *114*, 9096.
(231) Wang, Z.; Mingo, N. *Appl. Phys. Lett.* **2010**, *97*, 101903.
(232) Chan, M. K. Y.; Reed, J.; Donadio, D.; Mueller, T.; Meng, Y. S.; Galli, G.; Ceder, G. *Phys. Rev. B* **2010**, *81*, 174303.
(233) Hu, M.; Poulikakos, D. *Nano Lett.* **2012**, *12*, 5487.
(234) Lin, K.-H.; Strachan, A. *Phys. Rev. B* **2013**, *87*, 115302.
(235) Dames, C.; Chen, G. *J. Appl. Phys.* **2004**, *95*, 682.
(236) Tighe, T. S.; Worlock, J. M.; Roukes, M. L. *Appl. Phys. Lett.* **1997**, *70*, 2687.
(237) Fon, W.; Schwab, K. C.; Worlock, J. M.; Roukes, M. L. *Phys. Rev. B* **2002**, *66*, 045302.
(238) The Fibonacci chain of ref 201 is a one-dimensional quasicrystal, displaying local translational symmetries, but being aperiodic as a whole.
(239) Zhang, Y.; Xiao, Y. *Eur. Phys. J. B* **2008**, *63*, 425.
(240) Chen, J.; Zhang, G.; Li, B. *Nano Lett.* **2012**, *12*, 2826.
(241) Chen, J.; Zhang, G.; Li, B. *J. Chem. Phys.* **2011**, *135*, 104508.
(242) Hu, M.; Zhang, X.; Giapis, K. P.; Poulikakos, D. *Phys. Rev. B* **2011**, *84*, 085442.
(243) Kim, C.-J.; Yang, J.-E.; Lee, H.-S.; Jang, H. M.; Jo, M.-H.; Park, W.-H.; Kim, Z. H.; Maeng, S. *Appl. Phys. Lett.* **2007**, *91*, 033104.
(244) Seong, H.-K.; Jeon, E.-K.; Kim, M.-H.; Oh, H.; Lee, J.-O.; Kim, J.-J.; Choi, H.-J. *Nano Lett.* **2008**, *8*, 3656.
(245) Patolsky, F.; Zheng, G.; Lieber, C. M. *Nanomedicine* **2006**, *1*, 51.
(246) Lee, K.-Y.; Shim, S.; Kim, I.-S.; Oh, H.; Kim, S.; Ahn, J.-P.; Park, S.-H.; Rhim, H.; Choi, H.-J. *Nanoscale Res. Lett.* **2010**, *5*, 410.
(247) Jeon, E.-K.; Seo, H.; Ahn, C. W.; Seong, H.; Choi, H. J.; Kim, J.-J.; Kong, K.-J.; Buh, G.; Chang, H.; Lee, J.-O. *Nanotechnology* **2009**, *20*, 115708.
(248) Jang, D.; Lee, J. W.; Tachi, K.; Montes, L.; Ernst, T.; Kim, G. T.; Ghibaudo, G. *Appl. Phys. Lett.* **2010**, *97*, 073505.
(249) Rosaz, G.; Salem, B.; Pauc, N.; Potié, A.; Gentile, P.; Baron, T. *Appl. Phys. Lett.* **2011**, *99*, 193107.
(250) Cui, Y.; Zhong, Z.; Wang, D.; Wang, W.; Lieber, C. *Nano Lett.* **2003**, *3*, 149.
(251) Singh, N.; Agarwal, A.; Bera, L.; Liow, T.; Yang, R.; Rustagi, S.; Tung, C.; Kumar, R.; Lo, G.; Balasubramanian, N.; Kwong, D.-L. *IEEE Electron Device Lett.* **2006**, *27*, 383.
(252) Jiang, Y.; Singh, N.; Liow, T. Y.; Lo, G. Q.; Chan, D. S. H.; Kwong, D. L. *Appl. Phys. Lett.* **2008**, *93*, 253105.
(253) Kanungo, P. D.; Wolfsteller, A.; Zakharov, N.; Werner, P.; Gösele, U. *Microelectron. J.* **2009**, *40*, 452.
(254) Le, S. T.; Jannaty, P.; Luo, X.; Zaslavsky, A.; Perea, D. E.; Dayeh, S. A.; Picraux, S. T. *Nano Lett.* **2012**, *12*, 5850.
(255) Nah, J.; Liu, E.-S.; Varahramyan, K.; Tutuc, E. *IEEE Trans. Electron Devices* **2010**, *57*, 1883.
(256) Liang, G.; Xiang, J.; Kharche, N.; Klimeck, G.; Lieber, C. M.; Lundstrom, M. *Nano Lett.* **2007**, *7*, 642.
(257) Nah, J.; Dillen, D. C.; Varahramyan, K. M.; Banerjee, S. K.; Tutuc, E. *Nano Lett.* **2012**, *12*, 108.
(258) The values of the valence band-offset as a function of the composition of the alloy in a $Si_{1-x}Ge_x$-Ge interface were obtained by *kp* calculations where, for simplicity, the strain of the core and the shell was neglected. Notice also that in ref.[257] the alloy is defined as Si_xGe_{1-x} and thus x is the Si concentration, taking values of 0.7 and 0.5.
(259) Nah, J.; Liu, E.-S.; Shahrjerdi, D.; Varahramyan, K. M.; Banerjee, S. K.; Tutuc, E. *Appl. Phys. Lett.* **2009**, *94*, 063117.
(260) Nah, J.; Liu, E.-S.; Varahramyan, K.; Shahrjerdi, D.; Banerjee, S. K.; Tutuc, E. *IEEE Trans. Electron Devices* **2010**, *57*, 491.
(261) Katsaros, G.; Spathis, P.; Stoffel, M.; Fournel, F.; Mongillo, M.; Bouchiat, V.; Lefloch, F.; Rastelli, A.; Schmidt, O. G.; De Franceschi, S. *Nat. Nanotechnol.* **2010**, *5*, 458.
(262) De Franceschi, S.; Kouwenhoven, L.; Schöenberger, C.; Wernsdorfer, W. *Nat. Nanotechnol.* **2010**, *5*, 703.
(263) Zwiller, V.; Blom, H.; Jonsson, P.; Panev, N.; Jeppesen, S.; Tsegaye, T.; Goobar, E.; Pistol, M.-E.; Samuelson, L.; Björk, G. *Appl. Phys. Lett.* **2001**, *78*, 2476.
(264) Björk, M. T.; Thelander, C.; Hansen, A. E.; Jensen, L. E.; Larsson, M. W.; Wallenberg, L. R.; Samuelson, L. *Nano Lett.* **2004**, *4*, 1621.
(265) Roddaro, S.; Fuhrer, A.; Brusheim, P.; Fasth, C.; Xu, H. Q.; Samuelson, L.; Xiang, J.; Lieber, C. M. *Phys. Rev. Lett.* **2008**, *101*, 186802.
(266) Hu, Y.; Churchill, H. O. H.; Reilly, D. J.; Xiang, J.; Lieber, C. M.; Marcus, C. M. *Nat. Nanotechnol.* **2007**, *2*, 622.
(267) Kane, B. E. *Nature* **1998**, *393*, 133.
(268) Morton, J. J. L.; Tyryshkin, A. M.; Brown, R. M.; Shankar, S.; Lovett, B. W.; Ardavan, A.; Schenkel, T.; Haller, E. E.; Ager, J. W.; Lyon, S. A. *Nature* **2008**, *455*, 1085.
(269) Morello, A.; et al. *Nature* **2010**, *467*, 687.
(270) Simmons, S.; Brown, R. M.; Riemann, H.; Abrosimov, N. V.; Becker, P.; Pohl, H.; Thewalt, M. L. W.; Itoh, K. M.; Morton, J. J. L. *Nature* **2011**, *470*, 69.
(271) Yan, B.; Rurali, R.; Gali, A. *Nano Lett.* **2012**, *12*, 3460.
(272) Kloeffel, C.; Trif, M.; Loss, D. *Phys. Rev. B* **2011**, *84*, 195314.
(273) Bychkov, Y. A.; Rashba, E. I. *J. Phys. C* **1984**, *17*, 6039.
(274) Hao, X.-J.; Tu, T.; Caso, G.; Zhou, C.; Li, H.-O.; Guo, G.-C.; Fung, W. Y.; Ji, Z.; Guo, G.-P.; Lu, W. *Nano Lett.* **2010**, *10*, 2956.
(275) Hu, Y.; Kuemmeth, F.; Lieber, C. M.; Marcus, C. M. *Nat. Nanotechnol.* **2012**, *7*, 47.
(276) Xiang, J.; Vidan, A.; Tinkham, M.; Westervelt, R. M.; Lieber, C. M. *Nat. Nanotechnol.* **2006**, *1*, 208.
(277) Deng, C.; Sigmon, T. W.; Giust, G. K.; Wu, J. C.; Wybourne, M. N. J. *Vac. Sci. Technol. A* **1996**, *14*, 1860.

(278) Dayeh, S. A.; Wang, J.; Li, N.; Huang, J. Y.; Gin, A. V.; Picraux, S. T. *Nano Lett.* **2011**, *11*, 4200.
(279) Givargizov, E.; Sheftal, N. J. *Cryst. Growth* **1971**, *9*, 326.
(280) Mori, K.; Shoda, K.; Kohno, H. *Appl. Phys. Lett.* **2005**, *87*, 083111.
(281) Chang, H.-K.; Lee, S.-C. *Appl. Phys. Lett.* **2010**, *97*, 251912.
(282) Hsiao, T.-K.; Chang, H.-K.; Liou, S.-C.; Chu, M.-W.; Lee, S.-C.; Chang, C.-W. *Nat. Nanotechnol.* **2013**, *8*, 534.